12-2015

DESIGN AND SYNTHESIS OF POLYMER, CARBON AND COMPOSITE ELECTRODES FOR HIGH ENERGY AND HIGH POWER SUPERCAPACITORS

Margarita Arcila-Velez
Clemson University, marcila@g.clemson.edu

DESIGN AND SYNTHESIS OF POLYMER, CARBON AND COMPOSITE ELECTRODES FOR HIGH ENERGY AND HIGH POWER SUPERCAPACITORS

A Dissertation
Presented to
the Graduate School of
Clemson University

In Partial Fulfillment
of the Requirements for the Degree
Doctor of Philosophy
Chemical Engineering

---

by
Margarita Rosa Arcila Vélez
December 2015

Accepted by:
Dr. Mark E. Roberts, Committee Chair
Dr. Stephen Creager
Dr. Scott Husson
Dr. Rachel B. Getman

ABSTRACT

Supercapacitors (SCs) are promising energy storage devices because they deliver energy faster than Li-ion batteries and store larger amounts of charge compared to dielectric capacitors. SCs are classified in electrical double layer capacitors (EDLCs) and pseudocapacitors, based on their charge storage mechanism. EDLCs store charge electrostatically, i.e. by physical charge separation. This mechanism limits the storable amount of energy to the available surface area of the electrode, typically made of carbon materials, but grants good cycling stability of the SC device. Pseudocapacitor electrodes, commonly made of conducting polymers or metal oxides, store charge faradaically, i.e. through redox reactions throughout the bulk material, which allows them to store significantly larger amounts of energy than EDLCs, but their stability is compromised due to the partial irreversibility of the faradaic processes. To accomplish the commercialization of SCs, devices must show a combination of high charge storage capacities and long-term stability, besides being cost-effective.

To tackle the current issues of SCs, this field of study has taken mainly two directions: 1) the development of new architectures and nanostructures of the active materials, which has shown to increase the surface area, enhance stability, and facilitate ion diffusion; and 2) fabrication of composites between non-faradaic (carbon), faradaic materials, and/or redox-active components to achieve a balance between the amount of energy stored and the stability.

Following the first approach, a continuous process to grow vertically aligned carbon nanotubes (VACNTs) on cost-effective aluminum foil was developed. The

resulting electrodes were analyzed as SC electrodes and in symmetric cells, and the influence of the arrangement of the nanotubes and the synthesis conditions was studied. The performance of the VACNTs produced continuously showed similar performance to the VACNTs produced stationarily and the ordered structure of the VACNTs showed superior performance compared to randomly oriented CNTs. To increase the energy density, the second approach was taken, by combining pre-synthesized conducting polymers (CPs) and carbon nanotubes (CNTs) using a facile scalable dispersion filtration method to produce free-standing electrodes. Composites with the three main CPs were prepared, analyzed in various electrolytes, and their performance was comparable with polymer/ CNT films prepared with more complex techniques such as in-situ polymerization and pellet pressing. Then, based on the idea that the quinone molecules present in lignin store charge by undergoing a 2 proton, 2 electron redox reaction, a composite between polypyrrole, a stable conducting polymer, and the prototypical molecule p-benzoquinone was fabricated by electropolymerization of pyrrole in the presence of the redox molecule. A significant increase in capacitance and capacity was obtained with respect to polypyrrole films. Furthermore, an important obstacle in the application of CPs in SCs is the lack of easily reduced (n-dopable) polymers. Poly(aminoanthraquinone) (PAQ) is a conjugated polymer that shows electroactivity in the negative potential range of 0 to -2 V, due to the redox moieties of the polymer. PAQ was electropolymerized on free-standing CNT films and its performance as anode for SCs was studied. The materials and processing techniques described in this dissertation are useful to further develop high power/high energy electrodes for SCs.

DEDICATION

Esta tesis está dedicada a mi familia, amigos, y mentores que de una forma u otra han contribuido a mi formación académica y profesional. A todos los que me animaron y apoyaron a tomar el camino hacía mi doctorado y estuvieron conmigo durante mis estudios, especialmente a mis padres, Carlos y Lucy, por sus enseñanzas, sus consejos y su apoyo durante las dificultades y a través de la distancia. A Adam por ser mi compañero y apoyo incondicional, por hacer mis días más felices.

This dissertation is dedicated to my family, friends, and mentors who have contributed in any way to my personal and academic growth. To everyone who encouraged me to take this step in my life and to those who accompanied me throughout my doctoral studies, especially to my parents, Carlos and Lucy, for their guidance, advice and support during difficulties and through the distance. To Adam for his unconditional support, his guidance, and for making my days happier.

ACKNOWLEDGMENTS

I am most grateful to my advisor, Dr. Mark Roberts, for his mentorship, encouragement, trust and guidance and for teaching me how to be a successful and an integral researcher, for introducing me to the field of electrochemical energy storage and for allowing me to work in all these promising projects.

I would like to thank my research group, especially Dr. Jesse Kelly, Kryssia Diaz-Orellana and Robert Emmett, for their assistance, advice, and friendship, and all of the students who participated in any way in these research projects, including Dr. Apparao Rao's research group and Nicholas Degrood.

I would also like to thank my dissertation committee, Dr. Stephen Creager, Dr. Scott Husson, and Dr. Rachel Getman, for their valuable suggestions and feedback, their willingness to contribute to our research projects and help me throughout my doctoral studies.

Lastly, I would like to thank the Department of Chemical and Biomolecular Engineering for giving me the opportunity to pursue my PhD at Clemson University, for having a friendly and pleasant working environment and for their assistance and funding.

TABLE OF CONTENTS

Page

TITLE PAGE i

ABSTRACT ii

DEDICATION iv

ACKNOWLEDGMENTS v

LIST OF TABLES ix

LIST OF FIGURES ix

CHAPTER

I. INTRODUCTION 1

1.1 Electrochemical energy storage 1
1.2 Supercapacitors 2
1.2.1 Supercapacitor energy storage mechanisms 3
1.3 Commercial state of the art 5
1.4 Supercapacitor electrode materials 6
1.4.1 Carbon materials 6
1.4.2 Metal oxides 15
1.4.3 Conducting polymers 19
1.4.4 Electrode structure 24
1.5 Supercapacitor electrode manufacture 27
1.5.1 Wet coating methods 31
1.5.2 Printing methods 35
1.5.3 Electro-chemical methods 41
1.5.4 Non electrolytic reactive deposition 47
1.5.5 Other methods 53
1.6 Dissertation outline 57
1.7 References 60

II. ROLL-TO-ROLL SYNTHESIS OF VERTICALLY ALIGNED CARBON NANOTUBE ELECTRODES FOR ELECTRICAL DOUBLE LAYER CAPACITORS 89

2.1 Introduction 89

Table of Contents (Continued)

Page

2.2 Experimental methods 91
2.2.1 Materials 91
2.2.2 Electrode fabrication 93
2.2.3 Characterization 93
2.3 Results and discussion 94
2.4 Conclusions 104
2.5 References 105

III. A FACILE AND SCALABLE APPROACH TO FABRICATING FREE-STANDING POLYMER-CARBON NANOTUBE COMPOSITE ELECTRODES 109

3.1 Introduction 109
3.2 Experimental methods 112
3.2.1 Materials 112
3.2.2 Electrode fabrication 112
3.2.3 Characterization 113
3.3 Results and discussion 113
3.4 Conclusions 122
3.5 References 123

IV. PSEUDO-CAPACITOR ANODES COMPRISED OF ELECTROCHEMICALLY SYNTHESIZED AMINOANTHRAQUINONE REDOX POLYMERS 128

4.1 Introduction 128
4.2 Experimental methods 130
4.2.1 Materials 130
4.2.2 Electrode fabrication 131
4.2.3 Characterization 132
4.3 Results and discussion 132
4.4 Conclusions 144
4.5 References 145

V. REDOX SOLUTE DOPED POLYPYRROLE FOR HIGH-CHARGE CAPACITY POLYMER 151

5.1 Introduction 151
5.2 Experimental methods 156

Table of Contents (Continued)

Page

5.2.1 Materials 156
5.2.2 Electrode fabrication 156
5.2.3 Characterization 156
5.3 Results and discussion 157
5.4 Conclusions 169
5.5 References 171

VI. CONCLUSIONS AND RECOMMENDATIONS 179

6.1 Introduction 179
6.2 Roll-to-roll synthesis of vertically aligned carbon nanotube electrodes for electrical double layer capacitors 180
6.3 A facile scalable approach to fabricating free-standing polymer-carbon nanotube composite electrodes 182
6.4 Pseudo-capacitor anodes comprised of electrochemically synthesized aminoanthraquinone redox polymers 184
6.5 Redox solute doped polypyrrole for high-charge capacity polymer electrodes 184
6.6 References 186

LIST OF TABLES

Table Page

2.1 Table 1. Performance metrics of symmetric EDLC cells 103

LIST OF FIGURES

Figure Page

1.1 Ragone plot of energy storage devices 3

1.2 Mechanisms of SC operation: a) EDLC, and b) pseudocapacitance; c) current vs potential profiles for EDLCs and pseudocapacitors 4

1.3 Commercial supercapacitor configurations 6

1.4 SEM images of a) Activated carbon, b) multi-walled carbon nanotubes, c) graphene, and d) carbon nanofibers 8

1.5 Different carbon nanostructures and parameters affecting the material properties 9

1.6 SEM figures of: a) $NiCo_2O_4$/CF composites, b) honeycomb-like strongly coupled $CoMoO_4$–3D graphene hybrid, c) Co_3O_4/NiO core/shell nanowire arrays grown on FTO 17

1.7 Schematic illustrations showing the morphology of a) $NiCo_2O_4$/CF composites, b) NiO as spacer for GO, c) electrospun Mn_3O_4 nanofibers, and synthesis procedures to prepare: d) NiO nanoflakes/Co_3O_4 nanowires, and e) $CoMoO_4$/graphene 18

1.8 Different nanostructures of PPY obtained by varying the scan rate of cyclic voltammetric deposition. 22

1.9 Chemical vs electrochemical synthesis of PPY on carbon nano-onions and SEM images of the obtained materials 24

1.10 Wet coating methods: a) doctor blade coating technique, b) multilayer film deposition based on the dipping method, c) spray coating 31

1.11 Printing methods: a) ink-jet printing of active material, b) Gravure, c) Lithography. 36

1.12 Electro-chemical methods: a) electrophoresis, b) electrospinning, c) electrochemical synthesis 43

List of Figures (Continued)

Figure Page

1.13 Non-electrolytic reactive deposition techniques: a) electroless plating, b) chemical bath deposition, c) chemical vapor deposition. 47

1.14 Sputtering process schematic. 52

1.15 Other methods: a) laser treatment, b) filtration, c) pellet pressing, d) wet spinning 54

2.1 a) A schematic of the R2R process for growing vertically aligned CNTs on Al. foil. b) Al foil spools before and after CNT growth in the R2R process. c) a typical scanning electron microscopy (SEM) image of R2R-grown VACNTs 96

2.2 a) Spatial distribution of VACNT areal density in sCVD samples, b) CV profiles measured at a scan rate of 1000 mV s^{-1} in a standard three-electrode configuration with various electrolytes, c) Bode plots of the normalized imaginary capacitance (C") vs frequency for sCVD samples in the three electrolytes, and d) normalized capacitance vs voltage profiles (ν = 100 mV s^{-1}) for sCVD samples grown for 15, 30, 45, and 60 min (bars represent combined error from mass and CV data). The inset in panel d is a representative SEM image of sCVD VACNT forest grown for 1 h. 98

2.3 The capacitance of sCVD samples in three different electrolytes normalized by area shows a linear increase with increase in growth time. 98

2.4 Electrochemical properties of single electrodes comprised of sCVD, R2R, and BP samples. a) Cyclic voltammograms of various CNT electrodes in $TEABF_4$-MeCN electrolytes normalized by mass and scan rate (300 mV s^{-1}). b) normalized peak current (I_p) vs scan rate (ν) (inset: I_p vs $\nu^{1/2}$ for BP electrodes), c) galvanostatic discharge profiles (discharge current (ID) = 1 mA) in $TEABF_4$ - MeCN, and d) Bode plots of normalized imaginary capacitance (C") vs frequency for the three electrodes. 100

2.5 Nyquist plot for sCVD (blue), R2R (purple), and BP (red) electrodes..... 100

List of Figures (Continued)

Figure Page

2.6 Electrochemical characteristics of symmetric EDLC cells comprised of VACNT electrodes. a) photograph of the coin cell apparatus (inset: CNT electrodes and separator), b) cyclic voltammetry characteristics of and EDLC containing R2R electrodes at various scan rates, c) normalized CV profiles (F g^{-1}) for devices containing different CNT electrodes measured at a scan rate of 1000 mV s^{-1}, d) Nyquist plot for each of the devices described in (c), e) Charge-discharge measurements (1 full cycle at ±2 mA) for the devices consisting of sCVD (3.4 mg), R2R (3.2 mg), and BP (6.5 mg) electrodes, and f) Charge capacity of each device as a function of cycle number for more than 1000 cycles. 103

3.1 SEM images of composite electrodes made of a) CNT, b) PANI/CNT, c) PEDOT/CNT, and d) PPY/CNT; e) TGA profiles of the composite materials. f) EDAX of PPY/CNT composite, where P is polymer and C is carbon (%wt.) 116

3.2 Single electrode tests of CNT and ECP/CNT electrodes. a) CV in 3 M H_2SO_4 at 30 mV s^{-1}, b) CV in 1.5 M $TEABF_4$ in acetonitrile at 30 mV s^{-1}, c) scan rate dependence of capacitance in 3 M H_2SO_4 and d) 1.5 M $TEABF_4$ in acetonitrile, e) capacitance vs scan rate for PANI/CNT in 3 M H_2SO_4 and f) 1.5 M $TEABF_4$ in acetonitrile, g) Galvanostatic discharge curves with the inset figure showing the Nyquist plot in 3 M H_2SO_4 and h) 1.5 M $TEABF_4$ in acetonitrile..... 119

3.3 a) Picture of the electrodes, separator and testing set up of a symmetrical cell. Results for ECP/CNT symmetrical cells in 3 M H_2SO_4, and for PEDOT/CNT cell in 1.5 M $TEABF_4$ in acetonitrile (PEDOT/CNT-O), b) CV at 10 mV s^{-1}, c) scan rate dependence of capacitance. d) Nyquist plots with the inset figure showing an expanded view of the high frequency region, e) Bode plots of normalized imaginary capacitance (C") vs frequency, f) Galvanostatic discharge curves..... 121

4.1 Chemical structures of monomers used to electrochemically synthesize anode films: 1-aminoanthraquinone (1-AAQ), 1,5-diaminoanthraquinone (1,5-DAAQ) and 1,4-diaminoanthraquinone (1,4-DAAQ)..... 133

List of Figures (Continued)

Figure Page

4.2 a) CV polymerization of 1-AAQ (10 mM) in 1 M $LiClO_4$ in MeCN at 0.02 V s^{-1} and b) CV test in 1 M $LiClO_4$ in MeCN at 0.02 V s^{-1} 134

4.3 a) CV polymerization of 1-AAQ from 0 to 1.35 V vs Ag/Ag* at 20 mV s^{-1} in 1 M $LiClO_4$/MeCN electrolyte, b) capacitance vs potential for different scan rates. Inset: peak current vs scan rate$^{1/2}$. c) SEM images showing the morphology of PAQ on SS foil at magnifications of 500x and 3000x (inset), at an accelerating voltage of 5 kV 136

4.4 a) Cycling stability of PAQ deposited on SS foil (100 charge/discharge cycles), b) Cycling stability of PAQ/CT (1500 charge/discharge cycles) 137

4.5 CV test (30 mV s^{-1}) in 1 M $LiClO_4$/acetonitrile of PAQ polymerized on CT using a) chronoamperometry at 1.2, 1.35 and 1.5 V, and b) cyclic voltammetry from 0 V to 1.2, 1.35 and 1.5 V, c) CV test and d) charge/discharge and EIS (inset) of PAQ/CT electrodes in different salts (1 M) in acetonitrile at 10 mV s^{-1}. The black curves correspond to bare CT tests in 1 M $LiClO_4$/acetonitrile 140

4.6 SEM images of (a,b) CNT, (c,d) PAQ/CNT, (e,f) PPY/CNT. 141

4.7 a) CV test of AQ/CT anode and cathode, CT anode and cathode and PPY/CT cathode, b) CV of CT/CT, PAQ/PPY and PAQ/PAQ devices, and PAQ/PPY device after 3000 cycles, c) Stability of the 3 devices, d) C/D of the 3 devices, inset: EIS. e) C/D profiles for individual electrodes of PAQ/CT (green) and PPY/CT (blue) and the device of PAQ/PPY (red)..... 143

5.1 Illustrative schematic of the electrochemical processes occurring in a polypyrrole electrode doped with 1,4-benzoquinone..... 154

5.2 Electrode mass vs pyrrole concentration for polypyrrole/quinone composite (open circles) and reference polypyrrole (filled circles) films grown with a galvanostatic current density of 1.9 mA cm^{-2} for 360 seconds (total charge of 1.8 C). The quinone concentration is 0.092 M in each film. Linear correlations of the experimental data are displayed as solid lines..... 160

List of Figures (Continued)

Figure Page

5.3 Scanning Electron Microscopy (SEM) images showing the morphology of films grown on stainless steel mesh substrates with a pyrrole and quinone concentrations of 0.2 M and 0.092 M, respectively. Reference polypyrrole films are shown for magnification of (a) 500x and (b) 5000x, and PPy/QN films are similarly shown at (c) 500x (d) 5000x magnification 161

5.4 Electrochemical properties of reference polypyrrole (left column) and PPy/QN electrodes (right column) grown at different pyrrole concentrations measured in 0.1 M of $HClO_4$. Capacitance (F) vs potential is shown for (a) PPy and (b) PPy/QN, and specific capacitance (F g^{-1}) vs potential is shown for (c) PPy and (d) PPy/QN (0.01 V s^{-1}). Discharge curves, in terms of capacity ($mAhg^{-1}$), are shown for (e) PPy and (f) PPy/QN 164

5.5 a) Specific capacitance vs potential at a scan rate of 0.01 V s^{-1}, b) discharge curves, and c) average specific capacitance/deposition rate vs pyrrole concentration of PPy/QN electrodes deposited with pyrrole concentrations of: 0.085, 0.1, 0.15, 0.2, 0.3 and 0.4 M in the presence of quinone 0.092 M, along with reference polypyrrole control electrode 166

5.6 Cyclic voltammetry profiles (0.1 V s^{-1}) are shown for a) 5mM QN solutions, and b) PPy/QN films in electrolyte solutions with pH of 0.5, 1.5, 2.5 and 3.2. Figure insets show a) half wave potential (E1/2) vs pH and b) oxidation potential (Eox) vs pH 168

5.7 Electrode stability of reference polypyrrole and PPy/QN films prepared with 0.4 M pyrrole. a) Average specific capacitance between 0 to 0.8 V vs time in 0.1 M $HClO_4$ aqueous solution. Specific capacitance vs potential is shown for b) reference polypyrrole and c) PPy/QN electrodes after 1 h, 17.5 h, 21.5 h, 27 h, 84 h, and 262 h. CV profiles are recorded at a scan rate of 0.01 V s^{-1} 169

CHAPTER ONE

INTRODUCTION

1.1 Electrochemical energy storage

New materials and approaches to energy storage are being pursued in attempt to obtain energy security and reduced greenhouse gas emission from fossil fuels. Considerable resources are being expended on renewable energy sources, which require energy storage systems to store and deliver energy on demand, increasing the need such storage devices. Supercapacitors (SCs) and advanced battery systems (nickel, lithium, lead-acid, sodium-sulfur, etc.) have been identified as promising devices for supporting the emergence of renewable energy and offsetting the petroleum demands of transportation.[1] Supercapacitors, in particular, are attractive candidates due their ability to accommodate variable potential loads and rapid energy charge-discharge processes.

The push for new energy storage materials and systems is evidenced by the steady increase in federal funding. As the demand for energy storage increases, it is important to consider the availability of active materials and regardless of how mature Li-ion technology becomes, the world supply of lithium may not meet energy storage demands in the distant future.[2] In order to push technologies towards practical use, it is important to explore new directions using compatible and widely available materials. A primary consideration within the proposed research is how new materials and processes can be integrated in commercial technology.

1.2 Supercapacitors

Electrochemical capacitors (i.e. supercapacitors (SCs), electrical double layer capacitors (EDLCs), or ultracapacitors) are electrical energy storage devices that have the potential to achieve a combination of power and energy densities which is not attainable by either dielectric capacitors or batteries. Batteries generally exhibit high energy densities as a result of the utilization of the bulk electrode material for charge storage and their high charge capacity. However, the use of the electrochemical processes within the bulk of the electrode results in limitations on reaction kinetics and electron and ion transport, lowering the overall power delivery. Dielectric capacitors exhibit very high power densities, switching speeds, and high cyclability, but suffer from very low energy density. Supercapacitors combine the advantages of batteries and capacitors by incorporating similar electroactive materials to those found in batteries into high surface area configurations, paralleling concepts from capacitors. However, material selection and implementation of those materials into a rational design are critical. Ideally, all sites in the active electrode materials, surface and bulk, could be used to store charge, thereby boosting energy densities, while electroactive sites would be sufficiently close to electrolyte interfaces to allow for rapid electron and ion transport, resulting in increased power densities

Figure 1.1 shows a Ragone plot indicating the advantages and limitations of various energy storage devices with respect to their specific energy and power. As mentioned above, the drawback of dielectric capacitors is their inability to store large amounts of energy while batteries are incapable of fast charge/discharge cycles due to

longer times required for ion diffusion processes. This contrast in performance has been a major roadblock in electrochemical energy storage, and SCs have been proposed to bridge the gap between capacitors and batteries.

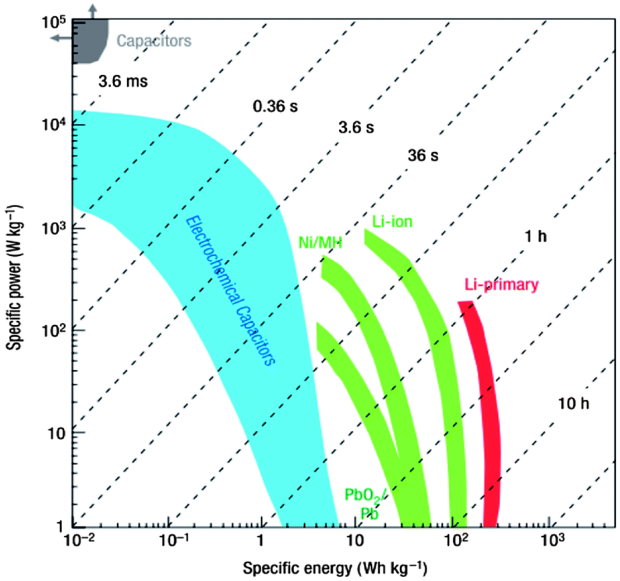

Figure 1.1. Ragone plot of energy storage devices. Reproduced from reference 3 with permission from Nature Publishing Group.

1.2.1 Supercapacitor energy storage mechanisms

The main components that make up a SC are two electrodes (cathode and anode), an electrolyte and separator. The electrolyte can be salts, acids, or bases, which dissociate into ions when dissolved in aqueous or organic solvents, and are necessary to support the flow of electricity across a load outside of the cell. Other types of electrolytes include polymer electrolytes and ionic liquids. The separator is a permeable polymeric membrane that keeps the electrodes apart, preventing a short circuit, while allowing the transport of ions.

SCs can be classified with respect to the energy storage mechanism of the electrodes in electrical double layer capacitors (EDLCs) and pseudocapacitors. EDLCs

store charge electrostatically, by ion adsorption-desorption processes along the polarized electrodes and pseudocapacitors store charge faradaically through reversible charge transfer reactions of the electrode material with the ions from the electrolyte. These storage mechanisms are illustrated in **Figure 1.2a** and **1.2b**.

Figure 1.2c shows the electrical response of an ideal EDLC (green line) and a pseudocapacitor (black line), which is represented as a current versus potential profile. The presence of peaks and the tilting in the profile of the pseudocapacitor are a result of Faradaic charge-transfer processes and the additional resistances associated with bulk electrodes, respectively. The integrated area of the current normalized by the scan rate and mass versus voltage is equal to the specific capacitance of the device; therefore, improved electrodes will show an increase in the peak capacitance and operating voltage.

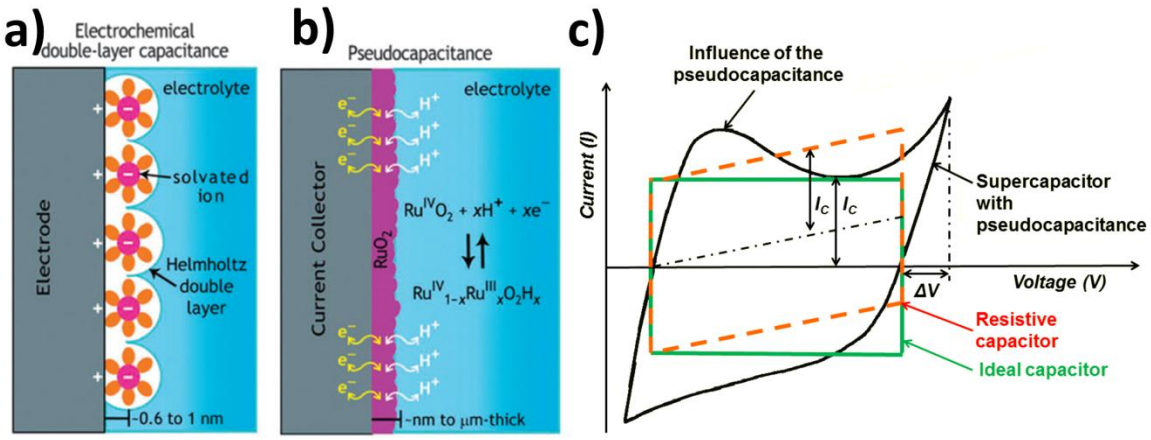

Figure 1.2. Mechanisms of SC operation: a) EDLC, and b) pseudocapacitance; Reproduced from reference 4 with permission from Cambridge University Press. c) current vs potential profiles for EDLCs and pseudocapacitors.[5]

1.3 Commercial state of the art

In general terms, supercapacitors may be considered to be “fast batteries” that can supply a reasonable amount in energy very quickly. In properly designed electrodes, high power and energy densities are attainable as charges can be stored at or near the high surface electrode area-electrolyte interface and through Faradaic electron transfer with the electroactive material. These attributes are ideal for applications requiring short power pulses of high power densities, rapid switching speeds, and high cycle stability which may include telecommunications, portable electronics, hybrid-electric vehicles, and pulsed power devices.

Common commercial supercapacitors are manufactured in jelly-roll type and stack configurations (**Figure 1.3)**, where the most important component is the carbon electrodes. They are made by mixing activated carbon with a conductivity enhancer and a non-conductive binder into a paste and coating aluminum foil current collectors. The standard electrolyte used for SCs is tetraethylammonium tetrafluoroborate in acetonitrile or propylene carbonate, and the separator can be cellulosic, polymeric, glass fiber-based, among others.

The main challenges that commercial supercapacitors are currently facing are low energy densities due to the limitations in surface area and non-faradaic nature, reduced power, and increased equivalent series resistance. This last problem arises from the electrode manufacture process, in which the AC requires a non-conductive binder and the active material is physically attached to the current collector.

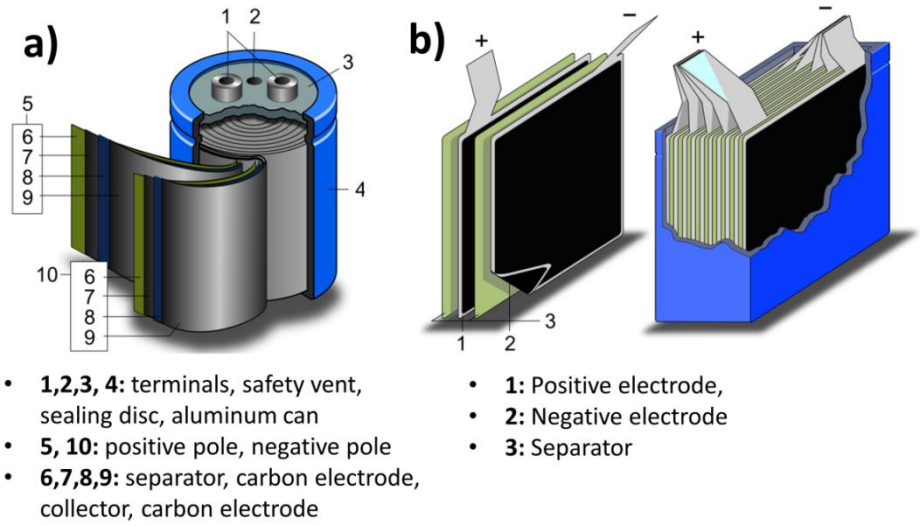

Figure 1.3. Commercial supercapacitor configurations. Adapted from 6.

1.4 Supercapacitor electrode materials

Depending on the energy storage mechanism of the SC, the electrode materials are classified in non-faradaic and faradaic. Carbon materials belong to the first group, while metal oxides (MOs) and conducting polymers (CPs) are the most common faradaic materials employed in SCs. Pseudocapacitors are similar to batteries in that the charge storage mechanism within the active electrodes is governed by Faradaic processes; however, they differ in that the processes in pseudocapacitors are limited by ion-adsorption (rather than ion diffusion), which leads to a relatively constant current profile with increasing voltage (capacitive-like behavior).

1.4.1 Carbon materials

Carbon materials (CMs), especially activated carbon (AC), are the most common material in commercial supercapacitors due to important features such as good electrochemical and thermal stability, electrical conductivity, abundance, high versatility

of texture, surface functionality, and low to moderate cost. EDLCs made of carbon electrodes can undergo 1 x10^6 charge discharge cycles with less than 20% loss in capacitance, while the same loss in conducting polymers has been recorded after less than 1000 cycles.[7, 8] Other properties of carbon include its amphoteric character, working well as anode and cathode, and good processability. As mentioned above, CMs store energy by physical charge separation on the materials surface, and therefore the most important parameter of these materials is the surface area of the interface between electrode and electrolyte. It has been observed that the maximum capacitance is attained when the pore size is very close to the ion size of the electrolyte.[9] As the pore size decreases, however, ion-diffusion becomes increasingly important, and can limit the overall power of the device. Intuitively, to increase the charge stored, it is necessary to increase the carbon surface area and tune porosity; this is usually achieved by using different precursors, as well as different synthesis conditions. Another option is to chemically modify (or functionalize) carbons through strong oxidation, which show pseudocapacitive properties at the cost of reduced stability.[10] In general, the main drawback of CMs is their low charge storage capacity compared to CPs and MOs, limited by the surface area of the material.

The performance of carbon materials varies based on structure, textures, and form. **Figure 1.4** shows common studied forms of carbon: activated carbon, single and multi-walled carbon nanotubes (MWCNTs), graphene, and nanofibers.[10, 11] **Figure 1.4** shows schematics of the same materials and a concise summary of the parameters affecting the material properties.

Activated carbons (ACs) are the materials employed in commercial EDLCs with capacitances of 100 F g^{-1} in organic electrolyte and 200 F g^{-1} in aqueous electrolyte.[12] AC is the preferred material due to its unique combination of very high surface area (~3000 m^2 g^{-1}), stable supply, well-established fabrication procedures, and decent conductivity.[9] Structurally, AC is comprised of discrete fragments of curved graphene sheets, in which pentagons and heptagons (defects) are distributed randomly throughout hexagon networks.[13]

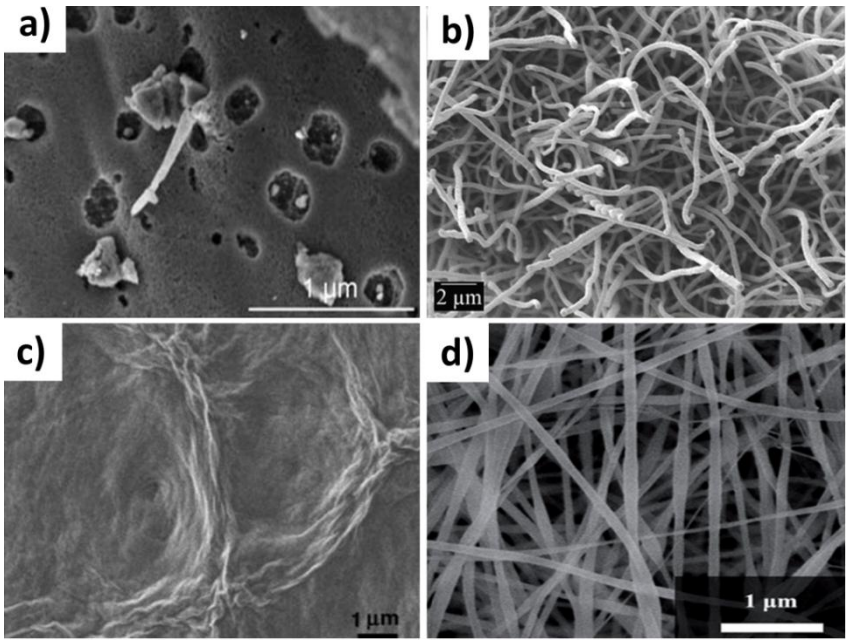

Figure 1.4. SEM images of a) activated carbon, b) multi-walled carbon nanotubes, c) graphene, and d) carbon nanofibers. Reproduced from reference 14, 15, 16, and 17 with permission from John Wiley and Sons, Centre National de la Recherche Scientifique (CNRS) and The Royal Society of Chemistry, and Elsevier.

AC can be fabricated from cheap materials, such as fruit and plant components and it is carried out in two steps.[18] The first step is carbonization, during which the carbon-rich organic precursor undergoes heat treatment to remove the non-carbon elements. Subsequently, to increase surface area, the carbon material is physically or

chemically activated using oxidizing gases or oxidizing agents (e.g. KOH, $ZnCl_2$, H_3PO_4), respectively.[19-21] Physical activation gasifies the char (the interstices) in steam to enhance the pores and chemical activation uses dehydrating agents to inhibit the formation of tar and enhance the yield of carbon (**Figure 1.5**).[19] Chemical activation is advantageous because it involves only one step and lower pyrolysis temperatures, it produces higher carbon yield of high surface area, and microporosity can be developed and controlled.[18, 20] Factors influencing the materials characteristics during activation are shown in **Figure 1.5**, from which the carbonization temperature is essential, because as temperature increases, the surface area decreases.

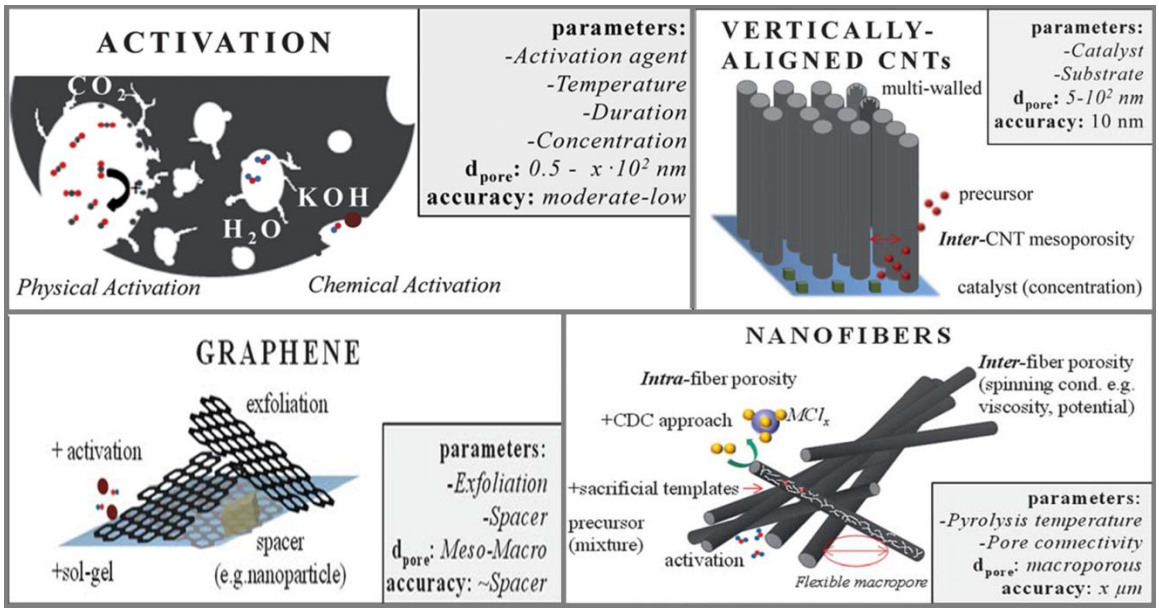

Figure 1.5. Different carbon nanostructures and parameters affecting the material properties. (Adapted from 22). Reproduced from reference 21 with permission from the Centre National de la Recherche Scientifique (CNRS) and The Royal Society of Chemistry.

Activation of carbon is a well-developed process that provides the ability to control, to some extent, the resulting properties of the material. On the downside, the pore

size distribution is not uniform, limiting the exposure of the developed area to the electrolyte.[12] AC electrode preparation is generally carried out by mixing the active material with conductivity enhancer and binder in a solvent and coating the mixture onto the current collector (CC), or by pressing the dry mixture into pellets without the loss of AC porosity.[20] Electrodes prepared by the former method with olive pits-derived and KOH-high temperature activated carbon showed a specific capacitance of up to 260 F g^{-1}.[23] Doctor blade coated AC electrodes derived from rice husk and activated with KOH showed a capacitance of 250 F g^{-1}.[24] AC electrodes prepared by pressing pellets with apricot shell-derived carbon, activated with NaOH, showed a capacitance of 339 F g^{-1}.[25] Coke-derived, KOH-activated carbon electrodes showed a capacitance of up to 350.96 F g^{-1} [26] and free-standing binder-free AC/carbon nanotubes (CNT) (95% AC) paper electrodes prepared by a filtration method showed a maximum capacitance 267.7 F g^{-1}.[27]

Graphene is an allotrope of carbon in the form of planar sheets of sp^2 bonded carbon atoms densely packed in a hexagonal lattice.[28] Graphene is obtained commonly by the reduction of graphene oxide (GO), which is commonly produced by the modified Hummers method from graphite.[29] Methods for graphene synthesis include mechanical and liquid phase exfoliation, chemical vapor deposition (CVD), chemical, thermal, or flame-induced reduction, epitaxial growth on metal surfaces, electrochemical synthesis, unzipping CNTs, and arc-discharge.[28, 30]

Graphene has great mechanical strength, which makes it useful for flexible and robust thin films; it has flexible pore structure, excellent conductivity, high stability and high surface area.[28] Due to its solubility in numerous solvents, it may be printed on

substrates for full integration with printable electronics. GO nanosheets inkjet-printed onto Ti foils and thermally reduced at 200 °C in N_2 attained capacitances as high as 132 F g^{-1} [16]. An important drawback from graphene is its tendency to aggregate in stacks of sheets, limiting the accessibility of electrolyte ions and degrading the unique properties of individual sheets.[31, 32] A proposed solution that has been frequently studied is combining graphene with CNTs, because CNTs act as a spacer between the graphene sheets reducing restacking and CNT agglomeration. Cheng et al.[33] used CNTs as spacer and as binder to hold the graphene nano-sheets together and electrodes prepared with vacuum filtration method achieved a capacitance of 290.6 F g^{-1}. Multi-layer graphene films prepared by chemical reduction of GO films obtained through layer-by-layer assembly showed an electrode capacitance of 247 F g^{-1}.[34] Holey graphene nanosheets prepared by ultra-rapid heating during the thermal reduction/exfoliation of graphite oxide exhibited a capacitance of up to 350 F g^{-1}.[35] Binder-free electrodes were produced by electro-spray deposition of a graphene oxide colloidal solution onto stainless steel CC and by reducing the GO with far-infrared radiation. The as-produced graphene electrode gave a specific capacitance of ~320 F g^{-1}.[29]

Carbon nanotubes (CNTs) can be classified in single-walled CNTs (SWCNTs) and multi-walled CNTs (MWCNTs), where SWCNTs are single graphene sheets rolled into cylinders and MWCNTs are concentric SWCNTs with increasing diameter. CNTs are synthesized from the catalytic decomposition of hydrocarbons. The three most common synthesis techniques are arc discharge, laser ablation, and chemical vapor

deposition (CVD), from which CVD is the most promising due to the lower temperatures needed (~600 – 800 ºC vs >1200 ºC).[36-38]

CNTs can possess high electrical conductivity, dictated by their chirality, purity, and number of walls, from which SWCNTs are highly conductive.[8] Due to their good mechanical properties, free-standing CNT films may be used as both electrode and current collector, eliminating the need for metallic CCs and the collector-electrode interface resistance.[39] CNTs can be directly grown on the substrate obviating the need for binder, reducing the contact resistance, CNT agglomeration, and maintaining the 3-dimensional nanostructure. In particular, vertically aligned CNTs (VACNTs) are promising due their organized structure, their fully accessible external surface area, and the ability to tune the inter-tube distance and film porosity. Vertically aligned double-walled carbon nanotubes synthesized via CVD, directly on substrates showed capacitances of around 200 F g^{-1}.[40, 41] CNTs can be solution or suspension-processed in a variety of ways to produce electrodes by using specific solvents, surfactants, or functionalizing the CNTs. Because SWCNTs can be solubilized in a variety of formulations and deposited from solution, thin films can be easily deposited using printing and coating techniques.[39] On the downside, the specific surface area of CNTs is significantly lower (100 – 400 m^2 g^{-1} [42]) than that of activated carbons or mesoporous carbons, resulting in lower energy density.[20, 43] Device capacitances, in the range of 20-80 F g^{-1} are attributed to the poorly developed microporous volume of CNTs.[12] Other limitations for commercial application of CNTs include their tendency to aggregate into bundles, their still-costly production process, low purity and yield, and reduced

conductivity due to the low control of chirality. Also, catalyst and reactor technology need to be optimized.[44] McArthur et al.[45] reduced agglomeration and introduced pseudocapacitance by functionalizing MWCNTs grown by thermal-CVD using an $Ar/C_2H_6/O_2$ glow discharge and the electrodes showed a specific capacitance of 288 F g^{-1}.

Carbon nanofibers (CNFs) are nanostructures with cylindrical shape of graphene layers similar to CNTs, but with different textural and structural characteristics. CNFs usually exhibit diameters of 100−300 nm and length of up to 200 μm. They can be classified in highly graphitic (high electrical conductivity, low specific surface area) and lowly graphitic CNFs (lower electrical conductivity, higher surface area, less crystalline).[46] CNFs are synthesized using CVD methods or from polymeric fibers such as rayon or polyacrylonitrile[47]. They can be used directly as electrode without the need for binder, achieve high electrical conductivities (200 – 1000 S cm^{-1}), and high surface area (once activated: 1000-2000 m^2 g^{-1}). This material has been studied for flexible electrodes, although their cost still restricts its application in commercial devices.

Coal based nanofibers and nitrogen-doped hollow activated CNFs were prepared by electrospinning, carbonization, and activation. Electrodes showed a specific capacitance of 230 F g^{-1} and N-doped CNFs achieved 197 F g^{-1}.[40, 45] Amorphous CNFs activated in KOH lead to new micropores and larger surface areas as well as a higher content of basic oxygen groups, enhancing the specific capacitance. Supercapacitor electrodes processed as cylindrical pellets with binder attained values as high as 255 F g^{-1}.[46] Mesoporous carbon nanofibres (CNFs) were prepared from furfuryl alcohol precursor coupled with a mesoporous silica template by vapor deposition polymerization strategy.

A specific capacitance of 222 F g^{-1} was obtained with electrodes prepared by mixing CNFs, conductivity enhancer and binder and pressing the mixture onto a nickel grid.[48]

Other important carbon materials include **carbon aerogels (CAs)**, **hydrogels**, and **carbide-derived carbon**. The first group is a large class of gels composed of particles with sizes in the nanometer range covalently bonded together. They have very high porosity (over 50%, with pore diameter under 100 nm) and high surface areas ranging between 400–1,000 m^2 g^{-1}.[10, 12] The three-dimensional mesoporous materials with interconnected ordered pore structure can provide efficient diffusion of electrolyte ions and electrons, leading to promising applications in supercapacitors.[49] CAs are prepared from the sol-gel route by the condensation reaction of resorcinol and formaldehyde and subsequent pyrolysis.[10] Capacitances of up to 150 F g^{-1} (aqueous) have been obtained with this material[49] and due to its very low density and therefore poor volumetric capacitance, it has been of less interest for supercapacitor applications.

Carbide-derived carbons are attractive because they are produced through one of the most accurate synthesis strategies to control micropore size with sub-Ångstrom accuracy based on the selective removal of metal atoms out of metal carbide matrices using gaseous halogens, primarily chlorine.[50] The extraction of metal atoms serves for the creation of micropores and takes place under full conservation of the original shape of the carbide allowing for a precise control over the resulting pore size, which depends on the used precursor. Their specific surface area exceeds 3000 m^2 g^{-1} [50] and in this case, higher temperatures usually lead to an increase in the pore size due to the self-organization of the highly mobile carbon atoms.[22, 51]

1.4.2 Metal oxides

Metal oxides (MOs) are compounds formed with a metal and an anion of oxygen typically in the form of O^{2-}. MOs can store significantly larger amounts of charge than carbon materials and, in some cases more than conducting polymers, with theoretical specific capacitances greater than 1200 F g^{-1}, with reasonable material stability.[52] MOs store charge faradaically through fast and reversible redox reactions on their surface, where the metal can exist in two or more oxidation states, and protons can freely intercalate allowing the reversible conversion of O^{2-} to OH^{-}. Surface functional groups, defects and grain boundaries can serve as redox centers for the charge transfer reactions.[52] Widely investigated MOs include ruthenium oxide (RuO_2), manganese oxide (MnO_2), nickel oxide (NiO) and cobalt oxide (Co_3O_4), from which RuO_2 and MnO_2 are considered the most promising materials for SCs, due to their high capacitance, and low cost/ natural abundance, respectively. Binary metal oxides (BTMOs), i.e. MOs that contain at least one transition metal ion and one or more electrochemically active or inactive ion have been also of interest. BTMOs are used to improve the capacitive performance by providing a larger potential operation range, superior conductivity, additional reactive sites and in some cases, improved stability. Practical challenges of BTMOs include difficulties to fabricate BTMOs that satisfy all the requirements of specific applications through a simple method. Both the synthesis parameters and material properties need to be optimized.[53] Some common BTMOs are $NiCo_2O_4$, $CoMoO_4$, and $NiMnO_3$.

Several reports have shown that bare metal oxide electrodes can deliver large specific capacitance and high energy density due to their redox reactions involving different ions. Metal oxides exhibit properties favorable for supercapacitor materials, such as a low molecular weight, low toxicity to the environment, and ease of large-scale fabrication. Synthesis methods of the material are relatively inexpensive, and the methods may be modified in order to tune the morphology to improve capacitance and power.[54-56] In addition, some metal oxides such as iron and manganese oxides are abundant in nature and thus low-cost.

The primary means of fabricating MOs directly on the CC is by electrodeposition, where a current is applied in three-electrode configuration to induce a redox reaction that forms metal oxides on a surface in solution. For instance, electrodeposited $NiCo_2O_4$ on carbon cloth achieved a capacitance of 2658 F g^{-1} [57] **(Figure 1.6a**, **Figure 1.7a)** and NiO/reduced graphene oxide (rGO) showed 569 F g^{-1} [58] (**Figure 1.7b**). Electrospinning is another viable synthesis method (see processing section); electrospun Mn_3O_4 nanofibers exhibited 360.7 F g^{-1} [59] (**Figure 1.7c**). MOs are also synthesized by the hydrothermal/ solvothermal method, precipitation technique, and sol-gel method, and the obtained material is combined with conductivity enhancer and binder and casted onto the CC or pressed into pellets. For instance, $CoMoO_4$ synthesized using the solvothermal method on 3D graphene foam showed 2741 F g^{-1} [60] (**Figure 1.6b, Figure 1.7e**), Co_3O_4 nanoparticle/rGO prepared with the hydrothermal technique showed 415 F g^{-1} [61] and electrodes based on Co_3O_4/NiO nanowires on nickel foam exhibited a specific capacitance of 853 F g^{-1} [62] (**Figure 1.6c, Figure 1.7d**). Thin NiO nanorods (10–15 nm in

diameter) grown directly on Ni foam demonstrated a specific capacitance of 1536 F g^{-1} [63]. Cr-doped Mn_3O_4 nanocrystals exhibit a maximum capacitance of 272 F g^{-1} [64] and Nio/rGO prepared by precipitation technique showed 525 F g^{-1}.[65] While record high capacitance values are observed in some cases, these values represent the performance of very thin films or low material quantities, and methods to prepare such materials are not conducive for large scale synthesis.

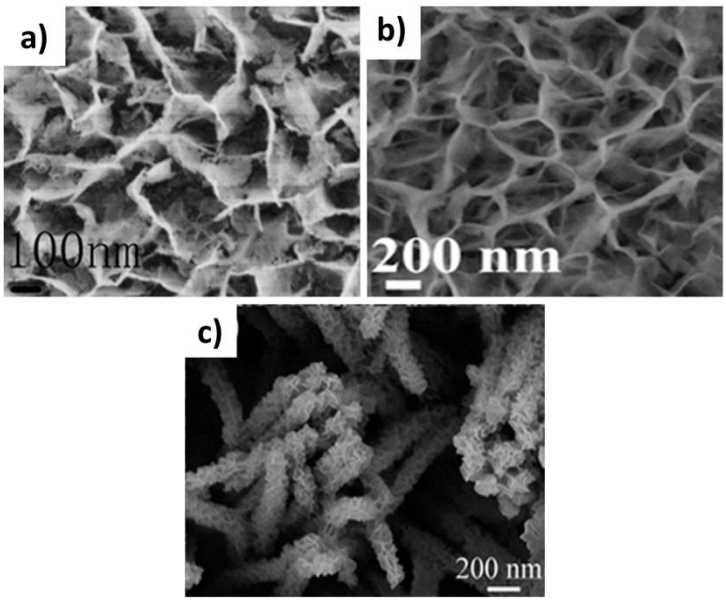

Figure 1.6. SEM figures of: a) $NiCo_2O_4$/CF composites, b) honeycomb-like strongly coupled $CoMoO_4$–3D graphene hybrid, c) Co_3O_4/NiO core/shell nanowire arrays grown on FTO. Reproduced from references 57, 60, and 62 with permission from the Centre National de la Recherche Scientifique (CNRS) and The Royal Society of Chemistry, John Wiley and Sons, and American Chemical Society.

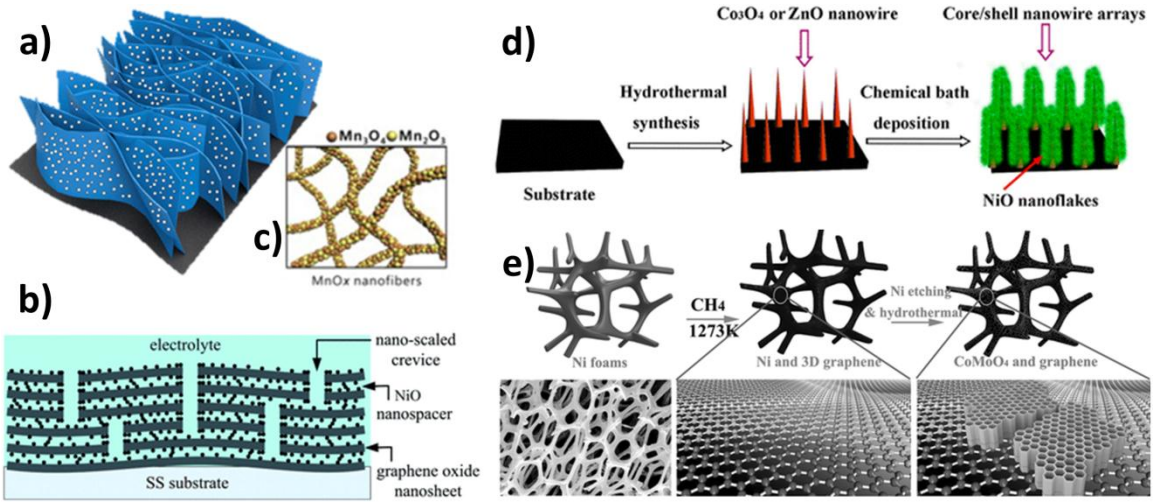

Figure 1.7. Schematic illustrations showing the morphology of a) $NiCo_2O_4$/CF composites, b) NiO as spacer for GO, c) electrospun Mn_3O_4 nanofibers, and synthesis procedures to prepare: d) NiO nanoflakes/Co3O4 nanowires, and e) $CoMoO_4$/graphene. Reproduced from references 57, 58, 59, 62, and 60 with permission from the Centre National de la Recherche Scientifique (CNRS) and The Royal Society of Chemistry, Elsevier, American Chemical Society, and John Wiley and Sons.

Nonetheless, metal oxides present unique limitations for use in SCs. The conductivity of most MOs except for RuO_2 is very low, since they belong to wide bandgap semiconductors or even insulators. MOs suffer from poor ion transport kinetics due to increased amount of grain boundaries. They are only suitable for use in aqueous electrolytes, limiting the nominal cell voltage to 1 V.[55] They also exhibit self-discharge behavior, breakdown of the material after charge-discharge cycling due to volume changes, corrosion of the current collector, and defects on the surface alter the electrochemical properties of the material.[66] The surface area, pore distribution, and the porosity are difficult to tailor in metal oxides. Some metal oxides, such as ruthenium oxide, maintain high costs not suitable for large-scale use in supercapacitors.[67] Therefore metal oxides may not be employed alone as supercapacitor electrodes for practical

applications.[52] Similarly to conducting polymers, MOs have been combined with carbon materials or developed into MO nanostructures to overcome these issues.[68]

1.4.3 Conducting polymers

Conducting polymers (CPs) conduct electricity and store energy due to their conjugated structure of alternating single and double bonds and/or atoms with p-orbitals (e.g. N,S) that, upon doping, allow charges to move along the polymer backbone with the array of delocalized electrons formed by overlapping p-orbitals.[69] Conducting polymers can be p-doped and n-doped by partial oxidation and partial reduction, respectively. Available conducting polymers can be easily p-doped and are most often conductive in their oxidized state; therefore research has focused on incorporating CPs into supercapacitors as cathode materials.[70] The most common conducting polymers,[69, 71] polyaniline (PANI),[72-74] polypyrrole (PPY),[71, 72, 75, 76] and poly(3,4-ethylenedioxythiophene) (PEDOT),[77-79] are fairly stable (over a few thousand of cycles) and have high theoretical charge capacities of 148 (doping degree: n=~0.51), 140 (n=~0.35) and 62 (n=~0.33) mAh g^{-1}, respectively.[80] PEDOT can be n-doped but it yields significantly reduced conductivity and specific capacitance relative to its p-doped form.[69]

Some favorable properties of CPs include the strong electrical conductivity, high specific capacitances, intermediate specific energies, ease of fabrication, and relatively cheap production.[69, 81, 82] However, to be viable commercially, CPs processability needs to be improved regarding their low solubility and inability to melt. Moreover, CPs electrical and physical properties are not yet suitable for commercial applications, and the materials and processing costs need to be further reduced. Another issue of CPs is the

poor mechanical stability, specifically resulting from repeated ion intercalation, which yields shorter life-cycles than supercapacitors utilizing CMs or MOs.[82] To tackle these shortcomings, research on CPs has predominantly focused on manufacturing composites with carbon materials, which have shown improved properties, as well as on nanostructured CPs and surfactant-stabilized CPs, which have shown better dispersibility and larger surface area.[83] Moreover, to increase charge capacity, CPs have also been combined with metal oxides.

The primary methods of synthesizing conducting polymers are electrochemical and chemical polymerization. The **electrochemical synthesis** consists on oxidizing the monomer, oligomers and polymer chains, by applying electric current, in the presence of an electrolytic solution (aqueous or organic) that contains the monomer. Some methods include constant potential or current, cyclic voltammetry, and pulsed potential or current. Electrochemical deposition can be carried out using a two- or three-electrode cell, where the electrode of interest is the substrate on which the polymer film forms and can be used directly as a SC electrode. An important advantage of this method is that it allows an efficient control of the morphology, thickness, polymerization rate, and electrochemical properties by adjusting parameters such as the applied current or potential, electrolyte, substrate type, and synthesis time.[84] **Figure 1.8**, for instance shows how the variation in the cyclic voltammetry scan rate produces different nanostructures, and influences the material performance. The obtained values of supercapacitance of these nanostructures are 327, 412 and 547 F g^{-1} for nanobelts, nanobricks, and nanosheets of PPy, respectively.[84]

Higher specific capacitances are normally obtained with electrodeposited CPs due to the more intimate contact between active material and current collector as well as the ease of producing large surface area nanostructured materials.[85] For instance, electrodeposited PANI on VACNT[86] and PANI nanowires on carbon cloth[87] achieved capacitances of 1030 F g^{-1} and 1079 F g^{-1}, respectively. PPy electrodes prepared by CV with varying scan rates form different nano/microstructures displayed a maximum capacitance of 586 F g^{-1} for multilayer PPy nanosheets.[84, 88] PEDOT micro/nanorods achieved a specific capacitance of 109.11 F g^{-1},[89] while PEDOT nanowires/carbon cloth nanocomposite showed 256.1 F g^{-1}.[90] Nanostructured electrodes can also be prepared via electrodeposition on templates, followed by its removal. Zhi et al.[85] achieved 960 F g^{-1} with PPy nanowires/GO deposited on an Al_2O_3 template. In this case, electrodeposition on porous carbon or MO materials, the polymer forms only on the accessible surfaces to the electrolyte, and as the polymer thickness increases, the effect of the interaction between the different materials in the composite is reduced. Electropolymerization is preferred for the synthesis of thin films, good-quality materials and material growth on the desired spot, rather than large-amount polymer production.[91]

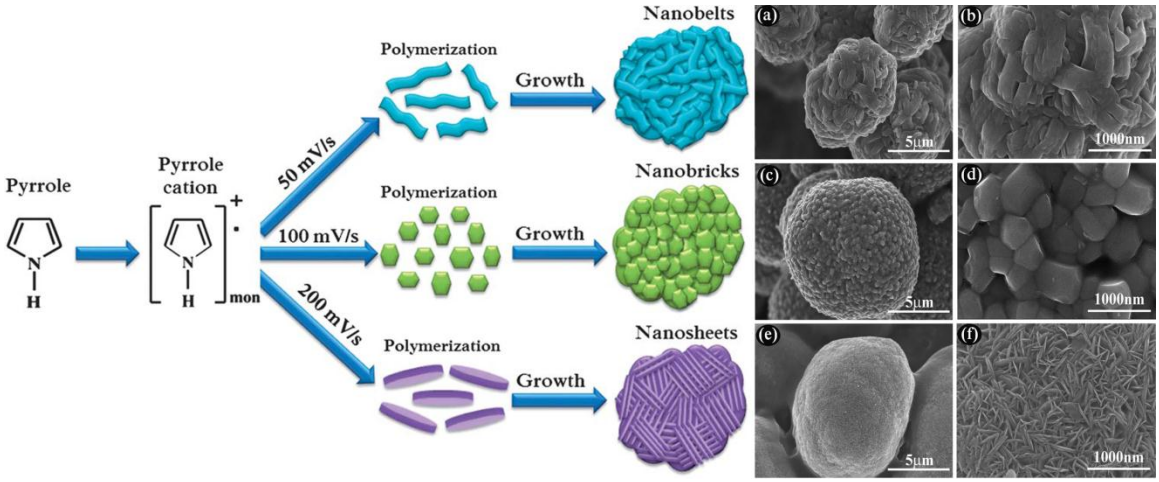

Figure 1.8. Different nanostructures of PPY obtained by varying the scan rate of cyclic voltammetric deposition.(Adapted from 84). Reproduced from reference 84 with permission from the Centre National de la Recherche Scientifique (CNRS) and The Royal Society of Chemistry.

In the **chemical synthesis**, monomers are oxidized by strong oxidants, yielding radicals that dimerize with other monomer radicals. The oxidization and radical-radical coupling process repeats itself causing the polymer to grow. Termination occurs by depletion of reactive radical species or by chain termination processes. After polymer bulk synthesis, the mixture is normally centrifuged, washed and the resulting material is filtered and dried. The chemical route allows the production of large quantities of CPs in the reaction solution and the direct assembly of the polymer to the CC by in situ polymerization. A common procedure to prepare electrodes for testing in lab scale is to combine the chemically polymerized CP with a conductive additive and binder in a solvent to form a slurry and spread it on the current collector. In the case of composites, it is a useful method to produce homogeneous mixtures of the materials, compared to electropolymerization. **Figure 1.9** shows how the deposition method (chemical vs electrochemical) affects the material distribution in the composite, as well as its

morphology. Electrochemically and chemically prepared PPy/CNOs showed capacitances of 428 and 652 F g^{-1}, respectively.[92] Wang et al.[93] achieved a capacitance of 746 F g^{-1} with PANI/GO composites on stainless steel CC. PPy/graphene and PPy/carbon aerogel electrodes prepared by the chemical route have shown capacitances of around 482 F g^{-1} and 433 F g^{-1}, respectively.[75, 94, 95] Sathish et al.[96] and Xu et al.[97] prepared electrodes by pressing PANI/rGO and PANI/GO sheets with binder and conductivity enhancer onto substrates and got capacitances of 626 F g^{-1} and 555 F g^{-1}, respectively. PPy/functionalized graphene sheets powder compressed into disc-shaped pellets showed a capacitance of 277.8 F g^{-1}.[98] Mondal et al.[99] prepared fibrous composites of graphene quantum dot-doped PANI that showed a specific capacitance of 1044 F g^{-1}. Grover et al.[100] prepared electrodes with PANI/rGO nanoribbons by spray-coating the material on graphite plates achieving capacitances of up to 1180 F g^{-1}. PEDOT/ rGO[101] and PEDOT/graphene[92] electrodes displayed a specific capacitances of 108 F g^{-1} and 380 F g^{-1}, respectively. Free standing PEDOT-PSS/single walled nanotube films made by filtration method had a specific capacitance of 133 F g^{-1}.[102] Despite the high throughput, the chemical route is not yet favorable for commercial synthesis, as limited availability of oxidants (dopants) and lack of control on the oxidizing power of the dopants leads to the inability to control the properties of the polymers produced.

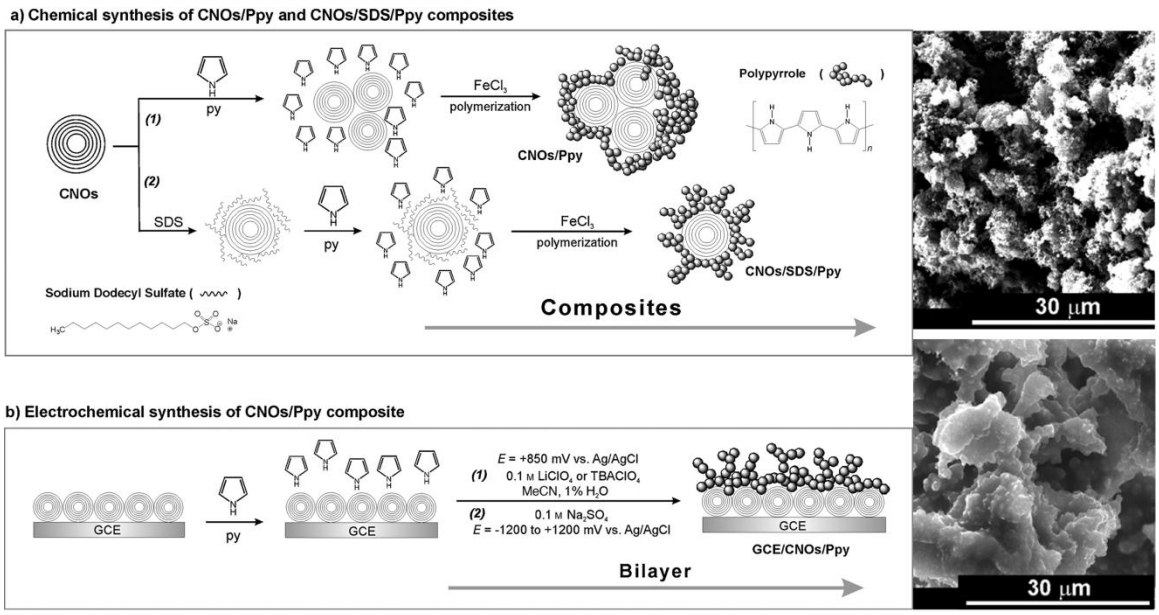

Figure 1.9. Chemical vs electrochemical synthesis of PPY on carbon nano-onions and SEM images of the obtained materials.(Adapted from 103). Reproduced from reference 103 with permission from John Wiley and Sons.

1.4.4 Electrode structure

The design and fabrication of CPs and composites is a major challenge facing future high-energy and high-power devices and is the subject of the proposed research. Compared with bulk conducting polymers, nanostructured materials have the potential to improve performance in energy storage devices. Some advantages of nanostructured materials include high surface area, short path lengths for ion transport, and improved electronic and ionic conductivity from reduced interfacial impedance.[104] In order to maximize capacitance, switching speed, and power, materials for supercapacitors must incorporate conductive, electroactive materials into high surface area structures that are engineered to provide optimized contact between redox active sites and electrolytes.

The physical structure of the electrode strongly dictates the energy storage performance, particularly power and energy densities. Within pseudocapacitive materials, Faradaic charge storage occurs within the first few nanometers of the surface; therefore, the material's architecture is essential and structural dimensions on the order of nanometers are necessary to achieve short diffusion lengths and rapid discharge rates.

Electrolyte. The choice of electrolyte will determine many aspects of material design, device operation and stability. The operational voltage range is fundamentally limited by the stability of the electrolyte, which inevitably will break down at a given potential. This limitation affects the device energy density, which is proportional to the square of the cell voltage. For example, changing electrolyte systems from aqueous to organic electrolytes in EDLC devices results in an increase in maximum potential from 1.0 V to 2.5-2.7 V. Factors that must be considered for the selection of electrolyte include conductivity, electrochemical and thermal stability, and toxicity.[105]

Aqueous. Operation in aqueous electrolytes is typically required for pseudocapacitive materials that require a proton source. These systems benefit from the use of benign salt electrolytes. The main limitation is the operating voltage window, which is restricted to below ~1.2 V. Furthermore, some metal oxides and conducting polymers are dependent on pH to show redox activity and be conductive. The stability of conducting polymer materials should be carefully considered as many materials, especially thiophene-based, are susceptible to overoxidation and can degrade in water.

Non-aqueous. The use of non-aqueous electrolytes has attracted attention due to the operating voltage limitation of water. Organic solvents have shown stability up to 2.7

V, and most materials, including metal oxides and polymers, function well without dissolving. However, non-aqueous solvents are more toxic than water based systems, potentially flammable, and typically possess lower conductivity than ionic aqueous systems. Some of these issues have been overcome by employing propylene carbonate instead of acetonitrile due to its lower flash point and toxicity, at the cost of significantly reduced conductivity.

Ionic liquids (ILs). ILs are non-flammable, solvent-free, room-temperature liquid salts that are quickly becoming a viable alternative to non-aqueous electrolyte systems. They are stable over a wide range of temperatures, their electrochemical stability is dependent on the individual ions, and operation voltages above 3 V have been demonstrated.[106] While these systems are typically used at higher temperatures due to their low ionic conductivity (few mS cm^{-1} at room temperature), prediction suggest that research in new ion combinations could lead to conductivities on the order of 40 mS cm^{-1} and operation stability at potentials greater than 4V.[3] Disadvantages of ILs include their high cost, toxicity, the difficulty to purify them since they cannot be distilled, and only small volumes are available commercially.[105]

Asymmetric and hybrid supercapacitors. An asymmetric SC is a device composed of electrode made of different pseudocapacitive materials.[107] Many examples exist with a metal oxide layer and a conducting polymer electrode[108, 109] and two distinct conducting polymer electrodes.[110, 111] Asymmetric SCs were initially investigated to expand the operating voltage window of SCs by incorporating materials with improved stability in their respective electrode voltage range. A hybrid supercapacitor consists of

two distinct electrodes, comprising a high surface area carbon electrode (EDLC) with a pseudo-capacitive electrode (redox-active). The concept of a hybrid supercapacitor arose due to chemical and electrical stability limitations of redox-active materials as anodes. Therefore, the anode material was replaced with carbon materials. The performance of these materials has similar limitations to EDLC devices.[112, 113]

1.5 Supercapacitor electrode manufacture

Besides the importance of the selection of active material for SC electrodes, the processing technique utilized to fabricate the electrode itself plays an essential role in the performance of the device. The development of process technologies scalable from the laboratory to the commercial level is critical to the implementation of carbon materials (CMs), conducting polymers (CPs), metal oxides (MOs), and composites in SC electrodes. The aim of this section is to explain the most common processing methods that are considered viable for the future mass production of SC electrodes, and to bridge the gap between the materials fabrication procedures and the ways of turning those materials into electrodes. To take full advantage of the synthesized material properties, the appropriate electrode fabrication method must be selected, taking into account the processability and the target application for the energy storage device. A combination between the material and the electrode fabrication processes determines attributes such as energy and power densities, conductivity, resistance, and capacitance, and important physical properties, such as thickness, uniformity, composition, morphology, porosity, adhesion to current collector (CC), and mechanical stability, that have direct influence in

the electrochemical performance of the material. Ultimately, for the industrial production of SCs, the electrodes must meet the performance requirements and the overall electrode manufacture process must be cost-effective.

The manufacturing techniques outlined below have been classified by the type of deposition or coating mechanism and they encompass the direct synthesis of electroactive materials on conductive substrates, the coating/deposition of pre-synthesized materials onto CCs, as well as free-standing electrode production. The advantages and challenges of each processing technique will be assessed. To this day, the aspects that hinder the commercialization of new materials are the high price of the active materials and the either inconvenient or ineffective fabrication methods in terms of equipment cost, process complexity, energy and material usage, throughput, and electrode performance. For instance, despite all the attention devoted to CNTs, their high cost and poor performance that has not met the expectations are still hindering their application. With the decrease of prices, increase in purity and low environmental effects, materials will become commercially viable for energy storage applications.[114] Simple spraying, spin coating or filtration methods all lead to random networks with various thickness and conductivities and can be tailored to the specific needs of the desired devices. At the same time, industrial scale fabrication will require roll-to-roll deposition (R2R), in terms of manufacture ability and cost control. Already R2R well-developed technologies include slot coating, gravure and flexo printing.

Raw/starting material. For mass production of SCs, the starting materials, substrate, template and reactants need to be cost-effective, as they influence the final

price of the devices. With respect to CPs and MOs, if the price of the monomers and metal oxide precursors is not competitive, this hinders the commercialization of pseudocapacitors significantly. The prices of the monomers are already competitive with the current price of AC for SCs (Pyrrole US$3000/t, aniline US$1650/t, EDOT US$2400/t, SC AC US$1500/t). The discussion of cheap raw materials pertains more to the sources of carbon materials, since they can be obtained from basically any organic matter, such as coconut shells,[115] bagasse,[116] and fermented rice.[117]

Binders and conductivity enhancers. Multiple electrode manufacturing techniques require the use of binders, which are non-conductive polymers that hold the material together as a whole and enhance or allow the adhesion of the active material to the CC. The most common binders are polyvinylidene fluoride (PVdF), polyvinylidene chloride (PVdC), ethyl cellulose, carboxy methyl cellulose, polytetrafluoroethylene (PTFE) and polyvinylpyrrolidone (PVP). Even though binders enhance the mechanical integrity of the electrode they add non-used mass and resistance to the electrodes, therefore their use should be minimized. Conductivity enhancers are used in many fabrication techniques as well, to counteract the insulating effect of the binder, to improve the overall conductivity of the electrode, and to enhance the contact between the active material and current collector and between individual active material particles. The most common conductivity enhancer is carbon black, which includes mesoporous carbon black and acetylene black. Carbon whiskers, carbon fibers, CNTs, graphite, metallic fibers and particles have been also employed.[118]

Substrates/current collector. While some techniques are useful for the production of free-standing electrodes, other methods allow the direct deposition of the material on a substrate. Normally, substrates are metal foils, foams, or grids made of stainless steel (SS), nickel, copper, aluminum, titanium or fluorine/indium doped tin oxides (FTO/ITO); flexible substrates (carbon cloth, cotton, polyester, and PET), or films made of carbon materials, such as CNTs, rGO, or graphene. The selection of substrate is dictated by multiple parameters, such as its conductivity, availability, price, thermal and chemical stability, interaction with active material, and mechanical properties.

Processing solvents and surfactants. The majority of processing techniques require the use of solvents to form solutions, suspension, or slurries of the active materials and additives. Water is clearly preferred over organic solvents because of its availability and non-toxicity, but it is limited for techniques that involve electricity, due to its low electrolysis potential. Organic solvents are used when it is the medium that provides stable dispersion of particles, and due to their relatively high density and good chemical stability. Their disadvantages are toxicity, cost, and flammability. For some materials, surfactants are needed to prepare stable suspensions for further processing. Common surfactants used are: sodium dodecylbenzenesulfonate (SDBS), cetyltrimethylammonium bromide (CTAB), and sodium dodecyl sulfate (SDS).[119-121]

Active material. The properties of each of the most common categories of electrode materials (CMs, MOs, CPs) were discussed in detail in the supercapacitor electrode materials section, however, the main features of the materials that influence the capacitance include the specific surface area, porosity, wettability and

pseudocapacitance.[122] The stability of the electrodes is primarily related to the type of material and it's interaction with the electrolyte components rather than the electrode fabrication method, where CMs are the most stable with slight degradation after multiple thousands of cycles, followed by MOs and CPs, which degrade faster due to their pseudocapacitive mechanism and volume changes during doping and de-doping.

1.5.1 Wet coating methods

This section encompasses the methods used to cover the current collector's surface with pre-synthesized solution-processed active material through a variety of coating methods. These methods are simple, cost effective, and industrial equipment has been developed for other coating applications.[114] Some challenges of these methods include contact resistance at the CC/active material interface, which is affected by the nature and quality of the adhesion and the presence of non-conductive binder.

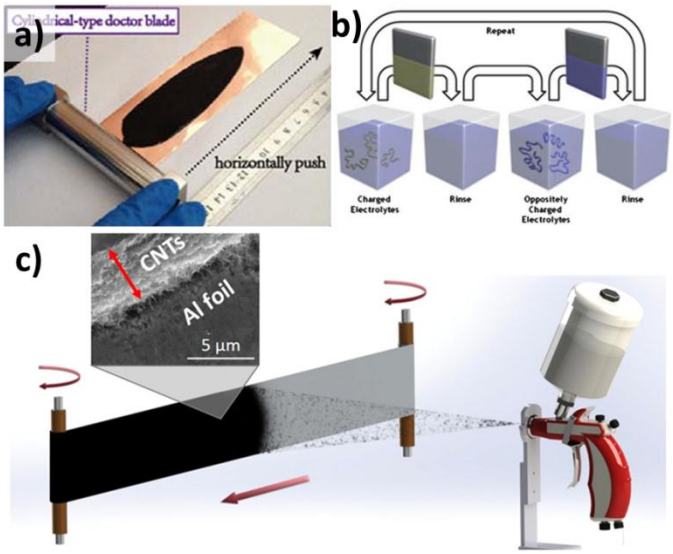

Figure 1.10. Wet coating methods: a) doctor blade coating technique, b) multilayer film deposition based on the dipping method, c) spray coating. Reproduced from references 123, 124, and 125 with permission from John Wiley and Sons, the Centre National de la Recherche Scientifique (CNRS) and The Royal Society of Chemistry, and AIP Publishing LLC.

Doctor blade coating. This technique utilizes a blade or a cylinder to distribute the active material, in the form of a slurry, throughout a substrate (**Figure 1.10a**). For lab-scale coating, the material is spread by manually or automatically sliding the blade over the substrate, and for large-scale R2R processes the blade is fixed over the moving substrate. Homogeneous slurries have been prepared with MOs,[126, 127] CPs,[128] and CMs[129] for SC electrodes. For the slurry preparation, binders, active materials and conductivity enhancers are dissolved in a solvent (organic or aqueous) using sonication to homogenize the mixture. The coating process should be carried out in a low-moisture environment, and the drying process should be slow, avoiding high temperatures to prevent cracking due to fast evaporation of the solvent. After drying, the films can be roll pressed to enhance particulate contact and adhesion to the current collector.[128, 130] The thickness (tens to hundreds of μm)[127] and uniformity of the films depend on the kind of material, distance between the blade and the substrate, and the volume and viscosity of the slurry, where low viscosities are required for efficient and repeatable coatings. The doctor blade technique prevails in electrode preparation as it is simple, cost-effective and versatile. It allows the fabrication of large area uniform porous films on rigid or flexible substrates at room temperature, with minimal ink waste.[123, 127, 131] This technique has shown some shortcomings, such as large internal resistance caused by poor adhesion to current collector and large film thicknesses.[132] Occasionally, multiple layers are needed to achieve sufficient conductivity and capacitance, and each layer must be allowed to dry to avoid delamination. It is still difficult to obtain crack-free, consistent quality films with even thickness throughout the substrate.[133]

Immersion/dip coating. In this method, the substrate is immersed in a coating solution at a constant speed, while the active material adsorbs onto the substrate due to cohesive, van der Waals or chemical attractive forces (**Figure 1.10b**). After a determined time in solution, the substrate, along with a thin layer deposited on its surface, is removed. Repetition of dipping cycles makes uniform and well-adherent coatings. Excess liquid drains from the surface and the solvent is allowed to evaporate at the air-liquid interface leaving a thin coat of active material.[37, 134] The thickness and density of the coating are determined by the withdrawal speed, solution concentration, duration of soaking and area exposed to the solution. Dip-coating pre-synthesized CMs, CPs, MOs and their composites has been used to prepare SC electrodes. CPs and MOs have also been deposited by submerging the substrate in monomer or metal oxide precursor solution and allowing the material to synthesize on the surface. This technique has been used to prepare flexible electrodes by coating fabric substrates (i.e. cotton and polyester), in which the solvent absorbability and retention play an important role, and are closely related to the fabric structure and thickness.[135] Dip coating is a simple process, in which binder and surfactant are optional;[37, 136] it can be conducted in ambient air and at room temperature, suggesting its potential for widespread commercial use. Automated continuous immersion systems have been developed to fabricate reproducible thin films,[137] although some shortcomings include long coating times, low throughput, low material loading on the substrate, and uneven liquid uptake in fabric substrates, resulting in non-uniform coatings.[135]

Spray/aerosol coating. Spray coating is a technique where a device continuously propels small drops of an active material suspension (aqueous or organic) out of a nozzle at a high speed through air onto a surface (**Figure 1.10c**). Common types of atomizers used to atomize and direct the liquid particles, at a constant distance from a substrate moving at a constant speed, are air blast, ultrasonic and electrostatic. The deposition on a heated substrate causes the solvent to evaporate and results in a homogeneous distribution of active material over a large area substrate. This technique produces well-adhered, highly porous films directly on CCs.[122] Common variations of the regular spray coating method for the fabrication of SC electrodes include spray pyrolysis and electrospray.[138, 139] In spray pyrolysis the sprayed precursor droplets thermally decompose on the heated substrate to form the desired chemical compound. Usually, the precursor is selected such that the compound decomposes to the desired material (e.g. $RuCl_3$ for RuO_2) at a high temperature during deposition or post-deposition calcination, and the remaining products are volatile. Some issues of spray pyrolysis is that hazardous fumes can be generated, high temperatures are needed (200 – 600 ˚C), and as the substrate temperature increases, the crystallinity of films is affected and the amount deposited decreases. In electrospray deposition (ESD) the solution is aerosolized at the nozzle by applying a high electric potential (in the kV range) through an emitter (usually a glass or metallic capillary) between the nozzle and the heated substrate.[140] After the formation of small and highly charged liquid droplets, they are attracted to the heated substrate by electrostatic forces, and upon solvent evaporation a solid film is formed. The morphology and thickness (from tens of nm to mm) of the deposited film can be controlled by adjusting deposition

parameters such as flow rate, deposition time, applied potential, substrate temperature, and solution composition. Electrodes of CMs (rGO, CNTs, nanospheres), CPs, MOs and its composites[114, 140] have been fabricated with this relatively quick technique yielding uniform films without significant agglomeration.[141] These electrodes have also shown excellent capacitive behavior, cycling performance as well as mechanical flexibility and durability, partially due to the good adhesion to the CC, even in the absence of binder.[142, 143] The spray deposition technique has been widely studied in the surface coating industry and provides significant potential for scalable processing of SC materials, because large area substrates can be continuously coated at low cost, with excellent uniformity and reproducibility.[140, 144] This method is high throughput, it can be integrated in R2R processes, and it is carried out at ambient pressure in open air and can be done at ambient temperature.[114, 138] It is a simple thin-film preparation method that does not require high-quality substrates, expensive equipment, chemicals, complicated formulation of suspensions, expensive substrates, vacuum apparatus and exotic gases, or extra assembly steps. There is no need for conductivity enhancers or binders.

1.5.2 Printing methods

Printing is a well-developed industrial technique to reproduce text, images or patterns based on an original master form or template, from which the electronics and energy storage field can take advantage.[145] It can be done on many surfaces such as paper, plastics, metals, cloth and composite materials. Recently there has been a noteworthy rise in the development of printable functional materials. Most printing inks have been developed considerably and the growing field of nanotechnology has brought

opportunities for further advancements. Additionally, computers and automated machinery are capable of fast and precise printing at low costs. Now techniques exist for printing nanoparticle dispersions, conductive polymers, and nanostructured carbons for applications in displays, biological tissue scaffolds, and energy storage devices, especially on flexible substrates.[146] Printing techniques are attractive mainly for microsupercapacitor manufacture since the electrodes can be patterned with high resolution (μm to nm). Printing has been applied mostly to CMs, since with the proper solvent, surfactant, or stabilizer chemistry they can be dispersed to produce inks compatible with diverse printing methods.[147, 148]

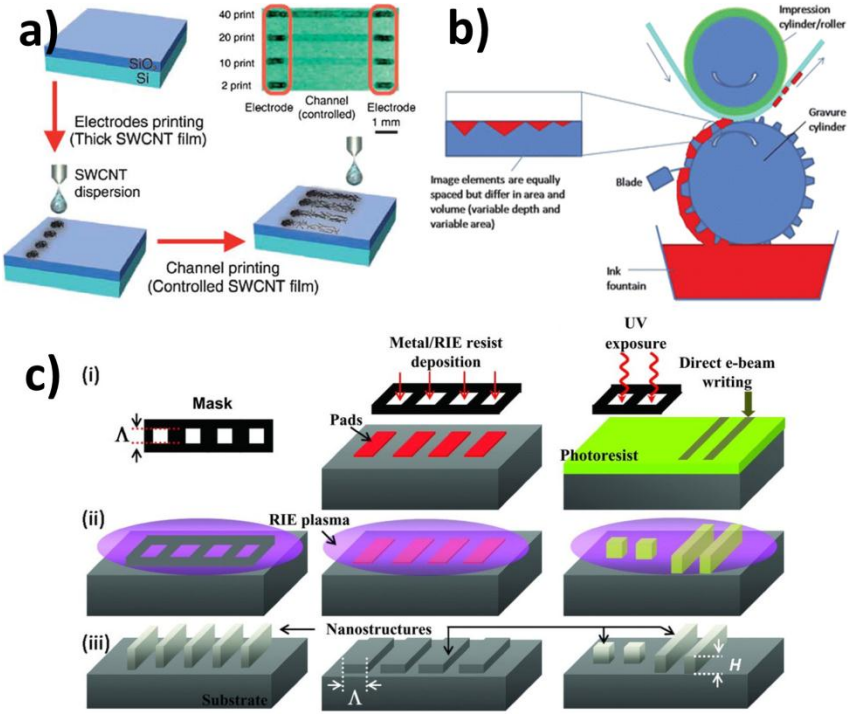

Figure 1.11. Printing methods: a) ink-jet printing of active material, b) gravure, c) lithography. Reproduced from references 149, 148, and 150 with permission from John Wiley and Sons, the Centre National de la Recherche Scientifique (CNRS) and The Royal Society of Chemistry, and Taylor & Francis.

Inkjet printing. Inkjet printing is the most common printing technique overall. In the field of SCs, inkjet printing has been successfully applied to fabricating SC and microsupercapacitor electrodes due to its high resolution (lines as thin as 20 μm).[146] CNTs [37, 151] and graphene and graphene oxide[152-154] are the most reported ink-jet printed materials, particularly for flexible devices, but CPs (PEDOT, PANI)[155, 156] have also been studied. Inkjet printing is based on digitally controlled generation and ejection of drops out of a series of nozzles (with diameters on the order of tens of microns) mounted on a printhead (**Figure 1.11a**). The three main stages of inkjet printing are: droplet ejection, droplet spreading, and droplet solidification. The printhead first moves to the desired position, where droplets are ejected through the nozzles and travel to the substrate. Upon impact, they spread along the surface and join with other droplets forming a thin film of liquid ink. Finally, the solvent evaporates, leaving the solid contents of the ink remaining on the substrate. Inkjet printing is realized by two modes of operation: continuous (CIJ) and drop-on-demand (DOD) printing. Today, the majority of inkjet printers are based on the DOD technology, which is also the standard choice for printing functional materials, because the nozzles eject material only when required, reducing waste and eliminating the need to recycle ink, which may result in ink degradation.[145]

Droplet ejection is dependent on the viscosity, surface tension, and density of the ink, the shape and size of the nozzle, and the ejection velocity of the droplet. Inkjet ink is a multi-component system that contains the active material in a liquid vehicle (aqueous or organic) and numerous additives, such as rheology and surface tension modifiers, humectants, binders, defoamers, surfactants, thickeners, and other stabilizers, that allow

to control the ink's physical properties. Since inks should provide good electrochemical properties, the active material content needs to be maximized and the non-conductive additives minimized. The inks should demonstrate good printability, good wettability, adhesion to specific substrates, and the printed film must show high resolution and stability to bending. Since agglomeration of solids can clog the printer nozzle, a rule of thumb states that the solids in the ink should be less than one-fiftieth the size of the printhead nozzles.[37] It is possible to tune the capacitance of printed electrodes by controlling the density and thickness of the film, which is related to the number of droplets and layers printed onto the substrate. Electrical resistivity can be significantly decreased by removing the additives and residual solvent through post-deposition thermal annealing (>300 °C), which is not compatible with certain substrates. Inkjet printing is cost effective and very suitable for manufacturing large area electronics by R2R printing, leading to simplified and large-scale manufacturing of carbon nanomaterials for SC electrodes.[37, 145, 146, 154] An important obstacle that needs to be overcome is the formulation of stable, uniform and effective inks with suitable properties.[145] Currently, the active material concentration in the inks is very low (e.g. 0.002–0.1 wt% for graphene and 0.1–1.0 wt% for graphene oxide) because of low viscosity requirements.[154, 157] For this reason, multiple layers are usually required (e.g. 190 layers[158]) and in some cases attempting thicker electrodes resulted in film delamination, indicating the need for a binder for thicker electrodes.[154] One of the major challenges of developing inks for inkjet printing is the ink gelation around the nozzles when the printer is not in use, which affects the printing process.[159]

Gravure printing. Gravure printing is a R2R method used traditionally for printing newspapers, magazines and packages. In the common gravure offset printing, ink is first doctored in the gravure grooves, then a silicone polymer blanket rubber roller or pad picks up the ink from the gravure grooves by rotating over the gravure or by pressing on it, respectively. Then the roller (or pad) with the ink on it transfers the ink to the substrate with a similar movement (**Figure 1.11b**).[160] As for inkjet, gravure for printing electrodes is strongly dependent on the rheology and composition of inks, which should be cured with minimum influences on the substrates to provide practical printing speed. Because of the lack of functional printing inks and the relative large line widths (minimum width: ~ tens of microns), this method is not commonly used in manufacturing of organic electronics. Nevertheless, the use of this simple method is attractive due to its high throughput, optimal control of feature size, ability to use very wide range of potential inks, and its compatibility with numerous substrates.[161] It has been used to print microsupercapacitors with inks made of CP, MO, and CM-based nanomaterials, especially on flexible substrates.[160] This printing technique yields porous structures leading to more effective utilization of the active material. On the downside, even though the speed of the general gravure offset printing step itself is fast, the overall manufacturing process time is limited by the post-printing thermal annealing (30-60 min) at high temperatures (100-350 ˚C).

Micro and nanolithography. Microlithography or photolithography is a microfabrication technique used in the microelectronics industry to make integrated circuits and microelectromechanical systems (**Figure 1.11c**).[162] Lithography is a versatile

and easy-to-implement process for producing well-aligned nanostructure arrays in various designed patterns on solid substrates, with micro or nanostructured designs, in particular nanowires.[138, 150, 162, 163] It is a rapid and effective method compatible with a large variety of materials. Broadly, micro and nanolithography can be divided into two sub-groups, one involving the conventional use of a mask (e.g. photolithography), and the other without a direct use of it (e.g. e-beam lithography, nanoimprint lithography).[150]

Photolithography is a radiation-based micropatterning process that involves pattern transference from a photomask onto a substrate surface followed by plasma or wet etching, and optional deposition. Photolithography is highly reliable for minimizing the footprint while maximizing the integration per substrate at a large scale, although it is mainly limited to 2D systems. The development of nanostructures requires the use of very short wavelength photons to circumvent the diffraction limit and reach a resolution in the sub-20 nm range. The use and the cost of complex optical systems and complicated particle sources such as extreme UV limit strongly its development. Factors affecting the dimensions of the nanomaterials formed by photolithography include mask dimensions and etching time. Instead of an external pre-fabricated mask, such as AAO or polystyrene beads, there are methods that use masks randomly generated in a chemical reaction.

Other lithographic techniques include electron-beam lithography, focused-ion-beam lithography, dip-pen nanolithography and nanoimprint lithography. In **e-beam lithography**, no mask is used and the electron beam can expose precise 20–40 nm wide lines on substrates.[150] **Nanoimprint** lithography is used for nano patterning because of its relatively inexpensive scale-up possibilities and deliverable pattern size challenging the

limits of e-beam lithography.[164] In nanoimprint lithography, a stamp replicated from a relief-structured master, can be used to transfer its pattern on a resist coated substrate followed by etching and subsequent metal deposition. Challenges remain such as proper choice and adhesion of the resist on various substrates, avoiding the collapse of high aspect ratio molds, and retaining lifetime of the molds. Patterns with sizes less than 10 nm could be obtained. Nano wires (NWs) of different materials (i.e. SnO/ZnO branch), nano-brushes, and nano-comb-like structures can be generated. Hierarchical structures can also be grown based on intrinsic crystalline defects.[165] Lithography is an appropriate technique when control on the nanostructure dimension and/or growth sites is necessary, but the high cost and low throughput for large-scale production are still challenges. Nanoimprint lithography based on contact has some drawbacks such as defect density, mask damage, and throughput for step-and-repeat. Research on nanoimprint lithography is recent and many alternative approaches for the fabrication of micropower sources are under development.[166] Due to the high degree of compatibility with integrated circuit technologies, the lithographic techniques are expected to become very important for the future development of on-chip energy storage. In summary, nanostructures can be grown with unprecedented precision in the control of length diameter and composition but it is expensive.[37]

1.5.3 Electro-chemical methods

The electro-chemical methods comprise all processing and direct synthesis techniques involving the use of direct electricity to chemically or physically deposit electroactive materials on a substrate. The benefits of the electrodeposition methods

include short processing times, low capital investment costs, precise control on parameters such as film thickness, deposition rate, high microstructural homogeneity and uniformity.[167] Some disadvantages are that some processes involve toxic and corrosive solvents and high voltages.

Anodization is used to produce nanostructured MO SC electrodes. It is carried out in a 3-electrode set up, where the anode is the substrate of interest and hydrogen evolution occurs at the cathode surface.[168, 169] The creation of metal oxides proceeds by oxidizing the metallic anode surface (precursor), which releases metal ions to the electrolyte and electrons to the external circuit. An oxide layer is formed on the metal surface from the chemical interaction of the released metallic ions and O^{2-} or OH^{-} ions from water electrolysis.

Electrophoretic deposition. Electrophoretic deposition (EPD) is the most basic form of electrochemical deposition method, in which charged particles in suspension move toward an electrode of opposite charge due to the influence of a spatially uniform electric field and then deposit to form a compact film (**Figure 1.12a**).[167, 170] It produces mechanically robust coatings, as well as functional nanostructured films. EPD is a versatile technique that can be applied to any powdered solid that forms a stable suspension in aqueous or organic (alcohols, ketones) medium, on a wide variety of substrates; it operates successfully with a wide range of particle sizes, from micro- to nanometer particles (colloidal suspensions), therefore interest in EPD is increasing to create advanced nanostructured coatings and nanoscale films with enhanced properties. Electrophoretic deposition has been a useful technique to deposit CMs (graphene, GO,

CNTs), MOs (NiO) and CPs on conductive substrates. EPD was proven to be a technique suitable for the production of graphene films with better packing and alignment compared to spray coating techniques, while avoiding the addition of crosslinking molecules or binders. The films provide good electrical contact, a high concentration of electroactive sites, as well as shorter transport and diffusion path lengths leading to high specific capacitances. Significantly, EPD offers the possibility of scaling up, although shortcomings such as the use of organic solvents and high voltages (~150 V) need to be considered.

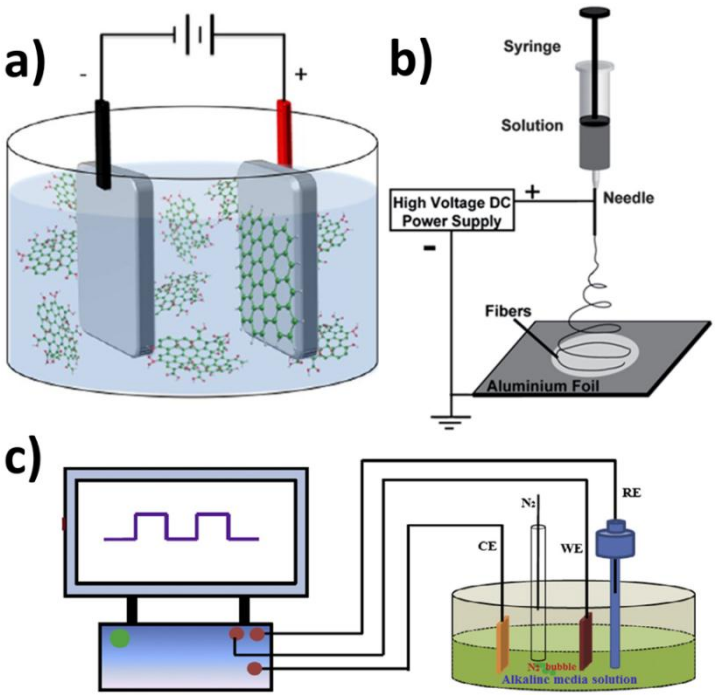

Figure 1.12. Electro-chemical methods: a) electrophoresis, b) electrospinning, c) electrochemical synthesis. Reproduced from references 170, 171, and 172 with permission from the American Chemical Society, the Centre National de la Recherche Scientifique (CNRS) and The Royal Society of Chemistry, and Elsevier.

Electrospinning. Electrospinning is an established technique for generating micro/nanofibers, in which the extrusion force is generated by the interaction between a charged polymer or MO solution and an external applied electric field.[171, 173, 174] A typical electrospinning setup is composed of a high voltage DC (or AC) power supply, a capillary (including a solution container and a spinneret) and a grounded metal collector (**Figure 12b**).[175] One electrode of the high voltage power supply (typically kV) is connected to the spinneret containing the solution and the other electrode is attached to the collector. Both are electrically conducting and separated an optimum distance. During electrospinning, the precursor solution is extruded from the spinneret to form a small droplet in the presence of an electric field. The interactions of the electrical charges in the fluid with the external electric field causes the pendant droplet to deform into a conical structure called the Taylor cone and a critical voltage is attained. When the applied voltage surpasses the critical voltage, the repulsive force of the charged polymer overcomes the surface tension of the solution and a fine charged jet is ejected from the tip of the Taylor cone. As the charged jet accelerates towards regions of lower potential, the solvent evaporates, and the resulting increase in the electrostatic repulsion of the charged particles causes the fibers to undergo a whipping motion and elongate until they are deposited onto a collector, resulting in the formation of fine fibers. If the applied voltage is not high enough, the jet will break up into droplets, a phenomenon called Rayleigh instability.

Almost any soluble polymer can be electrospun if its molecular weight is high enough. MOs (RuO_2, TiO_2, $LiCoO_2$), CPs (PEDOT, PANI) have been electrospun

directly on flexible substrates from their molecular precursors (e.g. monomers), and occasionally conductivity enhancers are added to the precursor to improve the electrical or mechanical properties.[171, 174, 175] Due to the limitations in molecular weight and unsuitable solubility for electrospinning, only a few conductive polymer solutions with appropriate viscosity have been directly electrospun, including polyaniline doped with sulfuric acid, camphorsulfonic acid, and polypyrrole doped with dodecylbenzene sulfonic acid. The addition of electrospinnable polymers may assist the formation of conducting polymer fibers, but the conductivity of the as-spun fibers decreases. The morphology and diameters of the electrospun fibers depend on parameters such as polymer type and molecular weight, conformation of the polymer chain, elasticity, applied voltage, solution feed rate and spinning distance; environmental parameters (e.g. temperature, humidity and air velocity in the chamber) and solution properties (e.g. conductivity, viscosity/concentration, polarity and surface tension).[174] Electrospinning may be highly beneficial to the supercapacitor field due to its ability to fabricate micro/nanofibers with large interconnected voids which create highly porous structures.[171] Nevertheless, the random orientation of fibrous mats fabricated by conventional electrospinning may limit the electrospun fibers applications that require direct, fast charge transfer or regular, uniform structures. Electrospinning does not require binder or conductivity enhancers; it is compatible with many substrates, and scalable.[173] It is a promising technique due to its comparative low cost and relatively high production rates. Nonetheless, it is difficult to achieve uniformity in the diameters of electrospun nanofibers below 50 nm. In addition, it is still a challenge to reach an adequate conductivity in highly flexible polymeric fibers,

and sufficient flexibility and mechanical stability in inorganic nanofibers that show excellent electrical properties. Finally, current electrospinning processes commonly involve toxic and corrosive organic solvents in the preparation of precursor solutions.

Electrochemical synthesis/deposition. Electrodeposition is a process that uses electrical current to induce the polymerization or deposition of a material in solution onto a substrate.[138] Electrodeposition is used to fabricate nanoporous and microporous films of CPs, MOs (nanorods, honeycombs, microspheres, nanosheets),[146, 176, 177] and graphene oxide has been also electrochemically reduced to fabricate 3D graphene networks by electrolyzing GO aqueous suspensions on metal electrodes at an applied potential.[152, 178] This method involves the use of an electrolyte in solution (aqueous or organic) containing the monomer or precursor, and a two-electrode or three-electrode electrochemical system composed of working (substrate), reference, and counter electrodes (**Figure 1.12c**).[179, 180] SC electrodes are prepared by depositing or electropolymerizing the electroactive material directly on the current collector, where the difference in potential causes the precursor to decompose or the monomer to oxidize and deposit on the substrate. Electrodeposition methods include: galvanostatic, potentiostatic, cyclic voltammetric, and pulse galvanostatic methods. Parameters that affect the morphology, size, conductivity and other properties of the electrodeposited material include the type of the electrolyte and its composition, electrodeposition technique, applied current density, potential, deposition time, and electrode separation. A variety of morphologies can be obtained and properties can be tailored by knowing how to select solution and electrical conditions.[138, 172] The primary advantage of electrodeposition as a processing technique is low internal

resistance because the active material is closely bound to the substrate, which also favoring the integrity of the electrode. Other advantages include short reaction time, operational simplicity and the absence of oxidant and binders, low-temperature operation process, and viability of commercial production. On the downside, CPs obtained by electropolymerization are more likely to form thin films and irregular structures.[176]

1.5.4 Non-electrolytic reactive deposition

These processing methods include direct chemical synthesis of the active material on the CC, simplifying the process as the synthesis and deposition occur simultaneously. One disadvantage of these methods is that the product might have low purity and purification steps might be needed.

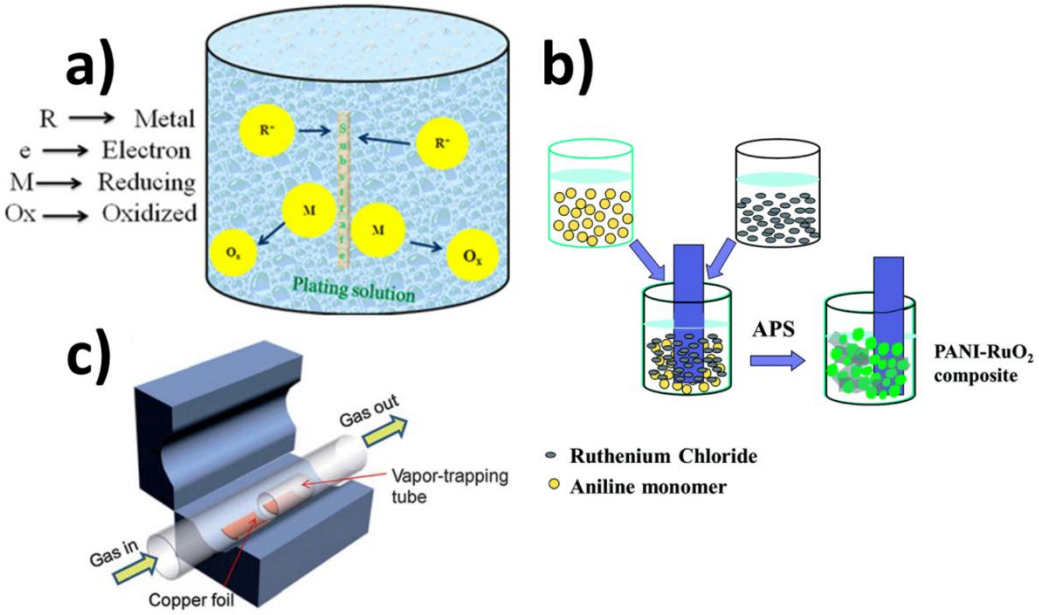

Figure 1.13. Non-electrolytic reactive deposition techniques: a) electroless plating, b) chemical bath deposition, c) chemical vapor deposition. Reproduced from references 138, 181, and 182 with permission from Elsevier, the Centre National de la Recherche Scientifique (CNRS) and The Royal Society of Chemistry, and the American Chemical Society.

Electroless plating. Electroless plating (EP) is an autocatalytic non-galvanic plating process where a metallic layer is deposited onto a surface using a chemical deposition process instead of an external electrical current.[183] When the substrate is dipped in an electroless solution, it develops a potential that causes ions to be attracted towards the substrate surface (**Figure 1.13a**). Normally, the EP bath is composed of metallic ions, which are the source of the metal to be deposited, a reducing agent that works as the electron source, a complexing agent to increase the metallic ion solubility and avoid hydroxide precipitation, a stabilizer and buffer to enhance the bath and pH stability, respectively, and a surfactant to increase the wettability of the surfaces.[183] EP is a well-established low-cost, non-hazardous chemical process and leads to better utilization of the metal deposited as compared to sputtering.[183] Because EP allows a constant metal ion concentration to bathe all parts of the substrate, it deposits metal evenly on irregularly shaped objects and through holes, which are difficult to plate evenly with electroplating. Other important advantages include its ability to selectively deposit thin metal films only on catalyzed areas of the substrate, easy control of the coating thickness, and independence on the electrical properties of the substrate. EP is also a low cost, highly reproducible and simple process that requires simple equipment. The main difficulty of this process is preventing spontaneous metal deposition with solution decomposition (loss of bath stability) and the deposits obtained by EP can have lower porosity than with other methods.

Chemical bath deposition. Chemical bath deposition (CBD) is used to deposit metal oxides directly on a substrate that is immersed in a solution containing the

precursors dissolved either in ionic or molecular form. The solid phase formation involves two steps, nucleation and particle growth (**Figure 1.13b**).[184] When the bath attains a determined temperature and the precursor solution becomes saturated, the ionic product starts to exceed the solubility product and positively charged and highly anisotropic nuclei are produced on both the substrate and in solution. Such nuclei assemble together to form nanostructures and precipitation occurs via heterogeneous growth on the substrate.[184, 185] Generally, metal ions are complexed in such a way that reactions take place between slowly released metal ions to form product in powder or thin film form.[167] Film thickness and growth strongly depend on the solution pH, temperature, precursor concentration, and topographical and chemical nature of the substrate.[184, 185] In the surfactant mediated CBD method, the surfactants do not directly take part in the reaction, but act as structure directing agents. After deposition, the films need to be annealed at temperatures such that the surfactants are removed.[167, 184, 186] CBD is a non-hazardous process that has various advantages such as large deposition area, reproducibility, and low cost of equipment.[134] It is a simple method to obtain a conducting additive-free and binderless electrode with high utilization of the active material. Any insoluble surface to which the solution has a free access will be a suitable substrate for the deposition. Other advantages of this method include easily controllable reaction conditions, and high yield in terms of the quantity of desired products. One of the drawbacks is the wastage of solution after every deposition.

Chemical vapor deposition. Chemical vapor deposition (CVD) is a process in which a substrate is exposed to one or more volatile precursors that react and/or

decompose on the substrate surface to produce a thin film or powder (**Figure 1.13c**).[167] Catalysts play an essential role in the properties of the deposited material, as well as substrate temperature and type, chamber pressure, molecule surface-diffusion rate, precursor type and concentrations of metal and oxygen vapors.[162] The CVD techniques include atmospheric-pressure, hot-filament, thermal-active, metal-organic, microwave-plasma, plasma-enhanced, low-temperature, and photo-assisted types.[167, 187] In the context of supercapacitor devices, the CVD process has become one of the most promising techniques to synthesize carbon materials, including CNTs, graphene and nanofibers. Carbon film deposition by the CVD process generally employs precursor molecules such as acetylene, ethylene, carbon monoxide, and methane. CVD is useful to grow highly pure and controlled number of layers of graphene sheets with low oxygen to carbon (O/C) ratio that is necessary for a better performance.[188-190] Recently, we[191] reported the continuous production on vertically aligned CNT directly on aluminum foil, which was possible due to the lower deposition temperature of 600 °C. Plasma-enhanced and hot-filament CVD are common for nanostructured metal oxides production.[138, 162] For the commercial CVD production of electrodes, an important problem to target is the high deposition temperatures, which increase cost and in some cases affect the morphology of the nanostructures and promote thin film growth.[162, 187] Other issues of CVD include precursor volatility at near room-temperature, slow deposition rates, low purity of product, and difficulty in depositing multicomponent materials (mixed metal-oxides) using multisource precursors because different precursors have different vaporization rates.

Sputtering. Sputtering is a process whereby atoms are ejected from a solid target material due to bombardment by a highly focused beam of inert gas (**Figure 1.14**).[138] Sputtered atoms ejected into the gas phase are not in their thermodynamic equilibrium state, and tend to deposit on all surfaces in the vacuum chamber. Before each sputter process the chamber is pumped down to a low pressure and the targets can be pre-sputtered to remove any contamination on surface.[138, 192] For SC materials, magnetron, radio frequency and reactive sputtering are prevalent. Magnetron sputtering is a physical vapor deposition method where the ions bombarding the target are primarily generated by the ionization of a working gas. In reactive sputtering a target of one chemical composition is bombarded by gas ions that react with the target to form a coating of a different chemical composition (e.g. SiO_2). The texture, surface morphology and uniformity of the deposits can be controlled by adjusting substrate temperature, sputtering time, power, and using different gases.[192] See-Hee et al.[193] deposited NiOx films and found that the less oxygen present in the sputtering chamber, the lower the hole concentration and hence the larger the specific capacitance. Graphene layers were synthesized by RF magnetron sputtering in a vacuum deposition system using a pure carbon target.[194] Liu et al.[195] found that with increasing sputtering temperature the specific capacitances of IrO2 thin-film electrodes gradually decrease, and crystallinity increases. The advantages of this method are solvent free synthesis, superior quality of the coated materials and the deposited film thicknesses can be tailored.[192] Since the synthesis method makes use of processes compatible with electronic device fabrication, it

can be implemented in manufacturing supercapacitors integrated with silicon chips. Nonetheless, sputtering cannot be yet applied on a large scale and is expensive.[183]

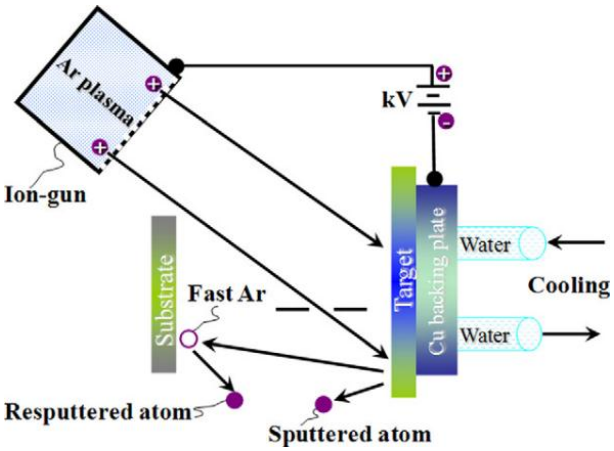

Figure 1.14. Sputtering process schematic. Reproduced from reference 138 with permission from Elsevier.

Evaporation-condensation technique. The inert gas evaporation–condensation (IGC) technique is used to produce nanoparticles via the evaporation of a metallic source in an inert gas. It is one of the most widely used methods for thin film deposition.[138] It is a physical vapor deposition method that decomposes the source materials, offering facile control of microstructure and morphology.[138] In its basic form, the method consists of evaporating a pure metallic source, using heating inside a chamber which has been previously evacuated to about 10^{-6} to 10^{-7} torr and backfilled with inert gas to a low pressure (~10^{-4} torr).[196] The metal vapor migrates from the hot source into the cooler inert gas by a combination of convective flow and diffusion. Ultimately, the particles undergo a homogeneous condensation to form atom clusters in the vicinity of a rotating cold surface. To prevent further aggregation, the formed clusters are removed from the region of deposition. This technique is mainly used for the synthesis of single-phase metals and

ceramic oxides. For applications in supercapacitors, the deposited metal films are then converted to metal oxides by oxidative annealing or electrochemical oxidation. A large amount of granular voids exist in these kinds of films, which is beneficial for cation storage and release and electrolyte penetration.

1.5.5 Other methods

Laser treatment. Laser printing technology has enabled the production of on-chip micro-supercapacitors in both an interdigitated planar form as well as conventional sandwich SC designs.[146] The most reported use of laser technologies for SC applications is to reduce graphene (or graphite) oxide.[146, 197] Gao et al.[198] fabricated an all-carbon, monolithic SC device using a CO_2 laser printer to induce the reduction followed by the patterning of self-standing graphite oxide films (**Figure 1.15a**). Several groups used a standard LightScribe DVD optical drive to reduce graphene oxide films, creating mechanically robust graphene with open networks and showed that the laser can change the initially stacked GO sheets into well-exfoliated rGO sheets, preventing restacking.[152, 187, 199, 200] However, the major shortage for laser-induced reduction is the poor frequency response, and downsizing of the necessary components remains a challenge.[146] Peng et al.[201] and In et al.[202] showed a method to rapidly produce laser-induced graphene for microsupercapacitors using laser induction of commercial polyimide sheets in ambient conditions that can be directly used as electrodes.

Laser treatment has been also used to grow MOs directly on substrates through pulsed laser deposition (PLD). In this technique a high-power laser beam is focused inside a vacuum chamber onto a metal target which produces a plasma plume consisting

of energetic species (such as neutral atoms, molecules, electrons, and ions) that react with an oxidizing agent. The ablated species experience multiple collisions with the oxidizing agent in the deposition chamber to generate metal oxide molecules in the expanding ablation beam that deposit on the substrate.[203] The advantages of PLD include stoichiometric transfer, growth from an energetic beam, reactive deposition, and inherent simplicity for the growth of multilayered structures.[204] The ultrathin feature can shorten the ion diffusion pathway, ensuring fast redox reactions, and good contact and adhesion to the CC eliminates the need for binder.

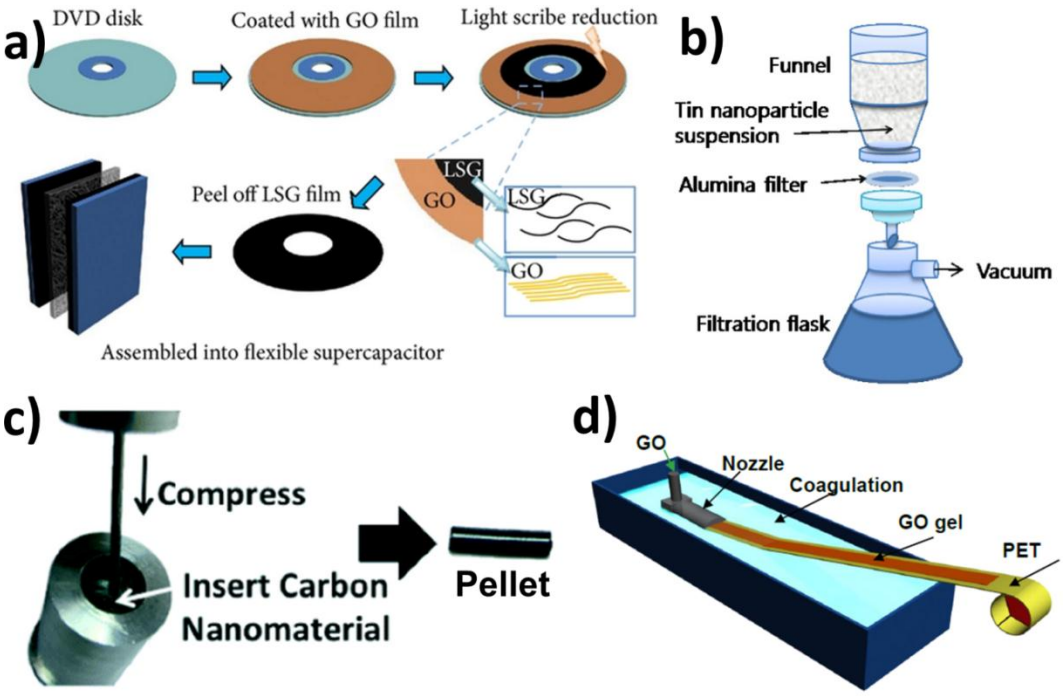

Figure 1.15. Other methods: a) laser treatment, b) filtration, c) pellet pressing, d) wet spinning. Reproduced from references 199, 132, 205, and 206 with permission from The American Association for the Advancement of Science, IOP Publishing, and the Centre National de la Recherche Scientifique (CNRS) and The Royal Society of Chemistry.

Filtration method. The filtration method is a simple and cost-effective way of creating free-standing electrodes. It consists on preparing a suspension of pre-synthesized materials by sonication and filtering through a membrane (**Figure 1.15b**). During filtration, the particles are stopped by the membrane and form a layered film on the membrane surface. The obtained cake is dried and peeled off the membrane, giving a free-standing electrode.[132, 207, 208] CNT, graphene, and conducting polymer films have been prepared with this method. Zhang et al.[207] produced SC electrodes by filtering a graphene-PVDF suspension through nickel foam, which worked as current collector. The filtration technology is easily scalable for device fabrication on an industrial scale and a large amount of working media can be incorporated into an electrode yielding larger energy capacities. Free-standing thin films provide a route to simplify the electrode-manufacturing process where conducting additives and binders are not necessary, and this method is also compatible with roll-to-roll thin-film fabrication technologies. The filtration method yields highly porous films and nanocomposites, with tunable components ratio, and the size of the electrodes is limited only by the filtration setup.[126] This method has the advantage of affording a high degree of dispersion of the electrode components. On the other hand, it is a time consuming method, because as the pores get covered by material, the filtration goes slower and it can take several hours. Intensive ultrasonication to form a homogenous mixture and binders is sometimes needed. Still significant internal resistances are observed, especially for thick films, and thin films electrodes show poor mechanical stability.

Punch pellets/press material onto CC. In this method pressure is applied to the pre-synthesized material to prepare self-standing films or pellets, or to attach the material to the current collector (**Figure 1.15c**). The general preparation procedure is as follows: the active material, conductivity enhancer, and binder are grinded and extensively mixed. Optionally the mixture is dissolved in a solvent, which is then evaporated by heating the system. A molder or press is used to press the sample into a pellet and the pellet can be heat-treated to avoid crack formation. Lastly, the pellet can be used as a free-standing electrode or it can be further pressed onto a current collector.[48, 165, 209] This method has been widely used to prepare electrodes of CMs, CPs, MOs and composites; it is simple and does not require complex equipment. Pellets produced with this method are stable, easy to handle, and do not require a supporting substrate. One of the biggest issues is its tendency of materials to irreversibly aggregate, especially when the material is being compressed during the electrode fabrication process, which results in the loss of accessible surface area. Besides, sufficiently thin films are difficult to obtain, and electrochemically inactive additives are often required. A portion of active material could be embedded in binder, making this portion inaccessible to the electrolyte, and impeding the contact between sections of active material.[140] These issues increase the overall electrode resistance which directly affects the power density of the devices.

Wet spinning. This process is used for materials that need to be dissolved in a solvent to be spun. The spinneret is submerged in a chemical bath that causes the fiber to precipitate and then solidify as it emerges (**Figure 1.15d**). Most of wet-spinning studies for SC electrodes have been carried out on graphene, because GO sheets can form liquid

crystals (LCs) with lamellar structures that can be dispersed at high enough concentrations, which makes them suitable for efficient alignment and effective coagulation.[206, 210-212] The continuous injection of liquid crystalline GO dispersions into coagulation baths generates continuous GO fibers. After chemical reduction, GO fibers turn into reduced GFs. With wet spinning fibers can be continuously spun at room temperature to tens of meters long. The orientation of the graphene nanosheets is beneficial for the penetration of the electrolyte, and for the mechanical stability and flexibility of the films.[206] The spinning process is simple, and non-toxic or corrosive although solvents are used. An interweaving yarn supercapacitor was prepared by interweaving polyelectrolyte-wrapped carbon nanomaterial core-sheath fibers (40 cm long) through a coaxial wet-spinning assembly strategy. The fibers were applied directly as contactable electrodes.[213] This approach of continuous wet-spinning represents an industrially viable production process for flexible SC electrodes opening up an avenue towards wearable devices.[210] An issue of spin coating is the waste of material, since only a portion of it is actually applied on the substrate.

1.6 Dissertation outline

To tackle the current issues of supercapacitors mentioned above, various approaches were studied in this doctoral work to make electrodes with carbon nanotubes, conducting polymers and electroactive polymers/dopants, employing chemical vapor deposition, dispersion filtration, and electrochemical polymerization fabrication techniques.

An important improvement towards the commercial production of MWCNT-based electrodes is described in chapter 2. MWCNTs were grown, as vertically aligned forests, directly on aluminum foil in a continuous roll-to-roll CVD system. With this method the need for a binder is eliminated since the catalyst particles are attached to aluminum and the synthesized CNTs grow chemically adhered to the CC. Furthermore, since the ordered structure of the vertically aligned carbon nanotubes is believed to decrease resistance and increase power density, due to reduced ion diffusion path length, the performance of these electrodes was compared with free-standing electrodes made of randomly oriented CNTs. To prove that the performance of the electrodes was not affected by the continuous process, electrodes produced by a stationary CVD process were also studied.

The objective of chapter 3 was to increase the energy density of free-standing CNT electrodes produced by a facile filtration method. It was hypothesized that by combining conducting polymers with carbon nanotubes, electrodes with increased capacitance would be obtained, due to the faradaic nature of the CPs and the efficient electron transport of the CNTs. The contribution and limitations of each material to the composite were analyzed.

An important limitation for the commercial application of conducting polymers is the lack of a conducting polymer that serves as anode. Since most common conjugated polymers are not n-dopable, a conjugated polymer with a quinone moiety redox-active in negative potentials was proposed as material for negative SC electrodes in chapter 4. The

influence of different types of electrolytes, substrates, and deposition techniques on the electrode performance and stability was studied.

Conducting polymers show intermediate charge storage capacities, due to the relatively low attainable doping degrees. The goal of chapter 5 was to increase the charge storage capacity of PPY by incorporating a high-charge capacity molecule, such as p-benzoquinone. It was believed that by entrapping the redox molecule dopant in a polypyrrole network by electropolymerization, this dopant would efficiently store charge along with the CP. The polymerization conditions were tuned and the stability of the electrodes was studied.

Each chapter is based on the following publications with minor revisions:

Chapter 2. Arcila-Velez, M.R., Zhu, J., Childress, A., Karakaya, M., Podila, R., Rao A.M, and Roberts, M.E. "Roll-to-roll synthesis of Vertically-Aligned Carbon Nanotube Electrodes for Electrical Double Layer Capacitors". Nano Energy, 8, 9 (2014)

Chapter 3. Arcila-Velez, M.R., Emmet, R., Karakaya, M., Podila, R., Diaz-Orellana, K.P., Rao A.M. and Roberts, M.E. "A Simple Approach to the Fabrication of Polymer/MWCNT Composite Electrodes". Submitted

Chapter 4. Arcila-Velez, M.R., and Roberts, M.E. "Pseudo-capacitor anodes comprised of electrochemically synthesized aminoanthraquinone redox polymers". Submitted

Chapter 5. Arcila-Velez, M.R., and Roberts, M.E. "Redox solute doped polypyrrole for high-charge capacity polymer electrodes". Chem. Mater., 4, 1601 (2014)

1.7 References

1. Liu, C.; Li, F.; Ma, L.-P.; Cheng, H.-M., Advanced Materials for Energy Storage. *Advanced Materials* **2010,** 22, (8), E28-E62.
2. Speirs, J.; Contestabile, M.; Houari, Y.; Gross, R., The future of lithium availability for electric vehicle batteries. *Renewable and Sustainable Energy Reviews* **2014,** 35, 183-193.
3. Simon, P.; Gogotsi, Y., Materials for electrochemical capacitors. *Nature Materials* **2008,** 7, (11), 845-854.
4. Long, J. W.; Bélanger, D.; Brousse, T.; Sugimoto, W.; Sassin, M. B.; Crosnier, O., Asymmetric electrochemical capacitors—Stretching the limits of aqueous electrolytes. *MRS Bulletin* **2011,** 36, (07), 513-522.
5. Elcap, Voltagram-Engl. In https://en.wikipedia.org/wiki/Pseudocapacitance.
6. Tosaka, Electric double-layer capacitor (Activated carbon electrode - BOX type). In 2008.
7. Pandolfo, A. G.; Hollenkamp, A. F., Carbon properties and their role in supercapacitors. *Journal of Power Sources* **2006,** 157, (1), 11-27.
8. Davies, A.; Yu, A., Material advancements in supercapacitors: From activated carbon to carbon nanotube and graphene. *The Canadian Journal of Chemical Engineering* **2011,** 89, (6), 1342-1357.
9. Pandolfo, T., Ruiz, V., Sivakkumar, S., Nerkar, J., *Supercapacitors: Materials, Systems, and Applications*. First ed.; Wiley-VCH Verlag GmbH & Co.: Weinheim, Germany, 2013.

10. Frackowiak, E.; Béguin, F., Carbon materials for the electrochemical storage of energy in capacitors. *Carbon* **2001,** 39, (6), 937-950.

11. Chen, S.-M.; Ramachandran, R.; Mani, V.; Saraswathi, R., Recent advancements in electrode materials for the high-performance electrochemical supercapacitors: a review. *Int. J. Electrochem. Sci* **2014,** 9, 4072-4085.

12. Simon, P., Taberna, P., Béguin, *Supercapacitors: Materials, Systems, and Applications*. First ed.; Wiley-VCH Verlag GmbH & Co.: Weinheim, Germany, 2013.

13. Harris, P. J. F., New Perspectives on the Structure of Graphitic Carbons. *Critical Reviews in Solid State and Materials Sciences* **2005,** 30, (4), 235-253.

14. Su , D. S.; Schlögl, R., Nanostructured Carbon and Carbon Nanocomposites for Electrochemical Energy Storage Applications. *ChemSusChem* **2010,** 3, (2), 136-168.

15. Cherusseri, J.; Kar, K. K., Hierarchically mesoporous carbon nanopetal based electrodes for flexible supercapacitors with super-long cyclic stability. *Journal of Materials Chemistry A* **2015,** 3, (43), 21586-21598.

16. Le, L. T.; Ervin, M. H.; Qiu, H.; Fuchs, B. E.; Lee, W. Y., Graphene supercapacitor electrodes fabricated by inkjet printing and thermal reduction of graphene oxide. *Electrochemistry Communications* **2011,** 13, (4), 355-358.

17. Zhao, H.; Wang, L.; Jia, D.; Xia, W.; Li, J.; Guo, Z., Coal based activated carbon nanofibers prepared by electrospinning. *Journal of Materials Chemistry A* **2014,** 2, (24), 9338-9344.

18. Al Bahri, M.; Calvo, L.; Gilarranz, M. A.; Rodriguez, J. J., Activated carbon from grape seeds upon chemical activation with phosphoric acid: Application to the adsorption of diuron from water. *Chemical Engineering Journal* **2012,** 203, 348-356.

19. Caturla, F.; Molina-Sabio, M.; Rodríguez-Reinoso, F., Preparation of activated carbon by chemical activation with ZnCl2. *Carbon* **1991,** 29, (7), 999-1007.

20. Sevilla, M.; Mokaya, R., Energy storage applications of activated carbons: supercapacitors and hydrogen storage. *Energy & Environmental Science* **2014,** 7, (4), 1250-1280.

21. Wang, J.; Kaskel, S., KOH activation of carbon-based materials for energy storage. *Journal of Materials Chemistry* **2012,** 22, (45), 23710-23725.

22. Borchardt, L.; Oschatz, M.; Kaskel, S., Tailoring porosity in carbon materials for supercapacitor applications. *Materials Horizons* **2014,** 1, (2), 157-168.

23. Redondo, E.; Carretero-González, J.; Goikolea, E.; Ségalini, J.; Mysyk, R., Effect of pore texture on performance of activated carbon supercapacitor electrodes derived from olive pits. *Electrochimica Acta* **2015,** 160, 178-184.

24. Xu, H.; Gao, B.; Cao, H.; Chen, X.; Yu, L.; Wu, K.; Sun, L.; Peng, X.; Fu, J., Nanoporous Activated Carbon Derived from Rice Husk for High Performance Supercapacitor. *Journal of Nanomaterials* **2014,** 2014, 7.

25. Xu, B.; Chen, Y.; Wei, G.; Cao, G.; Zhang, H.; Yang, Y., Activated carbon with high capacitance prepared by NaOH activation for supercapacitors. *Materials Chemistry and Physics* **2010,** 124, (1), 504-509.

26. Roldán, S.; Villar, I.; Ruíz, V.; Blanco, C.; Granda, M.; Menéndez, R.; Santamaría, R., Comparison between Electrochemical Capacitors Based on NaOH- and KOH-Activated Carbons. *Energy & Fuels* **2010,** 24, (6), 3422-3428.

27. Xu, G.; Zheng, C.; Zhang, Q.; Huang, J.; Zhao, M.; Nie, J.; Wang, X.; Wei, F., Binder-free activated carbon/carbon nanotube paper electrodes for use in supercapacitors. *Nano Research* **2011,** 4, (9), 870-881.

28. Tan, Y. B.; Lee, J.-M., Graphene for supercapacitor applications. *Journal of Materials Chemistry A* **2013,** 1, (47), 14814-14843.

29. Xiang, F.; Zhong, J.; Gu, N.; Mukherjee, R.; Oh, I.-K.; Koratkar, N.; Yang, Z., Far-infrared reduced graphene oxide as high performance electrodes for supercapacitors. *Carbon* **2014,** 75, 201-208.

30. Zhang, L. L.; Zhou, R.; Zhao, X. S., Graphene-based materials as supercapacitor electrodes. *Journal of Materials Chemistry* **2010,** 20, (29), 5983-5992.

31. Yu, A.; Roes, I.; Davies, A.; Chen, Z., Ultrathin, transparent, and flexible graphene films for supercapacitor application. *Applied Physics Letters* **2010,** 96, (25), 253105.

32. Fan, Z.; Zhao, Q.; Li, T.; Yan, J.; Ren, Y.; Feng, J.; Wei, T., Easy synthesis of porous graphene nanosheets and their use in supercapacitors. *Carbon* **2012,** 50, (4), 1699-1703.

33. Cheng, Q.; Tang, J.; Ma, J.; Zhang, H.; Shinya, N.; Qin, L.-C., Graphene and carbon nanotube composite electrodes for supercapacitors with ultra-high energy density. *Physical Chemistry Chemical Physics* **2011,** 13, (39), 17615-17624.

34. Yoo, J. J.; Balakrishnan, K.; Huang, J.; Meunier, V.; Sumpter, B. G.; Srivastava, A.; Conway, M.; Mohana Reddy, A. L.; Yu, J.; Vajtai, R.; Ajayan, P. M., Ultrathin Planar Graphene Supercapacitors. *Nano Letters* **2011,** 11, (4), 1423-1427.

35. Peng, Y.-Y.; Liu, Y.-M.; Chang, J.-K.; Wu, C.-H.; Ger, M.-D.; Pu, N.-W.; Chang, C.-L., A facile approach to produce holey graphene and its application in supercapacitors. *Carbon* **2015,** 81, 347-356.

36. Cheung, C. L.; Kurtz, A.; Park, H.; Lieber, C. M., Diameter-Controlled Synthesis of Carbon Nanotubes. *The Journal of Physical Chemistry B* **2002,** 106, (10), 2429-2433.

37. Park, S.; Vosguerichian, M.; Bao, Z., A review of fabrication and applications of carbon nanotube film-based flexible electronics. *Nanoscale* **2013,** 5, (5), 1727-1752.

38. Nessim, G. D., Properties, synthesis, and growth mechanisms of carbon nanotubes with special focus on thermal chemical vapor deposition. *Nanoscale* **2010,** 2, (8), 1306-1323.

39. Kaempgen, M.; Chan, C. K.; Ma, J.; Cui, Y.; Gruner, G., Printable Thin Film Supercapacitors Using Single-Walled Carbon Nanotubes. *Nano Letters* **2009,** 9, (5), 1872-1876.

40. Kim, B.; Chung, H.; Kim, W., Supergrowth of Aligned Carbon Nanotubes Directly on Carbon Papers and Their Properties as Supercapacitors. *The Journal of Physical Chemistry C* **2010,** 114, (35), 15223-15227.

41. Fedorovskaya, E. O.; Bulusheva, L. G.; Kurenya, A. G.; Asanov, I. P.; Rudina, N. A.; Funtov, K. O.; Lyubutin, I. S.; Okotrub, A. V., Supercapacitor performance of

vertically aligned multiwall carbon nanotubes produced by aerosol-assisted CCVD method. *Electrochimica Acta* **2014,** 139, 165-172.

42. Lota, G.; Fic, K.; Frackowiak, E., Carbon nanotubes and their composites in electrochemical applications. *Energy & Environmental Science* **2011,** 4, (5), 1592-1605.

43. Candelaria, S. L.; Shao, Y.; Zhou, W.; Li, X.; Xiao, J.; Zhang, J.-G.; Wang, Y.; Liu, J.; Li, J.; Cao, G., Nanostructured carbon for energy storage and conversion. *Nano Energy* **2012,** 1, (2), 195-220.

44. Zheng, C.; Qian, W.; Cui, C.; Xu, G.; Zhao, M.; Tian, G.; Wei, F., Carbon nanotubes for supercapacitors: Consideration of cost and chemical vapor deposition techniques. *Journal of Natural Gas Chemistry* **2012,** 21, (3), 233-240.

45. McArthur, M. A.; Hordy, N.; Coulombe, S.; Omanovic, S., A binder-free multi-walled carbon nanotube electrode containing oxygen functionalities for electrochemical capacitors. *Electrochimica Acta* **2015,** 162, 245-253.

46. Barranco, V.; Lillo-Rodenas, M. A.; Linares-Solano, A.; Oya, A.; Pico, F.; Ibañez, J.; Agullo-Rueda, F.; Amarilla, J. M.; Rojo, J. M., Amorphous Carbon Nanofibers and Their Activated Carbon Nanofibers as Supercapacitor Electrodes. *The Journal of Physical Chemistry C* **2010,** 114, (22), 10302-10307.

47. Boskovic, B. O.; Stolojan, V.; Khan, R. U. A.; Haq, S.; Silva, S. R. P., Large-area synthesis of carbon nanofibres at room temperature. *Nature Materials* **2002,** 1, (3), 165-168.

48. Yang, L.; Hou, L. R.; Zhang, Y. W.; Yuan, C. Z., Facile synthesis of mesoporous carbon nanofibres towards high-performance electrochemical capacitors. *Materials Letters* **2013,** 97, 97-99.

49. Wu, X.-L.; Xu, A.-W., Carbonaceous hydrogels and aerogels for supercapacitors. *Journal of Materials Chemistry A* **2014,** 2, (14), 4852-4864.

50. Presser, V.; Heon, M.; Gogotsi, Y., Carbide-Derived Carbons – From Porous Networks to Nanotubes and Graphene. *Advanced Functional Materials* **2011,** 21, (5), 810-833.

51. Gogotsi, Y.; Dash, R. K.; Yushin, G.; Yildirim, T.; Laudisio, G.; Fischer, J. E., Tailoring of Nanoscale Porosity in Carbide-Derived Carbons for Hydrogen Storage. *Journal of the American Chemical Society* **2005,** 127, (46), 16006-16007.

52. Zhi, M.; Xiang, C.; Li, J.; Li, M.; Wu, N., Nanostructured carbon-metal oxide composite electrodes for supercapacitors: a review. *Nanoscale* **2013,** 5, (1), 72-88.

53. Zhang, Y.; Li, L.; Su, H.; Huang, W.; Dong, X., Binary metal oxide: advanced energy storage materials in supercapacitors. *Journal of Materials Chemistry A* **2015,** 3, (1), 43-59.

54. Desilvestro, J.; Haas, O., Metal Oxide Cathode Materials for Electrochemical Energy Storage: A Review. *Journal of The Electrochemical Society* **1990,** 137, (1), 5C-22C.

55. Jiang, J.; Kucernak, A., Electrochemical supercapacitor material based on manganese oxide: preparation and characterization. *Electrochimica Acta* **2002,** 47, (15), 2381-2386.

56. Lang, X.; Hirata, A.; Fujita, T.; Chen, M., Nanoporous metal/oxide hybrid electrodes for electrochemical supercapacitors. *Nat Nano* **2011,** 6, (4), 232-236.

57. Du, J.; Zhou, G.; Zhang, H.; Cheng, C.; Ma, J.; Wei, W.; Chen, L.; Wang, T., Ultrathin Porous NiCo2O4 Nanosheet Arrays on Flexible Carbon Fabric for High-Performance Supercapacitors. *ACS Applied Materials & Interfaces* **2013,** 5, (15), 7405-7409.

58. Wu, M.-S.; Lin, Y.-P.; Lin, C.-H.; Lee, J.-T., Formation of nano-scaled crevices and spacers in NiO-attached graphene oxide nanosheets for supercapacitors. *Journal of Materials Chemistry* **2012,** 22, (6), 2442-2448.

59. Lee, E.; Lee, T.; Kim, B.-S., Electrospun nanofiber of hybrid manganese oxides for supercapacitor: Relevance to mixed inorganic interfaces. *Journal of Power Sources* **2014,** 255, 335-340.

60. Yu, X.; Lu, B.; Xu, Z., Super Long-Life Supercapacitors Based on the Construction of Nanohoneycomb-Like Strongly Coupled CoMoO4–3D Graphene Hybrid Electrodes. *Advanced Materials* **2014,** 26, (7), 1044-1051.

61. He, G.; Li, J.; Chen, H.; Shi, J.; Sun, X.; Chen, S.; Wang, X., Hydrothermal preparation of Co3O4@graphene nanocomposite for supercapacitor with enhanced capacitive performance. *Materials Letters* **2012,** 82, 61-63.

62. Xia, X.; Tu, J.; Zhang, Y.; Wang, X.; Gu, C.; Zhao, X.-b.; Fan, H. J., High-Quality Metal Oxide Core/Shell Nanowire Arrays on Conductive Substrates for Electrochemical Energy Storage. *ACS Nano* **2012,** 6, (6), 5531-5538.

63. Lu, Z.; Chang, Z.; Liu, J.; Sun, X., Stable ultrahigh specific capacitance of NiO nanorod arrays. *Nano Research* **2011,** 4, (7), 658-665.

64. Dong, R.; Ye, Q.; Kuang, L.; Lu, X.; Zhang, Y.; Zhang, X.; Tan, G.; Wen, Y.; Wang, F., Enhanced Supercapacitor Performance of Mn3O4 Nanocrystals by Doping Transition-Metal Ions. *ACS Applied Materials & Interfaces* **2013,** 5, (19), 9508-9516.

65. Zhao, B.; Song, J.; Liu, P.; Xu, W.; Fang, T.; Jiao, Z.; Zhang, H.; Jiang, Y., Monolayer graphene/NiO nanosheets with two-dimension structure for supercapacitors. *Journal of Materials Chemistry* **2011,** 21, (46), 18792-18798.

66. Reddy, A. L. M.; Ramaprabhu, S., Nanocrystalline Metal Oxides Dispersed Multiwalled Carbon Nanotubes as Supercapacitor Electrodes. *The Journal of Physical Chemistry C* **2007,** 111, (21), 7727-7734.

67. Lokhande, C. D.; Dubal, D. P.; Joo, O.-S., Metal oxide thin film based supercapacitors. *Current Applied Physics* **2011,** 11, (3), 255-270.

68. Jiang, J.; Li, Y.; Liu, J.; Huang, X.; Yuan, C.; Lou, X. W., Recent Advances in Metal Oxide-based Electrode Architecture Design for Electrochemical Energy Storage. *Advanced Materials* **2012,** 24, (38), 5166-5180.

69. Snook, G. A.; Kao, P.; Best, A. S., Conducting-polymer-based supercapacitor devices and electrodes. *Journal of Power Sources* **2011,** 196, (1), 1-12.

70. Park, H.-S.; Ko, S.-J.; Park, J.-S.; Kim, J. Y.; Song, H.-K., Redox-active charge carriers of conducting polymers as a tuner of conductivity and its potential window. *Scientific Reports* **2013,** 3, 2454.

71. Wang, K.; Wu, H.; Meng, Y.; Wei, Z., Conducting Polymer Nanowire Arrays for High Performance Supercapacitors. *Small* **2014,** 10, (1), 14-31.

72. Ramya, R.; Sivasubramanian, R.; Sangaranarayanan, M. V., Conducting polymers-based electrochemical supercapacitors—Progress and prospects. *Electrochimica Acta* **2013,** 101, (0), 109-129.

73. Ashok Kumar, N.; Baek, J.-B., Electrochemical supercapacitors from conducting polyaniline-graphene platforms. *Chemical Communications* **2014,** 50, (48), 6298-6308.

74. Wang, K.; Huang, J.; Wei, Z., Conducting Polyaniline Nanowire Arrays for High Performance Supercapacitors. *The Journal of Physical Chemistry C* **2010,** 114, (17), 8062-8067.

75. Zhang, D.; Zhang, X.; Chen, Y.; Yu, P.; Wang, C.; Ma, Y., Enhanced capacitance and rate capability of graphene/polypyrrole composite as electrode material for supercapacitors. *Journal of Power Sources* **2011,** 196, (14), 5990-5996.

76. Biswas, S.; Drzal, L. T., Multilayered Nanoarchitecture of Graphene Nanosheets and Polypyrrole Nanowires for High Performance Supercapacitor Electrodes. *Chemistry of Materials* **2010,** 22, (20), 5667-5671.

77. Cho, S. I.; Lee, S. B., Fast Electrochemistry of Conductive Polymer Nanotubes: Synthesis, Mechanism, and Application. *Accounts of Chemical Research* **2008,** 41, (6), 699-707.

78. Snook, G. A.; Peng, C.; Fray, D. J.; Chen, G. Z., Achieving high electrode specific capacitance with materials of low mass specific capacitance: Potentiostatically

grown thick micro-nanoporous PEDOT films. *Electrochemistry Communications* **2007,** 9, (1), 83-88.

79. Laforgue, A., All-textile flexible supercapacitors using electrospun poly(3,4-ethylenedioxythiophene) nanofibers. *Journal of Power Sources* **2011,** 196, (1), 559-564.

80. Naoi, K., Morita, M., Advanced Polymers as Active Materials and Electrolytes for Electrochemical Capacitors and Hybrid Capacitor Systems. *The Electrochemical Society Interface* **2008,** 17, 44-48.

81. Balint, R.; Cassidy, N. J.; Cartmell, S. H., Conductive polymers: Towards a smart biomaterial for tissue engineering. *Acta Biomaterialia* **2014,** 10, (6), 2341-2353.

82. Peng, C.; Zhang, S.; Jewell, D.; Chen, G. Z., Carbon nanotube and conducting polymer composites for supercapacitors. *Progress in Natural Science* **2008,** 18, (7), 777-788.

83. Pan, L.; Qiu, H.; Dou, C.; Li, Y.; Pu, L.; Xu, J.; Shi, Y., Conducting Polymer Nanostructures: Template Synthesis and Applications in Energy Storage. *International Journal of Molecular Sciences* **2010,** 11, (7), 2636-2657.

84. Dubal, D. P.; Lee, S. H.; Kim, J. G.; Kim, W. B.; Lokhande, C. D., Porous polypyrrole clusters prepared by electropolymerization for a high performance supercapacitor. *Journal of Materials Chemistry* **2012,** 22, (7), 3044-3052.

85. Chen, Z.; Yu, D.; Xiong, W.; Liu, P.; Liu, Y.; Dai, L., Graphene-Based Nanowire Supercapacitors. *Langmuir* **2014,** 30, (12), 3567-3571.

86. Zhang, H.; Cao, G.; Wang, Z.; Yang, Y.; Shi, Z.; Gu, Z., Tube-covering-tube nanostructured polyaniline/carbon nanotube array composite electrode with high capacitance and superior rate performance as well as good cycling stability. *Electrochemistry Communications* **2008,** 10, (7), 1056-1059.

87. Horng, Y.-Y.; Lu, Y.-C.; Hsu, Y.-K.; Chen, C.-C.; Chen, L.-C.; Chen, K.-H., Flexible supercapacitor based on polyaniline nanowires/carbon cloth with both high gravimetric and area-normalized capacitance. *Journal of Power Sources* **2010,** 195, (13), 4418-4422.

88. Fan, L.-Z.; Maier, J., High-performance polypyrrole electrode materials for redox supercapacitors. *Electrochemistry Communications* **2006,** 8, (6), 937-940.

89. Li, Y.; Wang, B.; Chen, H.; Feng, W., Improvement of the electrochemical properties via poly(3,4-ethylenedioxythiophene) oriented micro/nanorods. *Journal of Power Sources* **2010,** 195, (9), 3025-3030.

90. Hsu, Y.-K.; Chen, Y.-C.; Lin, Y.-G.; Chen, L.-C.; Chen, K.-H., Direct-growth of poly(3,4-ethylenedioxythiophene) nanowires/carbon cloth as hierarchical supercapacitor electrode in neutral aqueous solution. *Journal of Power Sources* **2013,** 242, 718-724.

91. Inzelt, G., *Conducting Polymers, A New Era in Electrochemistry*. First ed.; Springer: 2008.

92. Alvi, F.; Ram, M. K.; Basnayaka, P. A.; Stefanakos, E.; Goswami, Y.; Kumar, A., Graphene–polyethylenedioxythiophene conducting polymer nanocomposite based supercapacitor. *Electrochimica Acta* **2011,** 56, (25), 9406-9412.

93. Wang, H.; Hao, Q.; Yang, X.; Lu, L.; Wang, X., Effect of Graphene Oxide on the Properties of Its Composite with Polyaniline. *ACS Applied Materials & Interfaces* **2010,** 2, (3), 821-828.

94. Liu, Y.; Zhang, Y.; Ma, G.; Wang, Z.; Liu, K.; Liu, H., Ethylene glycol reduced graphene oxide/polypyrrole composite for supercapacitor. *Electrochimica Acta* **2013,** 88, 519-525.

95. An, H.; Wang, Y.; Wang, X.; Zheng, L.; Wang, X.; Yi, L.; Bai, L.; Zhang, X., Polypyrrole/carbon aerogel composite materials for supercapacitor. *Journal of Power Sources* **2010,** 195, (19), 6964-6969.

96. Sathish, M.; Mitani, S.; Tomai, T.; Honma, I., MnO2 assisted oxidative polymerization of aniline on graphene sheets: Superior nanocomposite electrodes for electrochemical supercapacitors. *Journal of Materials Chemistry* **2011,** 21, (40), 16216-16222.

97. Xu, J.; Wang, K.; Zu, S.-Z.; Han, B.-H.; Wei, Z., Hierarchical Nanocomposites of Polyaniline Nanowire Arrays on Graphene Oxide Sheets with Synergistic Effect for Energy Storage. *ACS Nano* **2010,** 4, (9), 5019-5026.

98. de Oliveira, H. P.; Sydlik, S. A.; Swager, T. M., Supercapacitors from Free-Standing Polypyrrole/Graphene Nanocomposites. *The Journal of Physical Chemistry C* **2013,** 117, (20), 10270-10276.

99. Mondal, S.; Rana, U.; Malik, S., Graphene quantum dot-doped polyaniline nanofiber as high performance supercapacitor electrode materials. *Chemical Communications* **2015,** 51, (62), 12365-12368.

100. Grover, S.; Goel, S.; Sahu, V.; Singh, G.; Sharma, R. K., Asymmetric Supercapacitive Characteristics of PANI Embedded Holey Graphene Nanoribbons. *ACS Sustainable Chemistry & Engineering* **2015,** 3, (7), 1460-1469.

101. Zhang, J.; Zhao, X. S., Conducting Polymers Directly Coated on Reduced Graphene Oxide Sheets as High-Performance Supercapacitor Electrodes. *The Journal of Physical Chemistry C* **2012,** 116, (9), 5420-5426.

102. Antiohos, D.; Folkes, G.; Sherrell, P.; Ashraf, S.; Wallace, G. G.; Aitchison, P.; Harris, A. T.; Chen, J.; Minett, A. I., Compositional effects of PEDOT-PSS/single walled carbon nanotube films on supercapacitor device performance. *Journal of Materials Chemistry* **2011,** 21, (40), 15987-15994.

103. Mykhailiv, O.; Imierska, M.; Petelczyc, M.; Echegoyen, L.; Plonska-Brzezinska, M. E., Chemical versus Electrochemical Synthesis of Carbon Nano-onion/Polypyrrole Composites for Supercapacitor Electrodes. *Chemistry – A European Journal* **2015,** 21, (15), 5783-5793.

104. Meyyappan, M., Nanostructured materials for supercapacitors. *Journal of Vacuum Science & Technology A* **2013,** 31, (5), 050803.

105. Azaïs, P., *Supercapacitors: Materials, Systems, and Applications*. First ed.; Wiley-VCH Verlag GmbH & Co.: Weinheim, Germany, 2013.

106. Brandt, A.; Pohlmann, S.; Varzi, A.; Balducci, A.; Passerini, S., Ionic liquids in supercapacitors. *MRS Bulletin* **2013,** 38, (07), 554-559.

107. Zhang, Y.; Feng, H.; Wu, X.; Wang, L.; Zhang, A.; Xia, T.; Dong, H.; Li, X.; Zhang, L., Progress of electrochemical capacitor electrode materials: A review. *International Journal of Hydrogen Energy* **2009,** 34, (11), 4889-4899.

108. Mak, W. F.; Wee, G.; Aravindan, V.; Gupta, N.; Mhaisalkar, S. G.; Madhavi, S., High-Energy Density Asymmetric Supercapacitor Based on Electrospun Vanadium Pentoxide and Polyaniline Nanofibers in Aqueous Electrolyte. *Journal of The Electrochemical Society* **2012,** 159, (9), A1481-A1488.

109. Khomenko, V.; Raymundo-Piñero, E.; Frackowiak, E.; Béguin, F., High-voltage asymmetric supercapacitors operating in aqueous electrolyte. *Applied Physics A* **2006,** 82, (4), 567-573.

110. Ghenaatian, H. R.; Mousavi, M. F.; Rahmanifar, M. S., High performance hybrid supercapacitor based on two nanostructured conducting polymers: Self-doped polyaniline and polypyrrole nanofibers. *Electrochimica Acta* **2012,** 78, 212-222.

111. Kurra, N.; Wang, R.; Alshareef, H. N., All conducting polymer electrodes for asymmetric solid-state supercapacitors. *Journal of Materials Chemistry A* **2015,** 3, (14), 7368-7374.

112. Wang, Q.; Wen, Z. H.; Li, J. H., A Hybrid Supercapacitor Fabricated with a Carbon Nanotube Cathode and a TiO2–B Nanowire Anode. *Advanced Functional Materials* **2006,** 16, (16), 2141-2146.

113. Khomenko, V.; Raymundo-Piñero, E.; Béguin, F., Optimisation of an asymmetric manganese oxide/activated carbon capacitor working at 2 V in aqueous medium. *Journal of Power Sources* **2006,** 153, (1), 183-190.

114. Zhao, X.; Sanchez, B. M.; Dobson, P. J.; Grant, P. S., The role of nanomaterials in redox-based supercapacitors for next generation energy storage devices. *Nanoscale* **2011,** 3, (3), 839-855.

115. Sun, L.; Tian, C.; Li, M.; Meng, X.; Wang, L.; Wang, R.; Yin, J.; Fu, H., From coconut shell to porous graphene-like nanosheets for high-power supercapacitors. *Journal of Materials Chemistry A* **2013,** 1, (21), 6462-6470.

116. Hao, P.; Zhao, Z.; Tian, J.; Li, H.; Sang, Y.; Yu, G.; Cai, H.; Liu, H.; Wong, C. P.; Umar, A., Hierarchical porous carbon aerogel derived from bagasse for high performance supercapacitor electrode. *Nanoscale* **2014,** 6, (20), 12120-12129.

117. Gao, S.; Chen, Y.; Fan, H.; Wei, X.; Hu, C.; Luo, H.; Qu, L., Large scale production of biomass-derived N-doped porous carbon spheres for oxygen reduction and supercapacitors. *Journal of Materials Chemistry A* **2014,** 2, (10), 3317-3324.

118. Azaıs, P., *Supercapacitors: Materials, Systems, and Applications*. First ed.; Wiley-VCH Verlag GmbH & Co.: Weinheim, Germany, 2013.

119. Zhang, L. L.; Zhao, S.; Tian, X. N.; Zhao, X. S., Layered Graphene Oxide Nanostructures with Sandwiched Conducting Polymers as Supercapacitor Electrodes. *Langmuir* **2010,** 26, (22), 17624-17628.

120. Mao, L.; Zhang, K.; On Chan, H. S.; Wu, J., Surfactant-stabilized graphene/polyaniline nanofiber composites for high performance supercapacitor electrode. *Journal of Materials Chemistry* **2012,** 22, (1), 80-85.

121. Bavio, M. A.; Acosta, G. G.; Kessler, T., Synthesis and characterization of polyaniline and polyaniline – Carbon nanotubes nanostructures for electrochemical supercapacitors. *Journal of Power Sources* **2014,** 245, 475-481.

122. Xin, Z.; Bryan, T. T. C.; Belén, B.; Weiliang, W.; Colin, J.; John, M. S.; Patrick, S. G., Spray deposition of steam treated and functionalized single-walled and multi-walled carbon nanotube films for supercapacitors. *Nanotechnology* **2009,** 20, (6), 065605.

123. Zhong, Y.; Yang, M.; Zhou, X.; Luo, Y.; Wei, J.; Zhou, Z., Orderly Packed Anodes for High-Power Lithium-Ion Batteries with Super-Long Cycle Life: Rational Design of MnCO3/Large-Area Graphene Composites. *Advanced Materials* **2015,** 27, (5), 806-812.

124. Hong, J.; Han, J. Y.; Yoon, H.; Joo, P.; Lee, T.; Seo, E.; Char, K.; Kim, B.-S., Carbon-based layer-by-layer nanostructures: from films to hollow capsules. *Nanoscale* **2011,** 3, (11), 4515-4531.

125. Karakaya, M.; Zhu, J.; Raghavendra, A. J.; Podila, R.; Parler, S. G.; Kaplan, J. P.; Rao, A. M., Roll-to-roll production of spray coated N-doped carbon nanotube electrodes for supercapacitors. *Applied Physics Letters* **2014,** 105, (26), 263103.

126. Kim, J.-H.; Kang, S. H.; Zhu, K.; Kim, J. Y.; Neale, N. R.; Frank, A. J., Ni-NiO core-shell inverse opal electrodes for supercapacitors. *Chemical Communications* **2011,** 47, (18), 5214-5216.

127. He, P.; Gao, X.-d.; Li, X.-m.; Jiang, Z.-w.; Yang, Z.-h.; Wang, C.-l.; Gu, Z.-y., Highly transparent silica aerogel thick films with hierarchical porosity from water

glass via ambient pressure drying. *Materials Chemistry and Physics* **2014,** 147, (1–2), 65-74.

128. Ryu, K. S.; Lee, Y.; Han, K.-S.; Park, Y. J.; Kang, M. G.; Park, N.-G.; Chang, S. H., Electrochemical supercapacitor based on polyaniline doped with lithium salt and active carbon electrodes. *Solid State Ionics* **2004,** 175, (1–4), 765-768.

129. Noked, M.; Okashy, S.; Zimrin, T.; Aurbach, D., Composite Carbon Nanotube/Carbon Electrodes for Electrical Double-Layer Super Capacitors. *Angewandte Chemie* **2012,** 124, (7), 1600-1603.

130. Zhang, Z.; Huang, X.; Jiang, J.; Wu, B., An improved dynamic model considering effects of temperature and equivalent internal resistance for PEM fuel cell power modules. *Journal of Power Sources* **2006,** 161, (2), 1062-1068.

131. Singh, P. K.; Kim, K.-W.; Park, N.-G.; Rhee, H.-W., Mesoporous nanocrystalline TiO2 electrode with ionic liquid-based solid polymer electrolyte for dye-sensitized solar cell application. *Synthetic Metals* **2008,** 158, (14), 590-593.

132. Jae Hyun, L.; Byung-Seon, K.; Youn-Kyoung, B.; Seung Bo, Y.; Hee-Tae, J., Tin nanoparticle thin film electrodes fabricated by the vacuum filtration method for enhanced battery performance. *Nanotechnology* **2009,** 20, (23), 235203.

133. Lepleux, L.; Chavillon, B.; Pellegrin, Y.; Blart, E.; Cario, L.; Jobic, S.; Odobel, F., Simple and Reproducible Procedure to Prepare Self-Nanostructured NiO Films for the Fabrication of P-Type Dye-Sensitized Solar Cells. *Inorganic Chemistry* **2009,** 48, (17), 8245-8250.

134. Sankapal, B. R.; Gajare, H. B.; Dubal, D. P.; Gore, R. B.; Salunkhe, R. R.; Ahn, H., Presenting highest supercapacitance for TiO2/MWNTs nanocomposites: Novel method. *Chemical Engineering Journal* **2014,** 247, 103-110.

135. Jost, K.; Perez, C. R.; McDonough, J. K.; Presser, V.; Heon, M.; Dion, G.; Gogotsi, Y., Carbon coated textiles for flexible energy storage. *Energy & Environmental Science* **2011,** 4, (12), 5060-5067.

136. Wang, K.; Zhao, P.; Zhou, X.; Wu, H.; Wei, Z., Flexible supercapacitors based on cloth-supported electrodes of conducting polymer nanowire array/SWCNT composites. *Journal of Materials Chemistry* **2011,** 21, (41), 16373-16378.

137. Mateos, A. J.; Cain, A. A.; Grunlan, J. C., Large-Scale Continuous Immersion System for Layer-by-Layer Deposition of Flame Retardant and Conductive Nanocoatings on Fabric. *Industrial & Engineering Chemistry Research* **2014,** 53, (15), 6409-6416.

138. Tiwari, J. N.; Tiwari, R. N.; Kim, K. S., Zero-dimensional, one-dimensional, two-dimensional and three-dimensional nanostructured materials for advanced electrochemical energy devices. *Progress in Materials Science* **2012,** 57, (4), 724-803.

139. Shinde, V. R.; Mahadik, S. B.; Gujar, T. P.; Lokhande, C. D., Supercapacitive cobalt oxide (Co3O4) thin films by spray pyrolysis. *Applied Surface Science* **2006,** 252, (20), 7487-7492.

140. Tang, H.; Yang, C.; Lin, Z.; Yang, Q.; Kang, F.; Wong, C. P., Electrospray-deposition of graphene electrodes: a simple technique to build high-performance supercapacitors. *Nanoscale* **2015,** 7, (20), 9133-9139.

141. Zhao, X.; Johnston, C.; Grant, P. S., A novel hybrid supercapacitor with a carbon nanotube cathode and an iron oxide/carbon nanotube composite anode. *Journal of Materials Chemistry* **2009,** 19, (46), 8755-8760.

142. Huang, C.; Grobert, N.; Watt, A. A. R.; Johnston, C.; Crossley, A.; Young, N. P.; Grant, P. S., Layer-by-layer spray deposition and unzipping of single-wall carbon nanotube-based thin film electrodes for electrochemical capacitors. *Carbon* **2013,** 61, 525-536.

143. Zhao, X.; Johnston, C.; Crossley, A.; Grant, P. S., Printable magnetite and pyrrole treated magnetite based electrodes for supercapacitors. *Journal of Materials Chemistry* **2010,** 20, (36), 7637-7644.

144. Sohn, K.; Joo Na, Y.; Chang, H.; Roh, K.-M.; Dong Jang, H.; Huang, J., Oil absorbing graphene capsules by capillary molding. *Chemical Communications* **2012,** 48, (48), 5968-5970.

145. Lawes, S.; Riese, A.; Sun, Q.; Cheng, N.; Sun, X., Printing nanostructured carbon for energy storage and conversion applications. *Carbon* **2015,** 92, 150-176.

146. Zhu, J.; Yang, D.; Yin, Z.; Yan, Q.; Zhang, H., Graphene and Graphene-Based Materials for Energy Storage Applications. *Small* **2014,** 10, (17), 3480-3498.

147. Secor, E. B.; Hersam, M. C., Emerging Carbon and Post-Carbon Nanomaterial Inks for Printed Electronics. *The Journal of Physical Chemistry Letters* **2015,** 6, (4), 620-626.

148. Weng, B.; Shepherd, R. L.; Crowley, K.; Killard, A. J.; Wallace, G. G., Printing conducting polymers. *Analyst* **2010,** 135, (11), 2779-2789.

149. Okimoto, H.; Takenobu, T.; Yanagi, K.; Miyata, Y.; Shimotani, H.; Kataura, H.; Iwasa, Y., Tunable Carbon Nanotube Thin-Film Transistors Produced Exclusively via Inkjet Printing. *Advanced Materials* **2010,** 22, (36), 3981-3986.

150. Ganguly, A.; Chattopadhyay, S.; Chen, K.-H.; Chen, L.-C., Production and Storage of Energy with One-Dimensional Semiconductor Nanostructures. *Critical Reviews in Solid State and Materials Sciences* **2014,** 39, (2), 109-153.

151. Hu, L.; Wu, H.; Cui, Y., Printed energy storage devices by integration of electrodes and separators into single sheets of paper. *Applied Physics Letters* **2010,** 96, (18), 183502.

152. Li, J.; Östling, M., Prevention of Graphene Restacking for Performance Boost of Supercapacitors—A Review. *Crystals* **2013,** 3, (1), 163.

153. Li, J.; Ye, F.; Vaziri, S.; Muhammed, M.; Lemme, M. C.; Östling, M., Efficient Inkjet Printing of Graphene. *Advanced Materials* **2013,** 25, (29), 3985-3992.

154. Ervin, M. H.; Le, L. T.; Lee, W. Y., Inkjet-Printed Flexible Graphene-Based Supercapacitor. *Electrochimica Acta* **2014,** 147, 610-616.

155. Crowley, K.; Smyth, M.; Killard, A.; Morrin, A., Printing polyaniline for sensor applications. *Chemical Papers* **2013,** 67, (8), 771-780.

156. Small, W. R.; Masdarolomoor, F.; Wallace, G. G.; in het Panhuis, M., Inkjet deposition and characterization of transparent conducting electroactive polyaniline composite films with a high carbon nanotube loading fraction. *Journal of Materials Chemistry* **2007,** 17, (41), 4359-4361.

157. Kordás, K.; Mustonen, T.; Tóth, G.; Jantunen, H.; Lajunen, M.; Soldano, C.; Talapatra, S.; Kar, S.; Vajtai, R.; Ajayan, P. M., Inkjet Printing of Electrically Conductive Patterns of Carbon Nanotubes. *Small* **2006,** 2, (8-9), 1021-1025.

158. Chen, P.; Chen, H.; Qiu, J.; Zhou, C., Inkjet printing of single-walled carbon nanotube/RuO2 nanowire supercapacitors on cloth fabrics and flexible substrates. *Nano Research* **2010,** 3, (8), 594-603.

159. Hoth, C. N.; Schilinsky, P.; Choulis, S. A.; Brabec, C. J., Printing Highly Efficient Organic Solar Cells. *Nano Letters* **2008,** 8, (9), 2806-2813.

160. Mäkelä, T.; Haatainen, T.; Majander, P.; Ahopelto, J., Continuous roll to roll nanoimprinting of inherently conducting polyaniline. *Microelectronic Engineering* **2007,** 84, (5–8), 877-879.

161. Xiao, Y.; Huang, L.; Zhang, Q.; Xu, S.; Chen, Q.; Shi, W., Gravure printing of hybrid MoS2@S-rGO interdigitated electrodes for flexible microsupercapacitors. *Applied Physics Letters* **2015,** 107, (1), 013906.

162. Devan, R. S.; Patil, R. A.; Lin, J.-H.; Ma, Y.-R., One-Dimensional Metal-Oxide Nanostructures: Recent Developments in Synthesis, Characterization, and Applications. *Advanced Functional Materials* **2012,** 22, (16), 3326-3370.

163. Yu, Q.; Lian, J.; Siriponglert, S.; Li, H.; Chen, Y. P.; Pei, S.-S., Graphene segregated on Ni surfaces and transferred to insulators. *Applied Physics Letters* **2008,** 93, (11), 113103.

164. Chou, S. Y.; Krauss, P. R.; Renstrom, P. J., Imprint Lithography with 25-Nanometer Resolution. *Science* **1996,** 272, (5258), 85-87.

165. Sun, Z.; Lu, X., A Solid-State Reaction Route to Anchoring Ni(OH)2 Nanoparticles on Reduced Graphene Oxide Sheets for Supercapacitors. *Industrial & Engineering Chemistry Research* **2012,** 51, (30), 9973-9979.

166. Ellis, B. L.; Knauth, P.; Djenizian, T., Three-Dimensional Self-Supported Metal Oxides for Advanced Energy Storage. *Advanced Materials* **2014,** 26, (21), 3368-3397.

167. Faraji, S.; Ani, F. N., Microwave-assisted synthesis of metal oxide/hydroxide composite electrodes for high power supercapacitors – A review. *Journal of Power Sources* **2014,** 263, 338-360.

168. Liu, G.; Wang, K.; Hoivik, N.; Jakobsen, H., Progress on free-standing and flow-through TiO2 nanotube membranes. *Solar Energy Materials and Solar Cells* **2012,** 98, 24-38.

169. Jun, Y.; Park, J. H.; Kang, M. G., The preparation of highly ordered TiO2 nanotube arrays by an anodization method and their applications. *Chemical Communications* **2012,** 48, (52), 6456-6471.

170. Chavez-Valdez, A.; Shaffer, M. S. P.; Boccaccini, A. R., Applications of Graphene Electrophoretic Deposition. A Review. *The Journal of Physical Chemistry B* **2013,** 117, (6), 1502-1515.

171. Sun, B.; Long, Y.-Z.; Chen, Z.-J.; Liu, S.-L.; Zhang, H.-D.; Zhang, J.-C.; Han, W.-P., Recent advances in flexible and stretchable electronic devices via electrospinning. *Journal of Materials Chemistry C* **2014,** 2, (7), 1209-1219.

172. Zhang, Q.; Zhang, K.; Xu, D.; Yang, G.; Huang, H.; Nie, F.; Liu, C.; Yang, S., CuO nanostructures: Synthesis, characterization, growth mechanisms, fundamental properties, and applications. *Progress in Materials Science* **2014,** 60, 208-337.

173. Dong, Z.; Kennedy, S. J.; Wu, Y., Electrospinning materials for energy-related applications and devices. *Journal of Power Sources* **2011,** 196, (11), 4886-4904.

174. Thavasi, V.; Singh, G.; Ramakrishna, S., Electrospun nanofibers in energy and environmental applications. *Energy & Environmental Science* **2008,** 1, (2), 205-221.

175. Pico, F.; Ibañez, J.; Lillo-Rodenas, M. A.; Linares-Solano, A.; Rojas, R. M.; Amarilla, J. M.; Rojo, J. M., Understanding RuO2·xH2O/carbon nanofibre composites as supercapacitor electrodes. *Journal of Power Sources* **2008,** 176, (1), 417-425.

176. Wang, L.; Lu, X.; Lei, S.; Song, Y., Graphene-based polyaniline nanocomposites: preparation, properties and applications. *Journal of Materials Chemistry A* **2014,** 2, (13), 4491-4509.

177. Xue, M.; Li, F.; Zhu, J.; Song, H.; Zhang, M.; Cao, T., Structure-Based Enhanced Capacitance: In Situ Growth of Highly Ordered Polyaniline Nanorods on Reduced Graphene Oxide Patterns. *Advanced Functional Materials* **2012,** 22, (6), 1284-1290.

178. Sheng, K.; Sun, Y.; Li, C.; Yuan, W.; Shi, G., Ultrahigh-rate supercapacitors based on eletrochemically reduced graphene oxide for ac line-filtering. *Scientific Reports* **2012,** 2, 247.

179. Wu, Z.; Zhu, Y.; Ji, X., NiCo2O4-based materials for electrochemical supercapacitors. *Journal of Materials Chemistry A* **2014,** 2, (36), 14759-14772.

180. Yuan, G.-Q.; Jiang, H.-F.; Lin, C.; Liao, S.-J., Shape- and size-controlled electrochemical synthesis of cupric oxide nanocrystals. *Journal of Crystal Growth* **2007,** 303, (2), 400-406.

181. Deshmukh, P. R.; Bulakhe, R. N.; Pusawale, S. N.; Sartale, S. D.; Lokhande, C. D., Polyaniline-RuO2 composite for high performance supercapacitors: chemical synthesis and properties. *RSC Advances* **2015,** 5, (36), 28687-28695.

182. Zhang, Y.; Zhang, L.; Kim, P.; Ge, M.; Li, Z.; Zhou, C., Vapor Trapping Growth of Single-Crystalline Graphene Flowers: Synthesis, Morphology, and Electronic Properties. *Nano Letters* **2012,** 12, (6), 2810-2816.

183. Faraji, S.; Ani, F. N., The development supercapacitor from activated carbon by electroless plating—A review. *Renewable and Sustainable Energy Reviews* **2015,** 42, 823-834.

184. Patil, U. M.; Gurav, K. V.; Fulari, V. J.; Lokhande, C. D.; Joo, O. S., Characterization of honeycomb-like "β-Ni(OH)2" thin films synthesized by chemical bath deposition method and their supercapacitor application. *Journal of Power Sources* **2009,** 188, (1), 338-342.

185. Dubal, D. P.; Gund, G. S.; Holze, R.; Jadhav, H. S.; Lokhande, C. D.; Park, C.-J., Surfactant-assisted morphological tuning of hierarchical CuO thin films for electrochemical supercapacitors. *Dalton Transactions* **2013,** 42, (18), 6459-6467.

186. Lee, W.; Mane, R. S.; Todkar, V. V.; Lee, S.; Egorova, O.; Chae, W.-S.; Han, S.-H., Implication of Liquid-Phase Deposited Amorphous RuO2 Electrode for

Electrochemical Supercapacitor. *Electrochemical and Solid-State Letters* **2007,** 10, (9), A225-A227.

187. Mahmood, N.; Zhang, C.; Yin, H.; Hou, Y., Graphene-based nanocomposites for energy storage and conversion in lithium batteries, supercapacitors and fuel cells. *Journal of Materials Chemistry A* **2014,** 2, (1), 15-32.

188. Huang, X.; Zeng, Z.; Fan, Z.; Liu, J.; Zhang, H., Graphene-based electrodes. *Advanced Materials* **2012,** 24, (45), 5979-6004.

189. Bansal, T.; Durcan, C. A.; Jain, N.; Jacobs-Gedrim, R. B.; Xu, Y.; Yu, B., Synthesis of few-to-monolayer graphene on rutile titanium dioxide. *Carbon* **2013,** 55, 168-175.

190. Brownson, D. A. C.; Banks, C. E., The electrochemistry of CVD graphene: progress and prospects. *Physical Chemistry Chemical Physics* **2012,** 14, (23), 8264-8281.

191. Arcila-Velez, M. R.; Zhu, J.; Childress, A.; Karakaya, M.; Podila, R.; Rao, A. M.; Roberts, M. E., Roll-to-roll synthesis of vertically aligned carbon nanotube electrodes for electrical double layer capacitors. *Nano Energy* **2014,** 8, 9-16.

192. Aravinda, L. S.; Nagaraja, K. K.; Nagaraja, H. S.; Bhat, K. U.; Bhat, B. R., ZnO/carbon nanotube nanocomposite for high energy density supercapacitors. *Electrochimica Acta* **2013,** 95, 119-124.

193. Lee, S.-H.; Tracy, C. E.; Roland Pitts , J., Effect of Nonstoichiometry of Nickel Oxides on Their Supercapacitor Behavior. *Electrochemical and Solid-State Letters* **2004,** 7, (10), A299-A301.

194. Ionescu, M. I.; Sun, X.; Luan, B., Multilayer graphene synthesized using magnetron sputtering for planar supercapacitor application. *Canadian Journal of Chemistry* **2014,** 93, (2), 160-164.

195. Liu, D.-Q.; Yu, S.-H.; Son, S.-W.; Joo, S.-K., Supercapacitive Studies on IrO2 Thin Film Electrodes Prepared by Radio Frequency Magnetron Sputtering. *Electrochemical and Solid-State Letters* **2008,** 11, (11), A206-A208.

196. Sarkar, A.; Satpati, A. K.; Rao, P.; Kumar, S., Electron beam deposition of amorphous manganese oxide thin film electrodes and their predominant electrochemical properties. *Journal of Power Sources* **2015,** 284, 264-271.

197. Zhiqiang, N.; Lili, L.; Peter, S.; Jun, C.; Xiaodong, C., Flexible Supercapacitors ? Development of Bendable Carbon Architectures. In *Nanotechnology for Sustainable Energy*, American Chemical Society: 2013; Vol. 1140, pp 101-141.

198. Gao, W.; Singh, N.; Song, L.; Liu, Z.; Reddy, A. L. M.; Ci, L.; Vajtai, R.; Zhang, Q.; Wei, B.; Ajayan, P. M., Direct laser writing of micro-supercapacitors on hydrated graphite oxide films. *Nat Nano* **2011,** 6, (8), 496-500.

199. El-Kady, M. F.; Strong, V.; Dubin, S.; Kaner, R. B., Laser Scribing of High-Performance and Flexible Graphene-Based Electrochemical Capacitors. *Science* **2012,** 335, (6074), 1326-1330.

200. Peng, X.; Peng, L.; Wu, C.; Xie, Y., Two dimensional nanomaterials for flexible supercapacitors. *Chemical Society Reviews* **2014,** 43, (10), 3303-3323.

201. Peng, Z.; Lin, J.; Ye, R.; Samuel, E. L. G.; Tour, J. M., Flexible and Stackable Laser-Induced Graphene Supercapacitors. *ACS Applied Materials & Interfaces* **2015,** 7, (5), 3414-3419.

202. In, J. B.; Hsia, B.; Yoo, J.-H.; Hyun, S.; Carraro, C.; Maboudian, R.; Grigoropoulos, C. P., Facile fabrication of flexible all solid-state micro-supercapacitor by direct laser writing of porous carbon in polyimide. *Carbon* **2015,** 83, 144-151.

203. Wang, H.; Yi, H.; Chen, X.; Wang, X., Asymmetric supercapacitors based on nano-architectured nickel oxide/graphene foam and hierarchical porous nitrogen-doped carbon nanotubes with ultrahigh-rate performance. *Journal of Materials Chemistry A* **2014,** 2, (9), 3223-3230.

204. Wang, H.; Wang, Y.; Wang, X., Pulsed laser deposition of large-area manganese oxide nanosheet arrays for high-rate supercapacitors. *New Journal of Chemistry* **2013,** 37, (4), 869-872.

205. Frazier, K. M.; Mirica, K. A.; Walish, J. J.; Swager, T. M., Fully-drawn carbon-based chemical sensors on organic and inorganic surfaces. *Lab on a Chip* **2014,** 14, (20), 4059-4066.

206. Kou, L.; Liu, Z.; Huang, T.; Zheng, B.; Tian, Z.; Deng, Z.; Gao, C., Wet-spun, porous, orientational graphene hydrogel films for high-performance supercapacitor electrodes. *Nanoscale* **2015,** 7, (9), 4080-4087.

207. Zhang, S.; Li, Y.; Pan, N., Graphene based supercapacitor fabricated by vacuum filtration deposition. *Journal of Power Sources* **2012,** 206, 476-482.

208. Zhang, L. L.; Zhao, X.; Stoller, M. D.; Zhu, Y.; Ji, H.; Murali, S.; Wu, Y.; Perales, S.; Clevenger, B.; Ruoff, R. S., Highly Conductive and Porous Activated Reduced Graphene Oxide Films for High-Power Supercapacitors. *Nano Letters* **2012,** 12, (4), 1806-1812.

209. An, K. H.; Kim, W. S.; Park, Y. S.; Choi, Y. C.; Lee, S. M.; Chung, D. C.; Bae, D. J.; Lim, S. C.; Lee, Y. H., Supercapacitors Using Single-Walled Carbon Nanotube Electrodes. *Advanced Materials* **2001,** 13, (7), 497-500.

210. Cheng, H.; Hu, C.; Zhao, Y.; Qu, L., Graphene fiber: a new material platform for unique applications. *NPG Asia Mater* **2014,** 6, e113.

211. Xu, Z.; Gao, C., Graphene in Macroscopic Order: Liquid Crystals and Wet-Spun Fibers. *Accounts of Chemical Research* **2014,** 47, (4), 1267-1276.

212. Xu, Z.; Gao, C., Graphene chiral liquid crystals and macroscopic assembled fibres. *Nat Commun* **2011,** 2, 571.

213. Kou, L.; Huang, T.; Zheng, B.; Han, Y.; Zhao, X.; Gopalsamy, K.; Sun, H.; Gao, C., Coaxial wet-spun yarn supercapacitors for high-energy density and safe wearable electronics. *Nat Commun* **2014,** 5.

CHAPTER TWO

ROLL-TO-ROLL SYNTHESIS OF VERTICALLY ALIGNED CARBON NANOTUBE ELECTRODES FOR ELECTRICAL DOUBLE LAYER CAPACITORS

2.1 Introduction

Electrochemical double layer capacitors (EDLCs), also known as supercapacitors, have emerged as a promising solution for applications requiring durable and reliable devices with high power and energy density.[1, 2] EDLCs offer comparable power densities to electrolytic capacitors while providing 2 to 3 orders of magnitude increase in energy density, thus allowing them to complement or serve as possible replacements for existing batteries.[3] Due to the prevalent use of activated carbon electrode materials, EDLC performance is often correlated with the electrode surface area, in which pore size distribution and the solvated electrolyte ion radius define the accessibility.[4] In this regard, the unique properties of carbon nanotubes (CNTs) make them suitable candidates for EDLC electrodes.[5] While the electrochemical stability of CNTs is necessary for long lifetime EDLCs, their high electrical conductivity allows for better electron transfer to the current collector and their high surface-to-volume ratio provides greater ion access.[4] Accordingly, vertically aligned arrays of multi-walled CNTs (VACNTs) have been considered for use in EDLCs due to their facile synthesis and the ability to control the ion-accessible surface by varying the CNT areal density on growth substrates.[6-10] VACNT electrodes have been used to achieve high power density EDLCs;[5, 11] however, continuous synthesis methods to prepare VACNTs directly on current collectors (e.g., Al foil) at relatively low costs are needed for commercially viable high power and high

energy density EDLCs. Additionally, when CNTs are grown from catalyst particles that are adhered to the current collector, the need for a binder is eliminated, thereby reducing inactive weight and contact resistance.[4]

Although CNTs can be synthesized in large quantities, present processes are not amenable for VACNT growth directly on current collectors for scalable manufacturing of EDLC electrodes.[12] Since the discovery of CNTs, several methods have been pioneered for their production, including electric arc discharge,[13, 14] laser ablation [15, 16] and chemical vapor deposition (CVD),[17, 18] however, only CVD has emerged as a practical and reliable method for synthesizing VACNT forests. While the CVD method is relatively versatile in terms of controlling CNT characteristics (e.g., tube diameter, number of walls, and dopant ratio),[19, 20] three factors that limit large scale VACNT synthesis are: i) substrate size set by reactor geometry, ii) requirements of a complex catalytic substrate preparation, and iii) high operating temperatures that are incompatible with traditional current collectors (e.g., Al foil).

Previously, Andrews et al.[21] developed a ferrocene-xylene liquid injection floating catalyst technique to grow VACNT forests on bare SiO_2/Si or quartz substrates, greatly simplifying the synthesis process.[21] Considering the startup and shutdown times for batch processing (which often consume >95% of runtime), a continuous roll-to-roll (R2R) process is expected to greatly reduce time, energy, and cost needed to produce VACNT forests.[22] Here, we describe a commercially viable low temperature R2R process for growing VACNTs on inexpensive Al foil current collectors to achieve continuous production of CNT-based EDLC electrodes. Our electrochemical studies on

single electrodes show that VACNT forests produced using our R2R method exhibit nearly four-times higher capacitance (~50 F g^{-1}) than randomly entangled buckypapers prepared from commercial CNTs (~13 F g^{-1}). Additionally, VACNTs produced using our R2R method displayed significantly lower contact resistance compared to CNT buckypapers. More importantly, we observed that symmetric supercapacitors comprised of R2R-produced VACNT electrodes exhibited high power densities (1270 W kg^{-1}) and energy densities (11.5 Wh kg^{-1}) with no loss in performance over more than a thousand cycles, compared to CNT buckypapers (650 W kg^{-1} and 5 Wh kg^{-1}).

2.2 Experimental methods

2.2.1 Materials

Tetrabutylammonium hexafluorophosphate ($TBAPF_6$, 98%), tetraethylammonium tetrafluoroborate ($TEABF_4$, >99%), O-xylene (98%), and ferrocene (98%) were purchased from Sigma-Aldrich. Al foil substrates were purchased from Sigma-Aldrich (99.9%) or from the local grocery store (Reynolds). Acetonitrile (Certified ACS) and propylene carbonate (99%) were obtained from Fisher Scientific. Multi-walled carbon nanotubes (30-50 nm outer diameter, SKU: 030106) were purchased from CheapTubes.com. Separators (Celgard® 2325, 25 μm-thick microporous trilayer PP/PE/PP membrane) were provided by Celgard. Deionized water was obtained from an in-house distillation apparatus followed by a water purification unit (Millipore™ Milli-Q Academic).

2.2.2 Electrode fabrication

Stationary CVD process. VACNT arrays were grown by CVD in a quartz tube with diameter of 2". Both ends of the tube were closed with stainless steel end-caps. The tube was placed in a furnace with two heating zones (reacting zone-40", and preheating zone-20"). A programmable syringe pump was used to inject the precursor (ferrocene in xylene, 0.5 at. % Fe), with the tip of the injection nozzle located at the center of the preheating zone. Al foils (Reynolds Wrap, 2 cm ×15 cm) cleaned with acetone were placed in the center of the reacting zone of the furnace. The system was heated up to 600 °C under a flow of Ar (500 sccm)/H_2 (100 sccm). At 600 °C, the precursor was injected into the tube at a rate of 1.5 ml h^{-1}, along with C_2H_2 (30 sccm).

R2R process. VACNT arrays were grown using ambient pressure CVD in a tube furnace (Thermo Fisher Scientific, TF55030A-1, Lindberg/Blue M Mini-Mite Tube Furnaces, 1100°C) that has an active zone of approximately 24 cm. The Al foil (Reynolds Wrap) which is used as the substrate is first swabbed clean with acetone. Al foil ribbon is then threaded through the quartz reaction tube and attached to the uptake spool before allowing the system to heat to 600°C under 500 sccm of Ar. Once the reaction temperature (600 °C) was reached, the uptake motor was activated to reel the foil at a rate of 0.5 cm min^{-1}. H_2 and C_2H_2 are then introduced at 50 sccm and 30 sccm respectively, as well as the precursor solution of 0.5 wt% ferrocene in xylene, which was injected into the tube at 0.3 ml h^{-1} using a programmable syringe pump (New Era NE-1000).

Preparation of CNT buckypapers (BP). CNTs (CheapTubes.com) were dispersed in 1 wt% aqueous solution of sodium dodecyl sulfate (SDS) using a tip

sonicator probe (1/8" diameter, Branson 250) with a power of 75 W for 15 minutes. Subsequently, the suspension was poured onto a polyamide filtration membrane (Whatman, 0.45 μm pore diameter) and filtered using a vacuum filtration setup (Synthware Filtration Apparatus, Kemtech America). The filter cake on the supporting filter membrane was washed with distilled water several times, and then oven dried at 60 °C for 8 h. The resulting film was peeled off the membrane to yield a freestanding CNT electrode (~125 μm thick).

2.2.3 Characterization

SEM. The surface morphology of the films was observed using scanning electron microscopy (SEM, Hitachi SU-6600) with an accelerating voltage of 20 kV.

Carbon content. Prior to electrochemical characterization, substrates were cut with dimensions of 1.1 cm x 1.4 cm and weighed in a balance (Ohaus Discovery Semi-Micro Balance, 0.01 mg). The mass of carbon on each unique sample was calculated after electrochemical characterization by mechanically removing the carbon from the aluminum substrate and weighing the aluminum substrate after drying at 90 °C.

Electrochemical analysis. Each sample was characterized in electrolyte solutions using cyclic voltammetry (CV) (1000, 300, 100 mVs^{-1}), galvanostatic charge/discharge cycles and electrochemical impedance spectroscopy (EIS) (0 V DC bias, 0.1 – 10000 Hz, 10 mV RMS). The CV current was normalized by scan rate (ν) and either substrate area to give F cm^{-2} or carbon mass to give F g^{-1}. Two analytical systems were used for electrochemical characterization: 1) a 3-electrode Teflon cell for single electrode evaluation and 2) a 2-electrode cell for symmetric supercapacitor testing (MTI Corp). In

the 3-electrode cell, the VACNT on Al foil substrates were fastened in a Teflon cell and contacted to the potentiostat (Princeton Applied Research VersaSTAT 4) leads with a Ti foil contact. A silver/silver ion electrode (Ag/Ag^{+}) was used as the pseudoreference electrode and a Pt mesh was used as the counter electrode. CV and galvanostatic charge discharge was carried out in the range of -1 to 1.3 V (up to 2 V). In the coin cell apparatus (2-electrode cell), EDLC devices were tested using symmetric samples as the electrodes separated by a Celgard (2325) trilayer separator. In this set up, one of the carbon samples is designated as the working electrode and the other designated as the reference/counter electrode. The cell performance was evaluated using CV, EIS and galvanostatic charge discharge measurements over a cell voltage range of 0 to 2.3 V.

2.3 Results and discussion

We developed a R2R process to synthesize VACNTs directly on a continuously drawn Al foil substrate (~ 2 cm wide, 0.63 mm thick) using the floating catalyst ferrocene-xylene method at a rate of 0.5 cm min^{-1} (**Figure 2.1**). At this rate, any given section of the foil has a reactor residence time of ~20 minutes, resulting in the growth of a forest containing 50 µm tall VACNTs (**Figure 2.1c**). As the foil is drawn through the slotted end caps of the CVD reactor, a solution of ferrocene in xylene (0.5 at. % Fe) is injected though the inlet nozzle at a rate of 0.3 ml h^{-1} in the presence of Ar, C_2H_2 and H_2 gases (500, 30 and 50 sccm, respectively). For comparison, VACNT electrodes were also prepared in a stationary CVD process by placing a long (15 cm x 2 cm) strip of Al foil at the center of a quartz tube and applying similar reaction conditions as described

above for the R2R process but with closed end caps. In the stationary and continuous CVD processes, we utilize a relatively low growth temperature of 600°C, which is safely below the melting point of aluminum (no changes in mechanical properties were observed on the Al foil). Also, we used commercially-available CNTs to prepare buckypapers containing randomly oriented nanotubes. For ease of discussion, samples are labeled as follows: i) R2R process VACNTs (R2R), ii) stationary CVD process (sCVD), and iii) buckypapers (BP).

In the stationary CVD process, the amount of CNTs grown depends on the runtime and substrate location relative to the injection nozzle (**Figure 2.2a**) due to the depletion of the precursor towards the downstream end of the furnace. We identified nearly uniform growth areas (see substrate locations 1-8 in **Figure 2.2a inset**) with CNT height ~50 μm (**Figure 2.2d inset**) and measured their electrochemical performance of each electrode type in three different electrolytes to determine optimal electrolyte properties (**Figures 2.2b-d**). It is worth noting that aqueous solutions (acidic or basic) are incompatible with Al foil substrates and therefore were not used.

The electrochemical properties of CNT electrodes were initially characterized using cyclic voltammetry (CV) and electrical impedance spectroscopy in a three-electrode configuration to determine the single electrode properties as a function of CNT growth time and electrolyte type. CV profiles were recorded at various scan rates and normalized by scan rate and mass to obtain specific capacitance (F g^{-1}) of the VACNT electrodes. The effect of the electrolyte type is apparent in **Figure 2.2b**, which shows the normalized CV profiles (1000 mV s^{-1}) for sCVD samples grown for 1 h in various

electrolytes. The higher conductivity of the organic salts in acetonitrile (MeCN) compared to propylene carbonate (PC) and the smaller ion size of $TEABF_4$ (~0.45 nm) relative to $TBAPF_6$ (~0.8 nm) led to the highest specific capacitance of 102 F g^{-1} in $TEABF_4$-MeCN. Slight non-idealities are observed in the CV profiles, which can be attributed to the weak (broad) redox peak of the Fe catalyst (~0.5 V) in the VACNT electrode, and the use of MeCN on Al foil, which leads to more noticeable electrode polarization effects compared to PC.

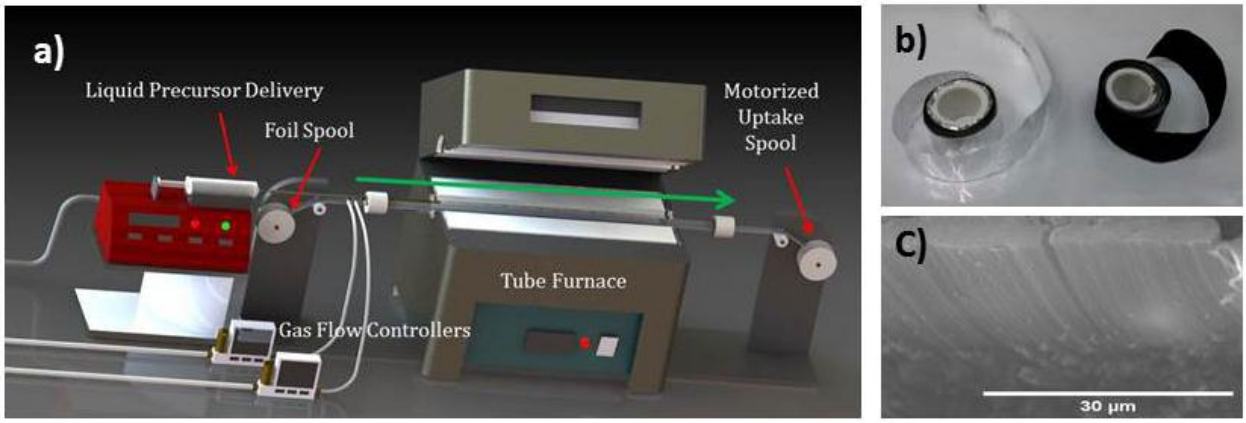

Figure 2.1. a) A schematic of the R2R process for growing vertically aligned CNTs on Al. foil, b) Al foil spools before and after CNT growth in the R2R process, c) a typical scanning electron microscopy (SEM) image of R2R-grown VACNTs.

Impedance analysis verifies the superior performance of the TEABF4-MeCN solution over the other electrolytes. Due to the nature of the ion-adsorption and ion-diffusion processes within a carbon electrode, each material exhibits a strong frequency dependent capacitance. On short time scales (high frequency), ions can only accumulate on the outermost surface of the polarized electrodes, whereas on long time scales (low frequency), ions have sufficient time to diffuse into the pores of the electrodes. The Bode plot of the imaginary component of the capacitance (C'') vs frequency (f) showed that the

sCVD samples exhibited shortest relaxation time ($\tau_0=1/f_{peak}$) in $TEABF_4$-MeCN, indicating the fastest discharge process (**Figure 2.2c**).[23, 24] At low (high) frequency, capacitance (resistance) dominates the impedance of the circuit and a crossover occurs at f_{peak}. Thus, τ_0 can be used as a factor of merit for supercapacitors and may be interpreted as the minimum time to discharge 50% of the total energy.[25]

The influence of CNT growth time on the specific capacitance is shown in **Figure 2.2d**, which shows an initial decrease, followed by a steady increase in capacitance with growth time. The higher capacitance values obtained for electrodes grown for 15 minutes is attributed to the capacitive contribution from the underlying Al foil that is not completely covered by VACNTs, and the possible error in measuring the mass of small amounts of VANCTs. For longer growth times, the increasing specific capacitance with mass arises from an increase in CNT areal density, which in turn affects the accessible surface area. Indeed, when normalized by the areal density, sCVD samples exhibited a linear increase in specfic capacitance (**Figure 2.3**).

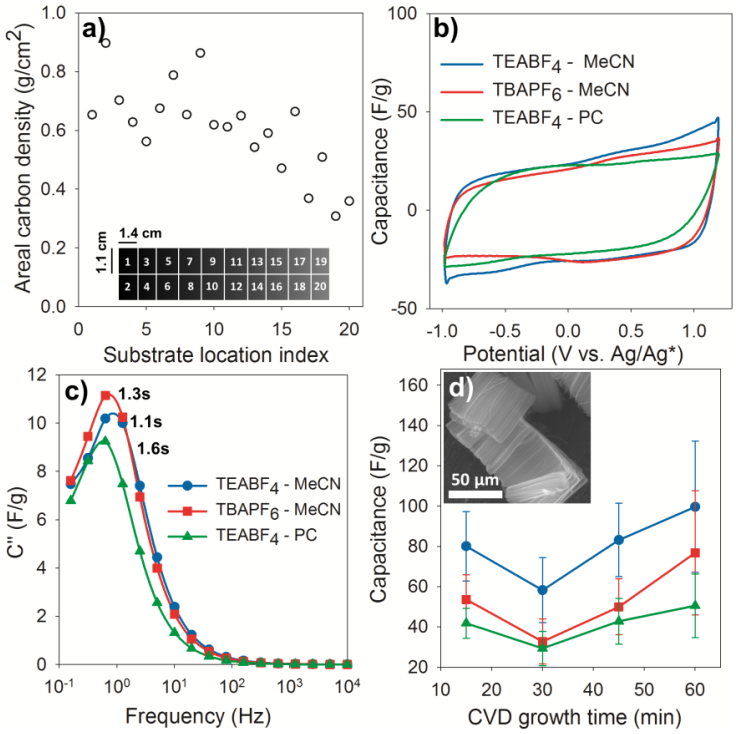

Figure 2.2. a) Spatial distribution of VACNT areal density in sCVD samples, b) CV profiles at 1000 mV s^{-1} in a three-electrode configuration with various electrolytes, c) Bode plots of the normalized imaginary capacitance (C") vs frequency for sCVD samples in the three electrolytes, and d) normalized capacitance vs voltage profiles (ν = 100 mV s^{-1}) for sCVD samples grown for 15, 30, 45, and 60 min (bars represent combined error from mass and CV data). The inset in panel d is a representative SEM image of sCVD VACNT forest grown for 1 h.

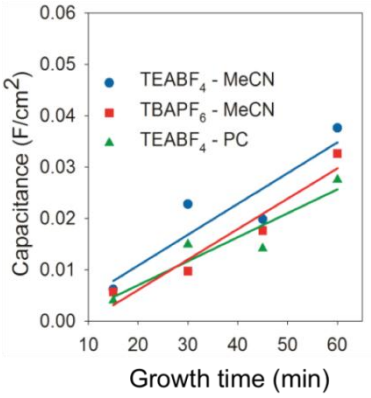

Figure 2.3. The capacitance of sCVD samples in three different electrolytes normalized by area shows a linear increase with increase in growth time.

Using the best conditions determined on sCVD electrodes in terms of VACNT growth time (1 h) and electrolyte type (TEABF4-MeCN), we compared the electrochemical performance sCVD, R2R, and BP electrodes at a scan rate of 100 mV s^{-1} (**Figure 2.4a**). Electrodes prepared at low temperature (600 °C), whether stationary (sCVD) or in the continuous R2R process (R2R), exhibited notably improved performance (51 F g^{-1}) compared to BP electrodes with randomly oriented CNTs (13.6 F g^{-1}). As shown in **Figure 2.4b**, sCVD and R2R electrodes show a linear dependence of current on scan rate, indicative of an ion-adsorption controlled energy storage mechanism. BP electrodes, however, exhibited a linear dependence of current on square root of scan rate (**Figure 2.4b inset**), indicating an ion-diffusion controlled process, which may be due to the thickness of the electrodes. Consistent with the CV analysis (cf. **Figure 2.4a**), galvonstatic discharge measurements (**Figure 2.4c**) show a similar trend in performance with CNT electrode type, where sCVD electrodes had the highest charge capacity of 36.7 mAh g^{-1} and R2R and BP electrodes showed values of 24.8 and 13.6 mAh g^{-1}, respectively.

Although the charge capacity of R2R electrodes is slightly lower relative to sCVD samples, they exhibit notably faster discharge times as reflected by their lower time constants (630 ms vs 1.26 s) determined from the Bode plots of *C''* vs frequency. Furthermore, the Nyquist plot of the electrical impedance measurements (**Figure 2.5**) showed that sCVD and R2R samples display a relatively low internal resistance compared to BP electrodes as the CNTs are directly grown from the current collector surface.

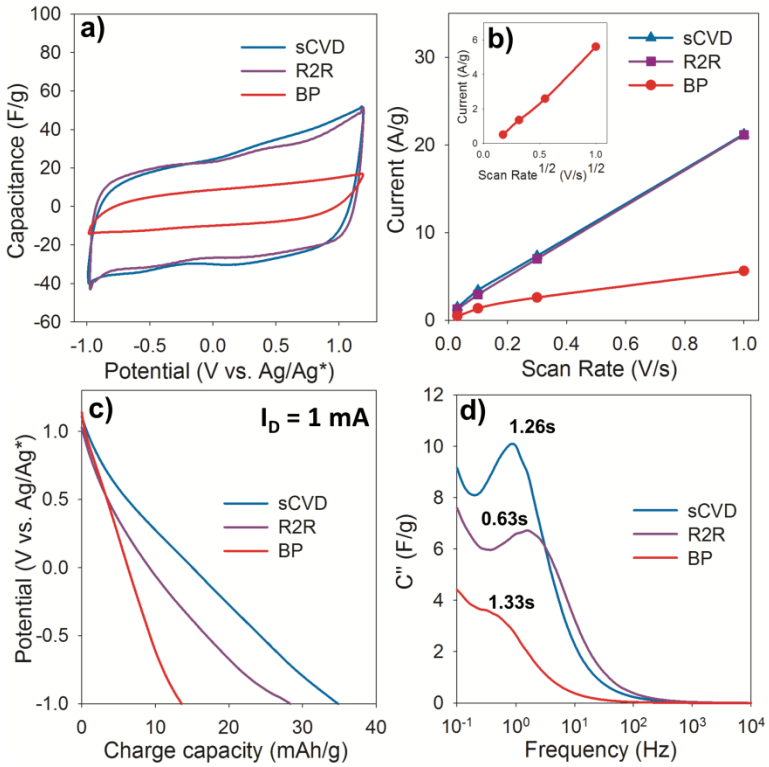

Figure 2.4. Electrochemical properties of single electrodes comprised of sCVD, R2R, and BP samples. a) Cyclic voltammograms of various CNT electrodes in $TEABF_4$-MeCN electrolytes normalized by mass and scan rate (300 mV s^{-1}), b) Normalized peak current (I_p) vs scan rate (v) (inset: I_p vs $v^{1/2}$ for BP electrodes), c) Galvanostatic discharge profiles (discharge current (I_D) = 1 mA) in $TEABF_4$ - MeCN, and d) Bode plots of normalized imaginary capacitance (C") vs frequency for the three electrodes.

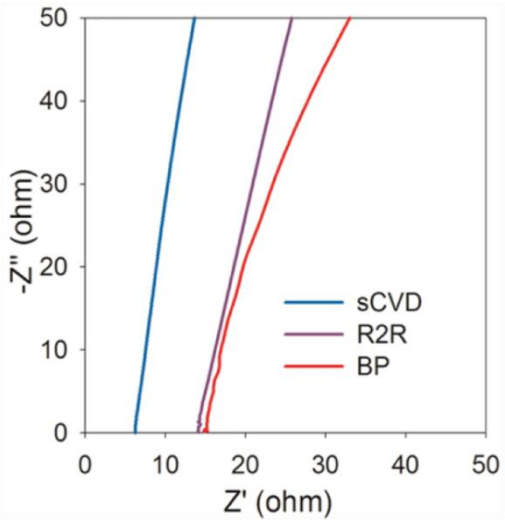

Figure 2.5. Nyquist plot for sCVD (blue), R2R (purple), and BP (red) electrodes.

Symmetric EDLC cells were fabricated using electrodes comprised of each type of VACNTs. Prior to cell assembly, each electrode and separator (Celgard 2325, 25 μm thick) were soaked overnight (~20 hours) in the $TEABF_4$-MeCN. The separator was placed between the two electrodes in a coin cell apparatus (MTI Corp), as shown in **Figure 2.6a**. CV profiles were recorded at various scan rates over a cell voltage range of 0 to 2.3 V, which are shown for R2R cells in **Figure 2.6b**. From the specific capacitance plots shown in **Figure 2.6c**, sCVD and R2R samples show similar electrochemical properties with a notably higher specific capacitance than BP electrodes. As observed in the single electrode measurements, the Nyquist plot for EDLC cells (**Figure 2.6d**) shows significantly lower internal resistance for sCVD and R2R samples compared to BP electrodes because the CNTs are chemically bound to the substrate rather than simply placed in physical contact.

The charge-discharge characteristics of EDLC cells containing different CNT electrodes with the same applied current (~2 mA) are shown in **Figure 2.6e**. Each cell displays a similar discharge profile; however, devices comprised of the VACNTs from the R2R process showed higher electrode polarization upon charging to the full-charge potential, possibly due to slight differences in electrode masses across the cell. It is difficult to determine the electrode mass prior to testing since the mass is determined by physically separating CNTs from Al foil, preventing us from fabricating a truly symmetric capacitor. When these discharge characteristics are normalized by mass and current (**Figure 2.6e**), we observe a similar trend in capacity as in the single electrode measurements, with the highest charge capacity of 9.55 mAh g^{-1} observed in the R2R

samples and 9.13 mAh g^{-1} in sCVD samples. From the discharge measurements, the energy and power density of the electrodes were calculated (**Table 2.1**) using the following equations:

$$W = \frac{1}{2}CV^2 \quad (1)$$

where *W* is the energy density, *C* is the device capacitance and *V* is the cell voltage, and

$$P = \frac{\Delta W}{\Delta t} \quad (2)$$

where *P* is the power density, and Δt is the discharge time. The specific capacitance of the devices was calculated from the cyclic voltammetry measurements using the following equation:

$$C_{sp} = \frac{\int I dV}{2\Delta V m \nu} \quad (3)$$

where I is current, ΔV is the voltage range, m is the carbon mass, and ν is scan rate (100 mV s^{-1}). As expected, we found good agreement between the single electrode capacitance values determined above, which are approximately 4 times the device capacitance (a device with 2 electrodes has half the capacitance and twice the mass). Lastly, we observed that the performance of all the EDLC cells was stable for over multiple thousand cycles without any degradation (**Figure 2.6f**) comparable to other inert carbon-based EDLCs.

Table 2.1. Performance metrics of symmetric EDLC cells.

Carbon (type)	Capacitance ($F\ g^{-1}$)	Power ($W\ kg^{-1}$)	Energy ($Wh\ kg^{-1}$)	τ_0 (sec)
R2R	9.6	1270	11.4	0.040
sCVD	9.1	1210	10.2	0.032
BP	4	650	4.9	0.013

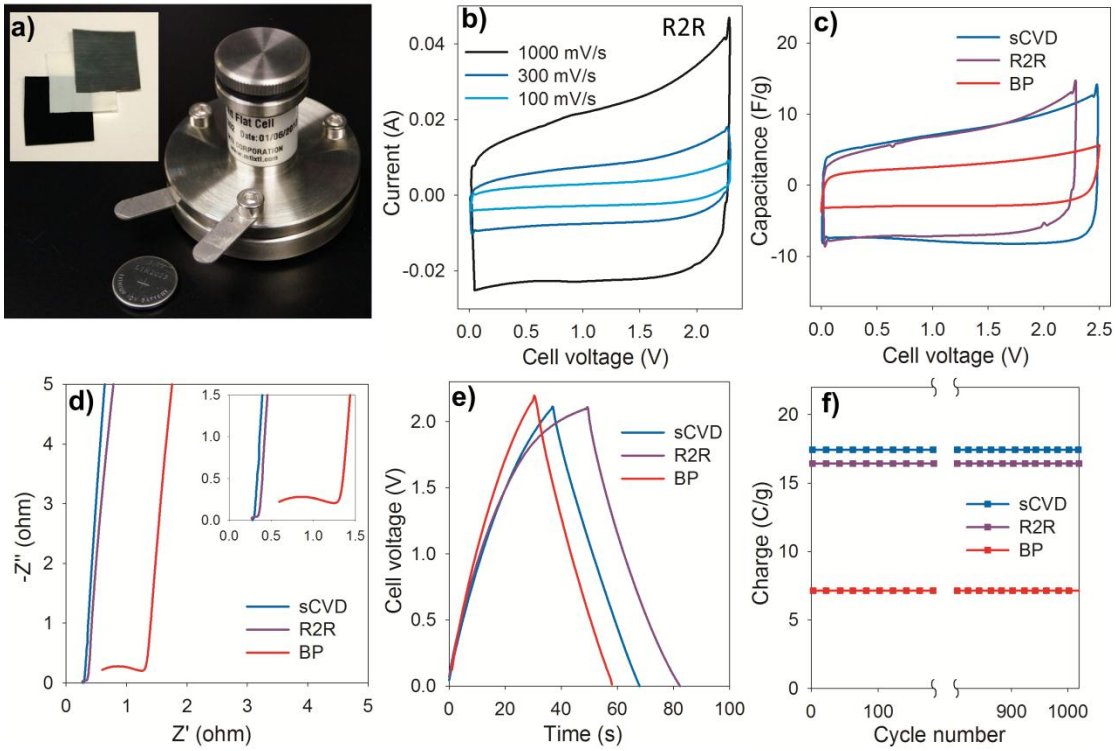

Figure 2.6. Electrochemical characteristics of symmetric EDLC cells comprised of VACNT electrodes. a) Photograph of the coin cell apparatus (inset: CNT electrodes and separator), b) Cyclic voltammetry characteristics of and EDLC containing R2R electrodes at various scan rates, c) Normalized CV profiles ($F\ g^{-1}$) for devices containing different CNT electrodes measured at a scan rate of 1000 $mV\ s^{-1}$, d) Nyquist plot for each of the devices described in (c), e) Charge-discharge measurements (1 full cycle at ±2 mA) for the devices consisting of sCVD (3.4 mg), R2R (3.2 mg), and BP (6.5 mg) electrodes, and f) Charge capacity of each device as a function of cycle number for more than 1000 cycles.

2.4 Conclusions

We have demonstrated a roll-to-roll process to synthesize VACNT electrodes directly on Al foils at a low temperature (600 °C) using a ferrocene-xylene solution-based method. Our R2R synthesis method is able to produce VACNTs on Al foils with comparable electrochemical performance to the stationary batch process. EDLC cells assembled with electrodes from the R2R process exhibited the highest performance in terms of capacitance (9.6 F g^{-1}), energy density (11.5 Wh kg^{-1}) and power density (1270 W kg^{-1}), which were significantly higher than cells comprising BP electrodes (650 W kg^{-1} and 4.9 Wh kg^{-1}). Each device demonstrated excellent cycle stability with no loss in performance over more than a thousand cycles suggesting R2R as a viable process for large scale manufacturing of EDLC electrodes. While the performance is not as good as activated carbon, these materials are promising for applications in li-ion batteries to reduce resistance at the electrodes.

2.5 References

1. Ghosh, A.; Lee, Y. H., Carbon-Based Electrochemical Capacitors. *ChemSusChem* **2012,** 5, (3), 480-499.
2. Miller, J. R.; Simon, P., Electrochemical Capacitors for Energy Management. *Science* **2008,** 321, (5889), 651-652.
3. Signorelli, R.; Ku, D. C.; Kassakian, J. G.; Schindall, J. E., Electrochemical Double-Layer Capacitors Using Carbon Nanotube Electrode Structures. *Proceedings of the IEEE* **2009,** 97, (11), 1837-1847.
4. Simon, P.; Gogotsi, Y., Charge storage mechanism in nanoporous carbons and its consequence for electrical double layer capacitors. *Philosophical Transactions of the Royal Society of London A: Mathematical, Physical and Engineering Sciences* **2010,** 368, (1923), 3457-3467.
5. De Volder, M. F. L.; Tawfick, S. H.; Baughman, R. H.; Hart, A. J., Carbon Nanotubes: Present and Future Commercial Applications. *Science* **2013,** 339, (6119), 535-539.
6. Jiang, Y.; Lin, L., A two-stage, self-aligned vertical densification process for as-grown CNT forests in supercapacitor applications. *Sensors and Actuators A: Physical* **2012,** 188, 261-267.
7. Honda, Y.; Takeshige, M.; Shiozaki, H.; Kitamura, T.; Yoshikawa, K.; Chakrabarti, S.; Suekane, O.; Pan, L.; Nakayama, Y.; Yamagata, M.; Ishikawa, M., Vertically aligned double-walled carbon nanotube electrode prepared by transfer methodology

for electric double layer capacitor. *Journal of Power Sources* **2008,** 185, (2), 1580-1584.

8. Rakesh, S.; Xianfeng, Z.; Saikat, T., Electrochemical double layer capacitor electrodes using aligned carbon nanotubes grown directly on metals. *Nanotechnology* **2009,** 20, (39), 395202.
9. Ren, Z. F.; Huang, Z. P.; Xu, J. W.; Wang, J. H.; Bush, P.; Siegal, M. P.; Provencio, P. N., Synthesis of Large Arrays of Well-Aligned Carbon Nanotubes on Glass. *Science* **1998,** 282, (5391), 1105-1107.
10. Khavrus, V. O.; Weiser, M.; Fritsch, M.; Ummethala, R.; Salvaggio, M. G.; Schneider, M.; Kusnezoff, M.; Leonhardt, A., Application of Carbon Nanotubes Directly Grown on Aluminum Foils as Electric Double Layer Capacitor Electrodes. *Chemical Vapor Deposition* **2012,** 18, (1-3), 53-60.
11. Niu, C.; Sichel, E. K.; Hoch, R.; Moy, D.; Tennent, H., High power electrochemical capacitors based on carbon nanotube electrodes. *Applied Physics Letters* **1997,** 70, (11), 1480-1482.
12. Endo, M.; Hayashi, T.; Kim, Y.-A., Large-scale production of carbon nanotubes and their applications. In *Pure and Applied Chemistry*, 2006; Vol. 78, p 1703.
13. Biró, L. P.; Horváth, Z. E.; Szalmás, L.; Kertész, K.; Wéber, F.; Juhász, G.; Radnóczi, G.; Gyulai, J., Continuous carbon nanotube production in underwater AC electric arc. *Chemical Physics Letters* **2003,** 372, (3–4), 399-402.

14. Bethune, D. S.; Klang, C. H.; de Vries, M. S.; Gorman, G.; Savoy, R.; Vazquez, J.; Beyers, R., Cobalt-catalysed growth of carbon nanotubes with single-atomic-layer walls. *Nature* **1993,** 363, (6430), 605-607.
15. Yudasaka, M.; Komatsu, T.; Ichihashi, T.; Iijima, S., Single-wall carbon nanotube formation by laser ablation using double-targets of carbon and metal. *Chemical Physics Letters* **1997,** 278, (1–3), 102-106.
16. Arepalli, S., Laser Ablation Process for Single-Walled Carbon Nanotube Production. *Journal of Nanoscience and Nanotechnology* **2004,** 4, (4), 317-325.
17. Qin, L. C., CVD synthesis of carbon nanotubes. *Journal of Materials Science Letters* **1997,** 16, (6), 457-459.
18. Huynh, C. P.; Hawkins, S. C., Understanding the synthesis of directly spinnable carbon nanotube forests. *Carbon* **2010,** 48, (4), 1105-1115.
19. Bandow, S.; Asaka, S.; Saito, Y.; Rao, A. M.; Grigorian, L.; Richter, E.; Eklund, P. C., Effect of the Growth Temperature on the Diameter Distribution and Chirality of Single-Wall Carbon Nanotubes. *Physical Review Letters* **1998,** 80, (17), 3779-3782.
20. Keskar, G.; Rao, R.; Luo, J.; Hudson, J.; Chen, J.; Rao, A. M., Growth, nitrogen doping and characterization of isolated single-wall carbon nanotubes using liquid precursors. *Chemical Physics Letters* **2005,** 412, (4–6), 269-273.
21. Andrews, R.; Jacques, D.; Rao, A. M.; Derbyshire, F.; Qian, D.; Fan, X.; Dickey, E. C.; Chen, J., Continuous production of aligned carbon nanotubes: a step closer to commercial realization. *Chemical Physics Letters* **1999,** 303, (5–6), 467-474.

22. Guzmán de Villoria, R.; Hart, A. J.; Wardle, B. L., Continuous High-Yield Production of Vertically Aligned Carbon Nanotubes on 2D and 3D Substrates. *ACS Nano* **2011,** 5, (6), 4850-4857.
23. Ghosh, A.; Le, V. T.; Bae, J. J.; Lee, Y. H., TLM-PSD model for optimization of energy and power density of vertically aligned carbon nanotube supercapacitor. *Scientific Reports* **2013,** 3, 2939.
24. Pech, D.; Brunet, M.; Durou, H.; Huang, P.; Mochalin, V.; Gogotsi, Y.; Taberna, P.-L.; Simon, P., Ultrahigh-power micrometre-sized supercapacitors based on onion-like carbon. *Nat Nano* **2010,** 5, (9), 651-654.
25. Taberna, P. L.; Simon, P.; Fauvarque , J. F., Electrochemical Characteristics and Impedance Spectroscopy Studies of Carbon-Carbon Supercapacitors. *Journal of The Electrochemical Society* **2003,** 150, (3), A292-A300.

CHAPTER THREE

A FACILE AND SCALABLE APPROACH TO FABRICATING FREE-STANDING POLYMER-CARBON NANOTUBE COMPOSITE ELECTRODES

3.1 Introduction

Rapid growth in the demand for electrical energy storage continues to encourage the development of new materials and devices. With their ability to improve the performance of batteries or provide high-power, a recyclable and safe alternative such as supercapacitors has experienced tremendous growth in this industry. Supercapacitors, which typically comprise high-surface area, inert carbonaceous electrode materials, offer the benefits of high power density, rapid charge/discharge, and long lifetime. Even with these important advantages, carbon materials (e.g., activated carbon, carbon nanotubes, graphene) are limited by relatively low energy density as a consequence of their physical charge storage mechanism, electrical double layer capacitance (EDLC), which is related to ion adsorption at the electrode surface. As we approach the maximum theoretical surface area in carbons, further increases in energy density are no longer attainable. On the other hand, electroactive materials such as metal oxides and electroactive conducting polymers (ECPs) can be prepared with relatively high surface areas, but are also able to store charge through Faradaic charge transfer in addition to EDLC. Metal oxides exhibit high Faradaic capacitance in aqueous solutions with good redox stability, but are limited by material cost, low operating voltage ranges, and the lack of scalable synthetic methods.[1,2]

ECPs, such as polypyrrole (PPY), polyaniline (PANI), and poly(3,4-ethylenedioxythiophene) (PEDOT), provide a low-cost, large specific capacitance alternative to carbon materials and metal oxides[3-6] and can be easily prepared through various routes[7] from cheap monomers in large quantities. However, ECPs often suffer from poor cycle stability due to polymer over-oxidation stresses caused by volumetric changes that accompany the charge-discharge processes associated with ion insertion and removal.[8] To improve their performance and stability, significant efforts have focused on creating micro or nanostructured ECP electrodes by modifying the synthesis processes, which enhances their mechanical and electrochemical properties.[8-10] Another approach to the same goal involves integrating a complementary material to reinforce and support the polymeric structure.[11, 12] Carbon nanotubes (CNTs) are attractive for this purpose due to their excellent structural properties, electronic conductivity and chemical stability. CNTs improve the cycle life and mechanical properties of ECPs since CNTs adapt easily to changes in volume,[13] and also introduce new electronic properties based on interactions between the two materials. Furthermore, the adaptation of such compositions helps overcome the low conductivity of ECPs in the neutral (or reduced) state and also increase electronic transport in thick electrodes.[14] Of equal importance, the addition of ECPs decreases CNT bundling and enhances the charge storage capacity compared to CNTs electrodes.

In-situ chemical polymerization is the prevalent method for preparing ECP/CNT composites, which consists of oxidative polymerization of ECPs in a CNT suspension and pressing the dry material into a pellet.[15] Through this approach, ECPs and CNTs are

integrated on a molecular scale[16-20], increasing conductivity[21], although, homogeneity depends on the CNT dispersion and ECPs often prefer to grow on themselves rather than distributing homogeneously along the CNTs leading to polymer aggregation[17] . High specific capacitance values (500 F g^{-1})[22] have been obtained by electrochemically polymerizing ECPs on CNTs due to strong electrochemical interaction between the two materials.[23] Nevertheless, this method is limited to low amounts of polymer because as the film grows thicker it blocks electrolyte access to the CNTs. In melt compounding, CNTs are directly dispersed into a polymer melt; however, locally homogeneous states are difficult to achieve without breaking down the entangled CNTs.[20] A simple alternative to produce ECP/CNT composites involves mixing pre-synthesized ECP with CNTs[24, 25], which is advantageous in terms of scalability and cost-effectivity.[14] Lota et al.[25] prepared composite electrodes by pressing a mixture of PEDOT and CNTs into pellets and obtained a single-electrode capacitance value of 95 F g^{-1} (at 2 mV s^{-1}), which possessed improved conductivity and cycle stability compared to PEDOT, albeit with significant diffusion limitations.

In this work, we present a simple, low-cost approach to fabricating free-standing ECP/CNT composite electrodes using a sequential dispersion-filtration process. After ECP synthesis, ECP/CNT dispersions (50/50 by wt.) are prepared in aqueous solutions containing sodium dodecyl sulfate (SDS) using ultrasonication, and then immediately filtered through a polyamide membrane with laboratory scale vacuum filtration. After electrodes are dried, robust, free-standing composite ECP/CNT paper electrodes are obtained, yielding high specific capacitance values up to 448 F g^{-1} (at 10 mV s^{-1}). In this

process, no binder or pressure is needed to obtain efficient electrode performance. Considering the process simplicity, low cost and amenability to high throughput processing, our new approach to composite electrode fabrication provides a unique application to scalable, high power and energy supercapacitor electrode manufacturing.

3.2 Experimental methods

3.2.1 Materials

Multi-walled carbon nanotubes were purchased from CheapTubes (dia.=30-50 nm, length=10-20 μm) and NanoTech Labs (dia.=70-80 nm, length=700-800 μm), and used as received. Polypyrrole (PPY), Polyaniline (PANI) and Poly(3,4-ethylenedioxythiophene) (PEDOT) were synthesized by a labmate using oxidative polymerization reported elsewhere. [26, 27, 28, 29] Briefly, PPy was prepared using 2.5 M $FeCl_3$ in methanol at 4°C for 6 h.[26] PANI was synthesized in aqueous HCl (1 M), using ammonium persulfate (0.54 M) as an oxidant at 4°C for 2 h.[27] PEDOT was synthesized using $Fe(NO_3)_3$ in an aqueous solution containing sodium poly(4-styrene sulfonate) (0.15 M) for 6 h.[28, 29] Deionized water was obtained from an in-house distillation apparatus followed by a water purification unit (Millipore™ Milli-Q Academic).

3.2.2 Electrode fabrication

The ECP/CNT composites were prepared by dispersing CNTs with an ECPs in aqueous solutions containing 1 wt.% SDS using a tip sonicator probe with a power of 75 W for 15 min. Subsequently, the suspension was poured onto a polyamide filtration membrane (Whatman, 0.45 μm pore diameter) and filtered using a vacuum filtration

setup. The filter cake on the supporting filter membrane was washed with distilled water several times, and then oven dried at 60 ˚C for 8h. The resulting films were peeled off the membrane yielding free-standing ECP/CNT resilient paper-like electrodes.

3.2.3 Characterization

Physical properties. The physical properties of the composite electrodes were investigated using scanning electron microscopy (SEM) and energy dispersive x-ray spectroscopy (EDAX).

Electrochemical properties. Composite electrodes were electrochemically evaluated as single electrodes using a potentiostat (Princeton Applied Research VersaSTAT 4) in aqueous 3 M H_2SO_4 solutions and in 1.5 M tetraethylammonium tetrafluoroborate ($TEABF_4$) in acetonitrile (MeCN). A Pt mesh was used as counter electrode, Ag/AgCl (sat'd KCl) and Ag/Ag* (0.1 M $AgNO_3$) electrodes were used as aqueous and non-aqueous pseudoreference electrodes, respectively. Electrochemical characterization included cyclic voltammetry (CV) at scan rates of 300 – 10 mV s^{-1}, electrochemical impedance spectroscopy (EIS) (0.5 V DC bias, 0.1 – 10000 Hz, 20 mV RMS) and galvanostatic charge/discharge cycles (C/D) at a current such that the discharge times equal ~60 s. The capacitance values were calculated from CV at a scan rate of 10 mV s^{-1}.

3.3 Results and discussion

In general, the introduction of ECPs into the MWNT papers created a more openly porous network (**Figure 3.1**) amenable to ion access to the electroactive materials

and enhanced the Faradaic processes. From the SEM at higher magnification (**Figure 3.1a**, >6000X), carbon nanotube agglomerates are observed sporadically throughout the electrode. With the addition of the ECP (**Figures 3.1 b-d**), it can be seen how the polymer acts as a binder and bridges the gaps between the CNT islands, enhancing the material's electrical properties. From **Figures 3.2b** and **3.2d**, the heterogeneous structure of PANI and PPY can be seen as well as these polymers tendency to aggregate in some areas forming clusters. In the PANI/CNT composites, the particles of 0.2 – 0.3 μm in size merge to form agglomerates with diameters of 2 – 6 μm. The PPY/CNT samples show a homogeneous distribution with uniform particle sizes of 0.1 – 0.3 μm, and unlike PANI, the individual particles did not fuse, although there is an uneven distribution of the polymer. PEDOT shows a webbed structure spread throughout the CNTs, suggesting the presence of a strong interaction between the two materials.

To find an estimate of the mass ratios present in the composite materials, thermal gravimetric analysis (TGA) and EDAX were performed (**Figures 3.1 e-f**). The decomposition of CNT paper occurs between 570 °C and 675 °C, while the ECP/CNT composites show an initial loss of moisture due to the hygroscopic nature of ECPs, followed by various mass loss transitions that include: structural decomposition, elimination of dopant molecules, thermal oxidation, and crosslinking.[30-32] The final decomposition at ~570°C is attributed to the oxidation of CNTs. From these TGA profiles, we estimated that the overall compositions of ECP in each composite are 70%, 57% and 50% for PANI, PPY and PEDOT, respectively. Interestingly, it appears that the CNTs exhibited a lower oxidation temperature when composites were more uniformly

mixed. It is plausible that the improved interaction between PEDOT/MWNT (compared to PPY/MWNT) prevents MWNT bundling which makes the CNTs more susceptible to oxidation.

Since the composite material is not completely homogeneous, EDAX was performed at different spots in the samples. **Figure 3.2f** shows the EDAX analysis of a section of a PPY/CNT sample. Areas where polymer seemed absent, elemental analysis confirmed that there was mainly carbon and the levels of oxygen were low indicating low water content in those areas. Where polymer was present, the levels of nitrogen (PANI, PPY) or sulfur (PEDOT) were higher, as well as the oxygen (water) levels, because ECPs absorb moisture, even when dried in vacuum for long times (>1 day). In the specific area evaluated with EDAX, PEDOT content ranged from 25 to 42 wt.%, due to its more homogeneous distribution along the sample. PANI and PPY were relatively localized because of their granular shape and tendency to aggregate, which resulted in compositions that varied from 7 to 70% and from 0 to 65%, respectively.

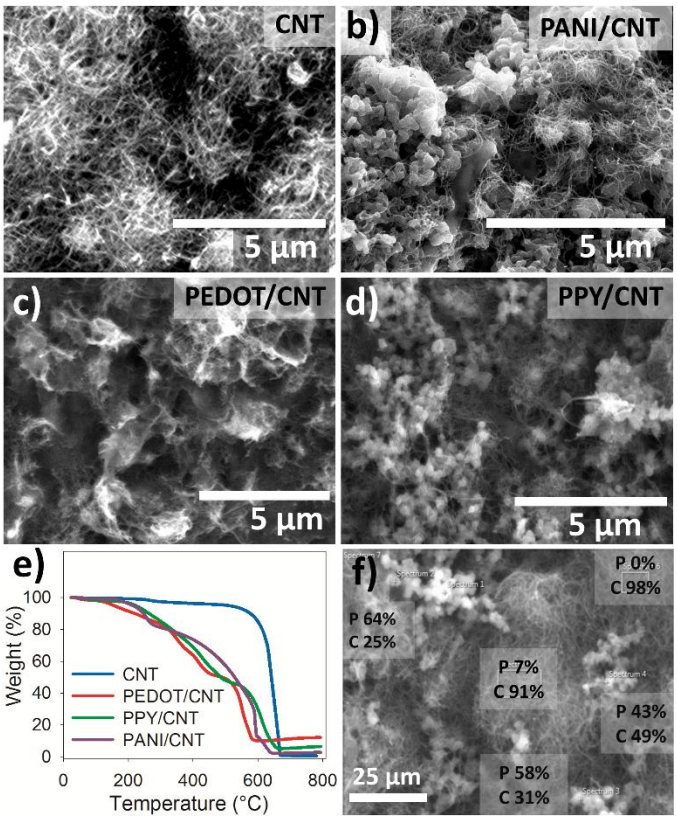

Figure 3.1. SEM images of composite electrodes made of a) CNT, b) PANI/CNT, c) PEDOT/CNT, and d) PPY/CNT, e) TGA profiles of the composite materials, f) EDAX of PPY/CNT composite, where P is polymer and C is carbon (%wt.).

Figures 3.2a and **3.2b** show the CV of ECP/CNT electrodes in aqueous and organic electrolytes, respectively. It can be observed from the area of the CV profiles, that the specific capacitances of CNT electrodes in aqueous and organic solutions of 27 F g^{-1} and 48 F g^{-1} are greatly increased with the incorporation of the conducting polymers, which are comparable to the highest values reported in literature.[13,25] PANI/CNT electrodes showed the highest specific capacitance values of 448 F g^{-1} in aqueous 3M sulfuric acid (aq) and 276 F g^{-1} in 1.5 M $TEABF_4$ in acetonitrile (org), which were similar to PPY/CNT (428 F g^{-1} aq, 315 F g^{-1} org). PEDOT/CNT electrodes displayed a notably lower specific capacitance (118 F g^{-1} aq, 95 F g^{-1} org) due to its relatively low theoretical

charge capacity of ~57 mAh g^{-1} compared to ~135 mAh g^{-1} and ~140 mAh g^{-1} for polypyrrole and polyaniline, respectively. It is also observed that although the active potential range of organic electrolytes is wider, the highest values of capacitance are obtained in aqueous electrolytes due to the higher conductivity of the electrolyte and smaller ion size. Nevertheless, there is an evident scan rate dependence of all the materials in both electrolyte types shown in **Figures 3.2c, 3.2d** for representative samples, which limits the material performance at very high charge/discharge rates. Compared to CNT electrodes, which display charge capacities of 10 mAh g^{-1} (20 mAh g^{-1}) in aqueous (organic) electrolytes, ECP/CNT composite electrodes exhibit improved charge capacities as high as 84 mAh g^{-1} (104 mAh g^{-1}) in similar electrolytes for PPY/CNT and PANI/CNT electrodes (**Figures 3.2g, 3.2h**). An increase of up to 8.4 times the CNT charge capacity is a result of the additional Faradaic energy storage in conducting polymers.

Figures 3.2e and **3.2f** show that the separation (ΔV), amplitude and width of the PANI redox peaks vary significantly with scan rate, which is attributed to the (i) granular structure of PANI that adds resistance to the mass diffusion and charge transfer processes and (ii) more open structure of PEDOT and PPY. The fact that the CNT electrodes also present diffusion limitations in the CV profiles indicates that the characteristics are associated with the electrode thickness (~125 μm), the presence of CNT bundles, and the random orientation of the CNTs.[14] As noted from the SEM images, this scan rate dependence is intensified for the ECP/CNT composites, because of polymer aggregates in some regions.

The presence of the electroactive polymer is also evidenced by the increase of diffusion and charge transfer resistances (inset of **Figures 3.2g** and **3.2h**), where the CNT electrode shows the fastest ion diffusion, followed by the PEDOT/CNT electrode. It can also be seen that the PEDOT/CNT electrode presents the smallest charge transfer limitations confirming a favorable interaction between the two materials. The effective charge transfer resistance of CNT electrode is associated with the resistance of ion transport into the CNT electrode and into the double layer within the porous structure. The highest resistance was found in PPY/CNT and PANI/CNT electrodes, which showed a bulky structure. The PEDOT/CNT electrode was quite similar to the bare CNT electrodes, presumably due to the intimate interaction between materials, thereby preventing further increases in ion adsorption or transfer resistance.

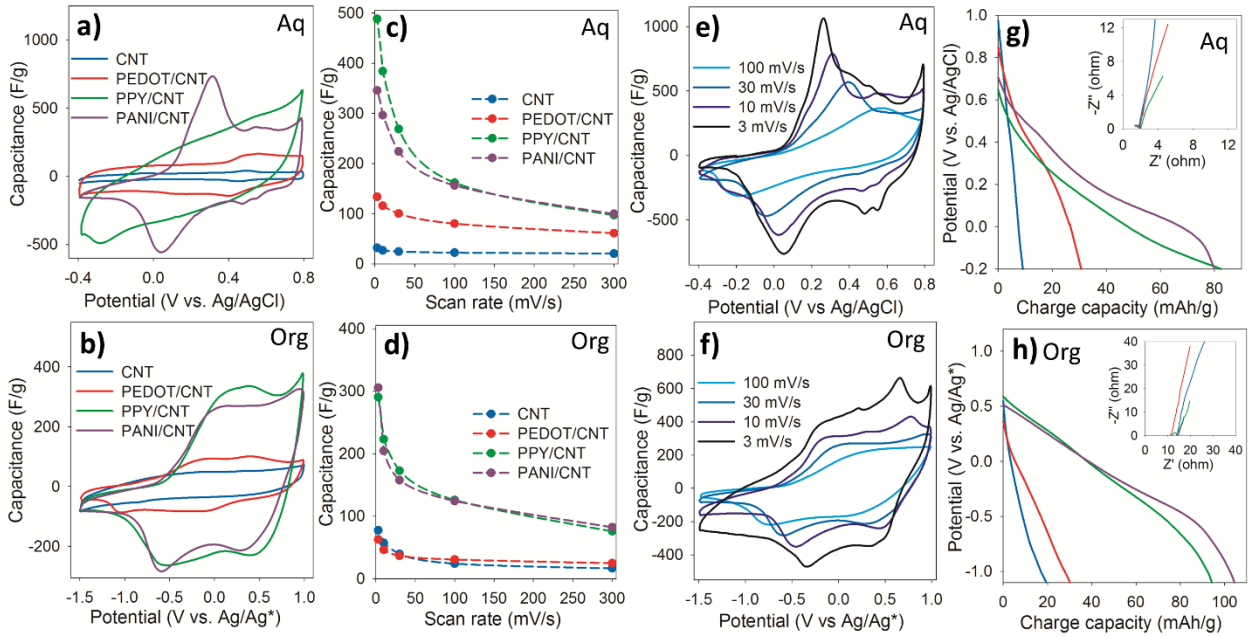

Figure 3.2. Single electrode tests of CNT and ECP/CNT electrodes. a) CV in 3 M H_2SO_4 at 30 mV s^{-1}, b) CV in 1.5 M $TEABF_4$ in acetonitrile at 30 mV s^{-1}, c) scan rate dependence of capacitance in 3 M H_2SO_4 and d) 1.5 M $TEABF_4$ in acetonitrile, e) capacitance vs scan rate for PANI/CNT in 3 M H_2SO_4 and f) 1.5 M $TEABF_4$ in acetonitrile. g) Galvanostatic discharge curves with the inset figure showing the Nyquist plot in 3 M H_2SO_4 and h) 1.5 M $TEABF_4$ in acetonitrile.

Symmetric cells of the composites were fabricated, as shown in **Figure 3.3a**, using Celgard 3401 and Celgard 2325 as separators for aqueous and organic systems, respectively. Results for cells comprising each ECP/CNT electrode with aqueous electrolyte are presented in addition to the results for devices comprising PEDOT/CNT in organic electrolyte. Since PPY and PANI are almost solely p-dopable, one electrode was polarized to 0.8 V and the other at 0 V in a 3 electrode cell prior to cell fabrication and testing. This allows both electrodes to alternately p-dope and de-dope during cell operation in the absence of an n-dopable material.

Figure 3.3b shows the device capacitive behavior at a 10 mV s^{-1}, in which cells comprising PANI/CNT showed the highest specific capacitance of 46 F g^{-1}, followed by PPY/CNT (20 F g^{-1}) and PEDOT/CNT (17 F g^{-1}). The organic PEDOT/CNT device showed similar capacitance (18 F g^{-1}) as the aqueous electrolyte, but over a much larger potential range. Since the energy and power densities depend on the voltage squared, the use of an electrolyte that can withstand a wide potential range, represents a significant increase in these properties, as calculated for PEDOT/CNT in acetonitrile: 744.3 W kg^{-1} and 12.2 Wh kg^{-1}, compared to the same material in aqueous system: 139.6 W kg^{-1} and 3.1 Wh kg^{-1} (for ~1 min discharge, current varies). PANI/CNT and PPY/CNT showed powers and energies of 283.4 W kg^{-1}, 4.8 Wh kg^{-1} and 114.6 W kg^{-1} and 2.3 Wh kg^{-1}, respectively, in aqueous electrolytes.

Each device exhibited a scan-rate dependence in the capacitance due to the diffusion-limited behavior in both electrolytes (**Figure 3.3c**), as expected from the performance of the individual electrodes. The highest scan-rate dependence was observed in the organic electrolyte, due to its lower ion conductivity evident from the Nyquist plot (**Figure 3.3d**). Even though the resistance of the organic electrolyte is notably larger, the effect of the larger potential range prevails. In the aqueous system, devices comprising the various ECP/CNT composites showed similar charge transfer resistances, with the lowest coming from PEDOT/CNT, as stated earlier due the presumed strong interaction between the two materials. From the Bode plot of imaginary capacitance vs frequency (**Figure 3.3e**), we found that cells with PEDOT/CNT had the shortest relaxation time constant,[14] indicating that this device can work efficiently at high discharge rates. The

PANI/CNT device shows the (i) slowest relaxation time constant due to polymer aggregation and redox kinetics, and (ii) largest charge capacity (8.1 mAh g^{-1}) due to its high theoretical charge capacity of ~140 $mAh^{-1}g$. This result is a direct evidence of the inherent trade-off between charge storage and discharge rate/efficiency.

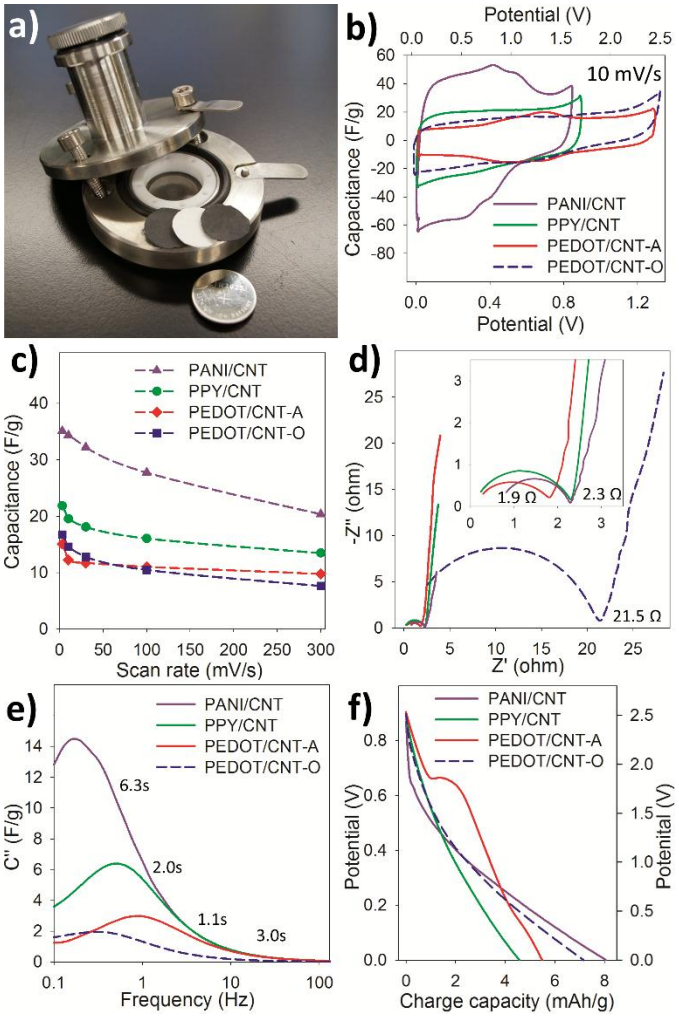

Figure 3.3. a) Picture of the electrodes, separator and testing set up of a symmetrical cell. Results for ECP/CNT symmetrical cells in 3 M H_2SO_4, and for PEDOT/CNT cell in 1.5 M $TEABF_4$ in acetonitrile (PEDOT/CNT-O), b) CV at 10 mV $^{s-1}$, c) scan rate dependence of capacitance, d) Nyquist plots with the inset figure showing an expanded view of the high frequency region. e) Bode plots of normalized imaginary capacitance (C") vs frequency, f) galvanostatic discharge curves.

3.4 Conclusions

In summary, we have developed a simple process for fabricating free-standing ECP/CNT electrodes that can be easily scaled to large size electrodes without the need for binder materials, substrate, or sophisticated processing techniques. Specifically, in this study, we prepared ECP/CNT composite electrodes (ECP = PPY, PANI and PEDOT) prepared with a routine dispersion-filtration process for immediate use in existing capacitor technologies. Electrochemical analysis of these composites showed an increase of up to 16 times in specific capacitance and 8 times in charge capacity compared to pure CNTs. Furthermore, the electrochemical properties of composite electrodes and devices obtained with our production method are comparable or superior to capacitors made with procedures such as pellet pressing, current collector coating, and in-situ chemical polymerization. Given its simplicity and the increased capacitance of our composite electrodes, they are posited to promote scalable manufacturing of superior supercapacitors.

3.5 References

1. Kearns, J. T.; Roberts, M. E., Enhanced performance of triarylamine redox electrodes through directed electrochemical polymerization. *Journal of Materials Chemistry* **2012,** 22, (6), 2392-2394.
2. Arcila-Velez, M. R.; Roberts, M. E., Redox Solute Doped Polypyrrole for High-Charge Capacity Polymer Electrodes. *Chemistry of Materials* **2014,** 26, (4), 1601-1607.
3. Kearns, J. T.; Roberts, M. E., Synthesis of high-charge capacity triarylamine-thiophene redox electrodes using electrochemical copolymerization. *Journal of Materials Chemistry* **2012,** 22, (48), 25447-25452.
4. Xu, Y.; Wang, J.; Sun, W.; Wang, S., Capacitance properties of poly(3,4-ethylenedioxythiophene)/polypyrrole composites. *Journal of Power Sources* **2006,** 159, (1), 370-373.
5. Fan, L.-Z.; Maier, J., High-performance polypyrrole electrode materials for redox supercapacitors. *Electrochemistry Communications* **2006,** 8, (6), 937-940.
6. Gupta, V.; Miura, N., High performance electrochemical supercapacitor from electrochemically synthesized nanostructured polyaniline. *Materials Letters* **2006,** 60, (12), 1466-1469.
7. Ramya, R.; Sivasubramanian, R.; Sangaranarayanan, M. V., Conducting polymers-based electrochemical supercapacitors—Progress and prospects. *Electrochimica Acta* **2013,** 101, (0), 109-129.

8. Peng, C.; Zhang, S.; Jewell, D.; Chen, G. Z., Carbon nanotube and conducting polymer composites for supercapacitors. *Progress in Natural Science* **2008,** 18, (7), 777-788.
9. Malinauskas, A.; Malinauskiene, J.; Ramanavičius, A., Conducting polymer-based nanostructurized materials: electrochemical aspects. *Nanotechnology* **2005,** 16, (10), R51.
10. Pan, L.; Qiu, H.; Dou, C.; Li, Y.; Pu, L.; Xu, J.; Shi, Y., Conducting Polymer Nanostructures: Template Synthesis and Applications in Energy Storage. *International Journal of Molecular Sciences* **2010,** 11, (7), 2636-2657.
11. Lahiff, E.; Lynam, C.; Gilmartin, N.; O'Kennedy, R.; Diamond, D., The increasing importance of carbon nanotubes and nanostructured conducting polymers in biosensors. *Analytical and Bioanalytical Chemistry* **2010,** 398, (4), 1575-1589.
12. Ates, M.; Sarac, A. S., Conducting polymer coated carbon surfaces and biosensor applications. *Progress in Organic Coatings* **2009,** 66, (4), 337-358.
13. Bose, S.; Kuila, T.; Mishra, A. K.; Rajasekar, R.; Kim, N. H.; Lee, J. H., Carbon-based nanostructured materials and their composites as supercapacitor electrodes. *Journal of Materials Chemistry* **2012,** 22, (3), 767-784.
14. Arcila-Velez, M. R.; Zhu, J.; Childress, A.; Karakaya, M.; Podila, R.; Rao, A. M.; Roberts, M. E., Roll-to-roll synthesis of vertically aligned carbon nanotube electrodes for electrical double layer capacitors. *Nano Energy* **2014,** 8, (0), 9-16.
15. Snook, G. A.; Kao, P.; Best, A. S., Conducting-polymer-based supercapacitor devices and electrodes. *Journal of Power Sources* **2011,** 196, (1), 1-12.

16. Khomenko, V.; Frackowiak, E.; Béguin, F., Determination of the specific capacitance of conducting polymer/nanotubes composite electrodes using different cell configurations. *Electrochimica Acta* **2005,** 50, (12), 2499-2506.
17. Frackowiak, E.; Khomenko, V.; Jurewicz, K.; Lota, K.; Béguin, F., Supercapacitors based on conducting polymers/nanotubes composites. *Journal of Power Sources* **2006,** 153, (2), 413-418.
18. Zheng, L.; Wang, X.; An, H.; Wang, X.; Yi, L.; Bai, L., The preparation and performance of flocculent polyaniline/carbon nanotubes composite electrode material for supercapacitors. *Journal of Solid State Electrochemistry* **2011,** 15, (4), 675-681.
19. Goh, R. G. S.; Motta, N.; Bell, J. M.; Waclawik, E. R., Effects of substrate curvature on the adsorption of poly(3-hexylthiophene) on single-walled carbon nanotubes. *Applied Physics Letters* **2006,** 88, (5), 053101.
20. Deng, H.; Lin, L.; Ji, M.; Zhang, S.; Yang, M.; Fu, Q., Progress on the morphological control of conductive network in conductive polymer composites and the use as electroactive multifunctional materials. *Progress in Polymer Science* **2014,** 39, (4), 627-655.
21. Long, Y.; Chen, Z.; Zhang, X.; Zhang, J.; Liu, Z., Synthesis and electrical properties of carbon nanotube polyaniline composites. *Applied Physics Letters* **2004,** 85, (10), 1796-1798.
22. Zhang, J.; Kong, L.-B.; Wang, B.; Luo, Y.-C.; Kang, L., In-situ electrochemical polymerization of multi-walled carbon nanotube/polyaniline composite films for electrochemical supercapacitors. *Synthetic Metals* **2009,** 159, (3–4), 260-266.

23. Zengin, H.; Zhou, W.; Jin, J.; Czerw, R.; Smith, D. W.; Echegoyen, L.; Carroll, D. L.; Foulger, S. H.; Ballato, J., Carbon Nanotube Doped Polyaniline. *Advanced Materials* **2002,** 14, (20), 1480-1483.

24. Weng, Y.-T.; Wu, N.-L., High-performance poly(3,4-ethylene-dioxythiophene):polystyrenesulfonate conducting-polymer supercapacitor containing hetero-dimensional carbon additives. *Journal of Power Sources* **2013,** 238, (0), 69-73.

25. Lota, K.; Khomenko, V.; Frackowiak, E., Capacitance properties of poly(3,4-ethylenedioxythiophene)/carbon nanotubes composites. *Journal of Physics and Chemistry of Solids* **2004,** 65, (2–3), 295-301.

26. Machida, S.; Miyata, S.; Techagumpuch, A., Chemical synthesis of highly electrically conductive polypyrrole. *Synthetic Metals* **1989,** 31, (3), 311-318.

27. Albuquerque, J. E.; Mattoso, L. H. C.; Balogh, D. T.; Faria, R. M.; Masters, J. G.; MacDiarmid, A. G., A simple method to estimate the oxidation state of polyanilines. *Synthetic Metals* **2000,** 113, (1–2), 19-22.

28. Lefebvre, M.; Qi, Z.; Rana, D.; Pickup, P. G., Chemical Synthesis, Characterization, and Electrochemical Studies of Poly(3,4-ethylenedioxythiophene)/Poly(styrene-4-sulfonate) Composites. *Chemistry of Materials* **1999,** 11, (2), 262-268.

29. Qi, Z.; G. Pickup, P., High performance conducting polymer supported oxygen reduction catalysts. *Chemical Communications* **1998**, (21), 2299-2300.

30. Meng, H.; Perepichka, D. F.; Bendikov, M.; Wudl, F.; Pan, G. Z.; Yu, W.; Dong, W.; Brown, S., Solid-State Synthesis of a Conducting Polythiophene via an

Unprecedented Heterocyclic Coupling Reaction. *Journal of the American Chemical Society* **2003,** 125, (49), 15151-15162.

31. Idris, N. H.; Wang, J.; Chou, S.; Zhong, C.; Rahman, M. M.; Liu, H., Effects of polypyrrole on the performance of nickel oxide anode materials for rechargeable lithium-ion batteries. *Journal of Materials Research* **2011,** 26, (07), 860-866.
32. Dhawale, D. S.; Salunkhe, R. R.; Jamadade, V. S.; Dubal, D. P.; Pawar, S. M.; Lokhande, C. D., Hydrophilic polyaniline nanofibrous architecture using electrosynthesis method for supercapacitor application. *Current Applied Physics* **2010,** 10, (3), 904-909.

CHAPTER FOUR

PSEUDO-CAPACITOR ANODES COMPRISED OF ELECTROCHEMICALLY SYNTHESIZED AMINOANTHRAQUINONE REDOX POLYMERS

4.1 Introduction

With the continuous increase in portable electronics and technologies, high energy/high power energy storage devices must be developed to achieve long operation times with the adequate energy supply. Supercapacitors (SCs) represent a high energy/high power alternative to existing batteries and capacitors due to their combination of high-surface area, non-faradaic carbon materials, and redox active or conductive polymers/dopants.[1-5] Current state of the art commercial SCs utilize activated carbon (AC) anodes and cathodes, because of the large capacitance associated with its high surface area available for ion adsorption, and the outstanding cycle life arising from its chemical stability over wide potential windows.[6-11] Albeit these properties, capacitance is limited by a maximum achievable surface area in contact with the electrolyte; conductivity enhancers are needed and the addition of a non-conductive binder to cast the material on the current collector increases ESR.

As their price decreases and purity increases, other forms of carbon, such as carbon nanotubes (CNTs), are attracting interest for SC electrodes due to their high conductivity and their outstanding mechanical properties, which allows the preparation of free-standing CNTs films, eliminating the need for a current collector, binder, and conductivity enhancers.[12-15] Conducting polymers (CPs), metal oxides (MOs) and redox active polymers/dopants are of interest as well, due to their considerably larger charge

capacities arising from their faradaic processes, although stability is partially compromised.[16-19] Another aspect that prevents the integration of faradaic SCs to the market is that most of these materials only function as cathodes because their reduction occurs at potentials more negative than the limits of most electrolyte systems, imparting insurmountable instability. Accordingly, anode polymeric materials with comparable capacitances to state-of-the-art cathodic polymers is lacking, preventing the ability to construct asymmetric pseudo-capacitors with access to a wide potential range.

Previously, quinone-containing (QN) polymers and compounds have been subject of research for energy storage applications[20-26] due to their high charge storage capacity achieved through stable 2-electron 2-proton redox reactions. Nevertheless, quinones are not conductive and need to be chemically or physically incorporated into a conductive medium that transports electrons to and from the quinone redox sites. When polymerized, different types of aminoanthraquinones have a conjugated and therefore conductive backbone, eliminating the need for an extra conductive matrix. Some aminoanthraquinones studied for SC electrodes include poly(1,5-diaminoanthraquinone),[27] which works as anode and cathode material[28] and poly(1-aminoanthraquinone) (PAQ).[29] PAQ is an interesting material since its backbone corresponds to polyaniline, which is a high capacitance conducting polymer, and the quinone moieties store larger amounts of charge.

In this work, we demonstrate the use of electrochemically polymerized poly(1-aminoanthraquinone) as an anode material for SCs. The importance of the electrochemical polymerization method is discussed, in addition to how the applied

voltage and current affect the redox behavior of the resulting film. When prepared under optimized conditions, PAQ shows a pronounced redox couple in the range of 0 to -2 V vs Ag/Ag* with an average capacitance of 176 F g^{-1} on stainless steel substrates. The polymer stability was dramatically improved when polymerized on free-standing CNT mats (CTs), yielding capacitances of 81 F g^{-1} for the complete electrode (210 F g^{-1} based on PAQ mass). Asymmetric pseudo-capacitors fabricated using PAQ/CT as the anode and a polypyrrole (PPY)/CT cathode showed increased specific power of 606 W kg^{-1} and energy of 5.9 Wh kg^{-1}, compared to CT/CT device which had 247 W kg^{-1} and 1.71 Wh kg^{-1}.

4.2 Experimental methods

4.2.1 Materials

Multi-walled carbon nanotubes were purchased from CheapTubes (dia.=30-50 nm, length=10-20 μm). Sodium dodecyl sulfate (SDS, 98.5%), 1-aminoanthraquinone (97%), lithium perchlorate ($LiClO_4$, 95%), and tetrabutylammonium perchlorate ($TBAClO_4$, 99%) were purchased from Sigma-Aldrich. Propylene carbonate (PC, 99.5%), acetonitrile anhydrous (MeCN, 99.9%), and tetrabutylammonium tetrafluoroborate ($TBABF_4$, 98%) were acquired from Acros Organics. All materials were used as received. Deionized water was obtained from an in-house distillation apparatus followed by a water purification unit (Millipore™ Milli-Q Academic).

4.2.2 Electrode fabrication

CNT free-standing film preparation.[34] CNTs were dispersed in 1 wt% aqueous SDS using a tip sonicator probe (1/8″ diameter, Branson 250) with a power of 75 W for 15 min. Subsequently, the suspension was poured onto a polyamide filtration membrane (Whatman, 0.45 μm pore diameter) and filtered using a vacuum filtration setup (Synthware Filtration Apparatus, Kemtech America). The filter cake on the supporting filter membrane was washed with distilled water several times, and then oven dried at 60 °C for 8 h. The resulting film was peeled off the membrane to yield a freestanding CNT electrode (~125 μm thick).

PAQ Electrode Preparation. Organic solvents, propylene carbonate and acetonitrile, were chosen to polymerize and test materials in due to the monomers' low solubility in water and the wider operational potential ranges. The conditions for electropolymerization of 1-AAQ were initially surveyed in propylene carbonate (PC) and acetonitrile (MeCN) solvents but PC was discarded because its lower ion conductivity and higher viscosity caused the reduction peak to appear below -2 V, where the electrolyte starts degrading. All the results reported in this chapter are in acetonitrile and were carried out in sealed cells to prevent solvent evaporation, which can deteriorate the materials performance and stability.

Solutions were prepared with 10 mM 1-aminoanthraquinone in 1 M lithium perchlorate ($LiClO_4$) in acetonitrile (MeCN), stirred and purged with N_2 prior to use. Polymer films were grown on 0.46 cm^2 stainless steel (SS) foil substrates (McMaster-Carr) or free-standing carbon nanotube films (CT) using chronoamperometry or cyclic

voltammetry with a VersaSTAT4 potentiostat/galvanostat and VersaStudio v1.50 Electrochemistry Software (Princeton Applied Research). Prior to polymer deposition, SS substrates were washed with ethanol, DI water and treated in UV-ozone (Novascan, PSD-UV8) for 30 minutes in air and at room temperature. A platinum mesh was used as counter electrode and an Ag/Ag* pseudoreference electrode. Stainless steel was chosen as the substrate to analyze the performance of thin films and to find adequate polymerization conditions and CT was used to further test polymer performance and to fabricate the supercapacitor cells.

4.2.3 Characterization

The surface morphology of the samples was observed using scanning electron microscopy (SEM, Hitachi SU-6600) with an accelerating voltage of 5 kV. Each polymer electrode was characterized in a three-electrode cell containing 1 M $LiClO_4$, $TBABF_4$ or $TBAClO_4$ in MeCN using cyclic voltammetry (ν = 300 to 10 mV s–1), galvanostatic charge–discharge cycles (0 to -1.5 V) with current densities selected to achieve a total discharge time of ca. 60 s.

4.3 Results and discussion

The redox behavior of three aminoanthraquinone monomers was evaluated with the goal of generating polymeric electrodes that function as anode materials: 1-aminoanthraquinone (1-AAQ), 1,5-diaminoanthraquinone (1,5-DAAQ) and 1,4-diaminoanthraquinone (1,4-DAAQ) (**Figure 4.1**). Various electrochemical

polymerization techniques were applied to stainless steel electrodes immersed in 10 mM monomer solutions in 1 M lithium perchlorate ($LiClO_4$)/acetonitrile electrolyte.

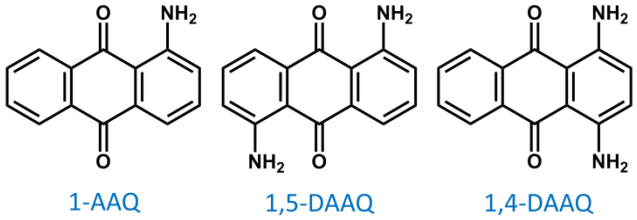

Figure 4.1. Chemical structures of monomers used to electrochemically synthesize anode films: 1-aminoanthraquinone (1-AAQ), 1,5-diaminoanthraquinone (1,5-DAAQ) and 1,4-diaminoanthraquinone (1,4-DAAQ).

When cyclic voltammetric (CV) polymerization scans from -1.5 V to +1.5 V were applied, a redox couple formed in the range of -0.5 V to -1.5 V (**Figure 4.2a**), but when testing the film in fresh electrolyte in the same potential range, this peak decreased rapidly upon cycling towards positive potentials (**Figure 4.2b**). Hence, polymer formation was found to occur by oxidative polymerization at positive potentials, while the quinone redox peaks appear in the negative potentials. Each monomer exhibited similar behavior, but 1-AAQ was selected for subsequent analysis as its polymer films were consistently homogeneous with a clearly defined and symmetrical redox couple and good adherence to the substrate. Reductive polymerization was also attempted using each monomer, but no films could be obtained with this method.

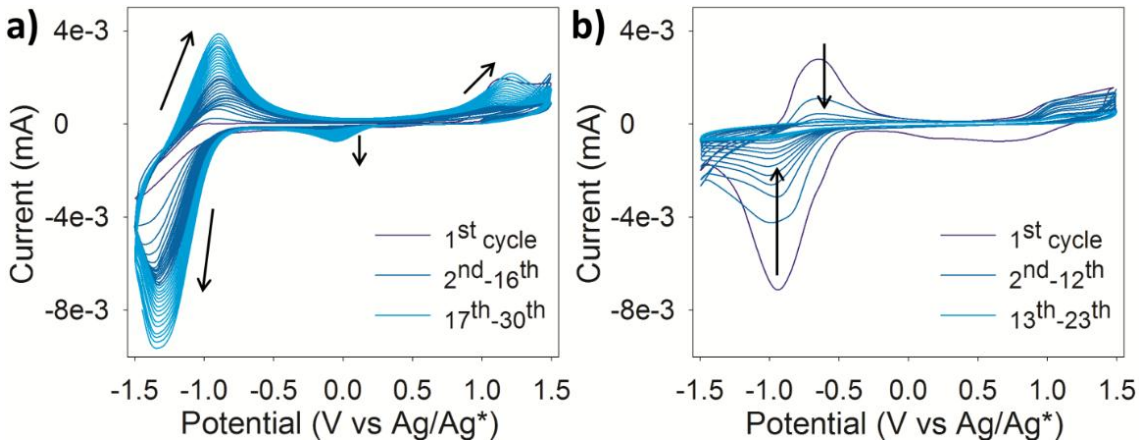

Figure 4.2. a) CV polymerization of 1-AAQ (10 mM) in 1 M $LiClO_4$ in MeCN at 0.02 V s^{-1} and b) CV test in 1 M $LiClO_4$ in MeCN at 0.02 V s^{-1}.

To synthesize PAQ films, cyclic voltammetry was performed from 0 V to increasingly positive potentials at a rate of 20 mV s^{-1}. When the positive potential vertex was above 1.2 V, a dark layer was observed on the substrate. Polymer films could be obtained at higher rates by further increasing the upper potential limited up to 1.5 V; however, polymer films could not be obtained above 1.6 V due to overoxidation of the polymer and film delamination. From these experiments, it was concluded that the optimal potential range for the PAQ growth is between 1.2 and 1.5 V, whether the film is prepared using CV, constant current, or constant voltage methods. As noted above, voltammetric cycling in the negative range during electrode synthesis resulted in degradation of the reduction peak; therefore, the minimum potential during oxidative polymerization was set to 0 V.

Figure 4.3a shows how the CV deposition profile evolves during cycling from 0 to 1.35 V. As the polymer is growing on the substrate, the initial oxidation potential decreases from 1.02 V to 0.60 V, as expected for growing electroactive polymers. A

second peak at lower potential at 0.42 V appears after 2 cycles, presumably due to the cross-linking within the polymer and the formation of polyaniline-like or arylamine linkages that exhibit redox potentials around 0.4 V.[30-32] Continued cycling causes this peak to shift positively due to the increasing density of the cross-linking in the polymer. The appearance of shoulders in the final CV profile indicates the redox behavior is a combination of electrochemical process resulting from linear polymer chains (peak around 0.8-0.9 V) and cross-linking regions (peak around 0.5-0.6 V).

After synthesis, PAQ films were electrochemically analyzed in fresh electrolyte (monomer free) from 0 to -2 V and CV profiles were normalized by scan-rate and mass (**Figure 4.3b**). At faster scan rates, above 50 mV s^{-1}, the redox couple appeared highly reversible with symmetric peaks; however, the formation of a second reduction peak was observed at low scan rates, which may be attributed to a reaction between anionic (QN•–) and dianonic (QN2–) QN species.[33] Furthermore, the disproportion between the reduction and oxidation peaks continued to increase with decreasing scan rate, indicating irreversible processes occurring at low rates. For example, at 10 mV s^{-1}, the electrode exhibited an average capacitance of 176 F g^{-1}; however, the peak oxidation and reductive capacitance values were 330 F g^{-1} and 425 F g^{-1}, respectively, at this rate. The inset of **Figure 4.3b** shows the scan-rate dependence of peak current, which exhibits a linear relationship with the square root of scan rate, indicating a diffusion-limited redox process at all rates. The irreversibility observed at low scan rates is evident by the increasing slope on the cathodic peak (reduction) relative to the anodic peak.

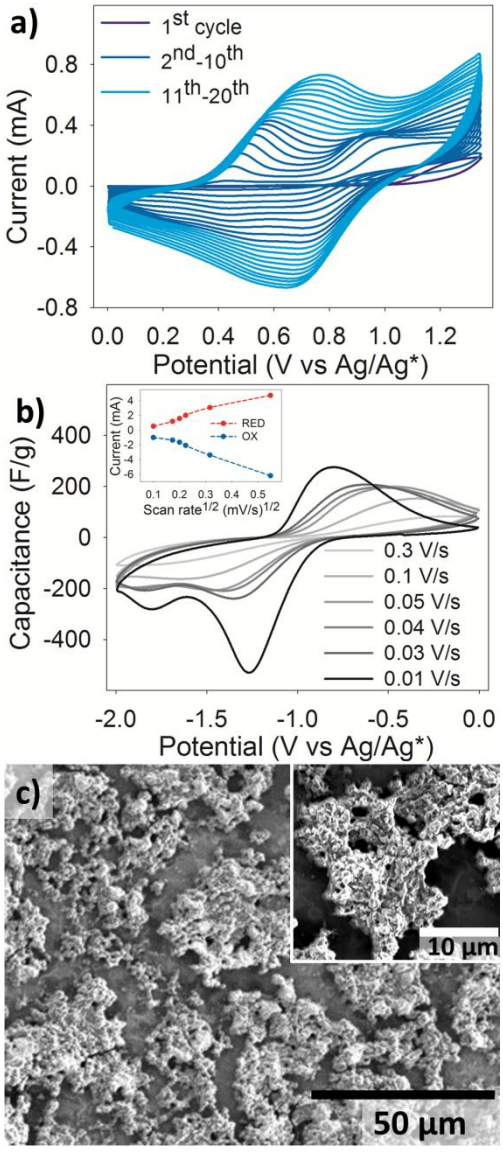

Figure 4.3. a) CV polymerization of 1-AAQ from 0 to 1.35 V vs Ag/Ag* at 20 mV s^{-1} in 1 M $LiClO_4$/MeCN electrolyte, b) capacitance vs potential for different scan rates. Inset: peak current vs scan rate$^{1/2}$, c) SEM images showing the morphology of PAQ on SS foil at magnifications of 500x and 3000x (inset), at an accelerating voltage of 5 kV.

Charge discharge cycling were performed over a potential range from 0 to -1.5 V on PAQ films, and by the 80th cycle the charge capacity of the electrode had decreased to 57% of the initial value (**Figure 4.4a**). Studies have been carried out to analyze the

factors driving the degradation of quinone materials, which include high applied current, the presence of water in the solvent, high pH, and reactions involving the electrolyte.[33] Furthermore, the reduction of quinones in aprotic media occurs in two successive one-electron steps forming the anion radical, $Q^{\bullet-}$, and the dianion, Q^{2-} and usually the first reduction is reversible, whereas the second is electrochemically quasi-reversible.[33] As mentioned previously, CPs, such as polyaniline, do not perform as well as an anode material, in part due to poor conductivity at negative potentials, so the polyaniline-like backbone of the PAQ films may not transport electrons efficiently to and from the redox sites, thus affecting the reversibility at high potential.

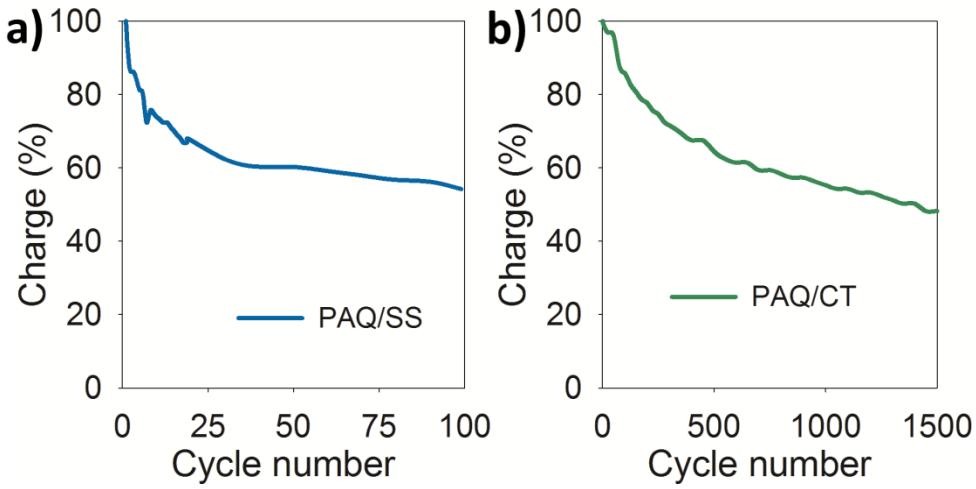

Figure 4.4. a) Cycling stability of PAQ deposited on SS foil (100 charge/discharge cycles), b) cycling stability of PAQ/CT (1500 charge/discharge cycles).

The way in which the polymer grows on the SS may also affect the film stability and reversibility. SEM images taken from PAQ films on SS (**Figure 4.3c** and inset) show that a layer of the flake-structured polymer covers the whole SS area, which in this case can be unfavorable due to the lower conductivity of the polymer. Upon further growth,

the polymer forms densely packed islands throughout the sample that are only partially interconnected or not connected at all, affecting the performance of the film.

To improve electrode conductivity and adhesion, which is especially problematic for thicker polymer films, PAQ was polymerized on free-standing CNT mats (CTs) which would serve as a conductive matrix and allow for radial polymer expansion and contraction during oxidation-reduction processes. These free-standing CTs were prepared through a dispersion filtration method.[34] Polymer films were initially deposited using CV from 0 to 1.35 V, based on the previous experiments on SS. Stability studies were performed on the PAQ/CT electrodes and the decrease to 60% of the charge occurred after 900 cycles, compared to 80 cycles for the PAQ on SS foil, significantly improving, but not solving the stability issues (**Figure 4.4b**).

The influence of the electropolymerization method on the polymer performance was examined by cyclic voltammetry tests (**Figures 4.5a and 4.5b**). These CV tests were carried out on PAQ films synthesized on CT using chronoamperometry (CA) and CV at different potentials and potential ranges, with a synthesis time of 45 minutes. CA and CV depositions that surpassed 1.5 V showed decreased capacitance due to overoxidation of the polymer. The remaining films deposited below the polymer overoxidation potential show similar performance with the highest specific capacitance of ~54 F g^{-1} (30 mV s^{-1}) for films prepared using CV from 0 V to 1.35 V. It was also observed that electrolyte degradation is slowed by the presence of the polymer, broadening the active potential range of the electrode. With CT as the substrate, the redox peaks are also more symmetrical at slower scan rates, which indicates enhanced reversibility.

The electrolyte contents and electrode structure are known to affect the performance and stability of Faradaic electrode materials. Testing electrolyte conditions were investigated using PAQ/CT films in three different salts in acetonitrile: tetrabutylammonium tetrafluoroborate ($TBABF_4$), tetrabutylammonium perchlorate ($TBAClO_4$) and $LiClO_4$, and the results were compared to bare CT electrodes in 1M $LiClO_4$. As shown in **Figures 4.5a and 4.5b**, larger ion sizes (radius TBA+: 4.94 Å vs Li+: 0.9 Å) lead to a significant decrease of the redox peaks, capacitance (81 F g^{-1} vs 46 and 48 F g^{-1}), charge capacity, and an increase in resistance due to the inaccessibility of ions to the QN active sites.[33] On CT, the overall capacitance is lower than that obtained on the SS foil due to the added weight and reduced capacitance of the CNTs. If only the mass of the polymer is considered, a PAQ capacitance of 210 F g^{-1} is obtained for the film deposited with CV from 0 to 1.35 V and tested in 1 M $LiClO_4$.

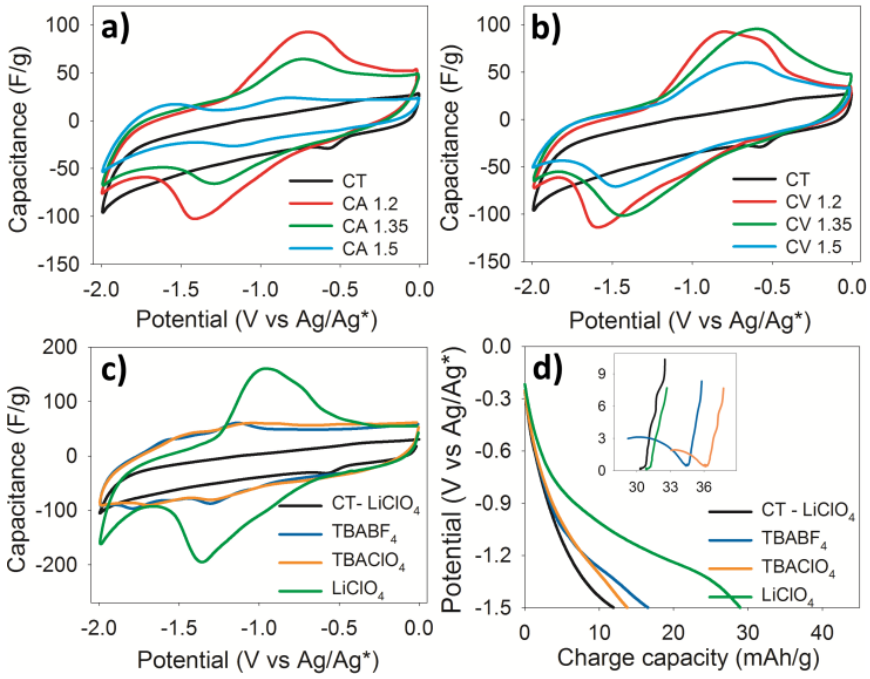

Figure 4.5. CV test (30 mV s^{-1}) in 1 M $LiClO_4$/acetonitrile of PAQ polymerized on CT using: a) chronoamperometry at 1.2, 1.35 and 1.5 V, and b) cyclic voltammetry from 0 V to 1.2, 1.35 and 1.5 V; c) CV test and d) charge/discharge and EIS (inset) of PAQ/CT electrodes in different salts (1 M) in acetonitrile at 10 mV s^{-1}. The black curves correspond to bare CT tests in 1 M $LiClO_4$/acetonitrile.

SEM images were also recorded for the bare CT electrodes (**Figures 4.6a and 4.6b**) where the randomly oriented entangled carbon nanotubes can be seen. **Figures 4.6c and 4.6d** show the electropolymerized PAQ on the carbon nanotube mat. At a magnification of x350 (**Figure 4.6c**), it was observed that a PAQ layer deposited on the CT substrate and coated the carbon nanotubes, which cannot be distinguished. Some polymer agglomerates can be seen as well scattered throughout the sample but more spaced out and notably smaller in size, compared to the PAQ islands on SS. It is believed that these agglomerates form at long polymerization times (45 min), when after covering the CT surface, PAQ further selectively polymerizes on certain sections. Due to the

random orientation of the CNTs and the smaller polymer particle sizes, porous materials are obtained, which facilitate the electrolyte access to the active redox sites. In the higher magnification SEM picture (**Figure 4.6d**) the polymer layer is visible on the CNTs.

To evaluate the performance of the PAQ/CT anodes in SC cells, pseudocapacitors were constructed using either PAQ/CT (symmetric) or PPY/CT (asymmetric) as cathodes. PPY/CT was synthesized using standard polymerization conditions: 0.8 V was applied to CT in a 0.5 M Py solution in 1 M $LiClO_4$/acetonitrile for 6 minutes. SEM pictures of PPY/CT (**Figures 4.6e and 4.6f**) show that the PPY film coated the CNTs in a homogeneous manner, similar to PAQ/CT.

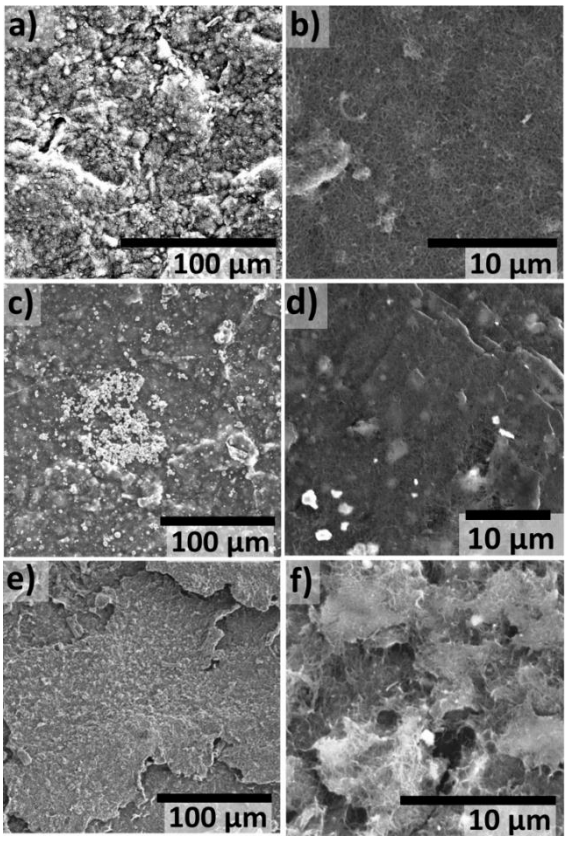

Figure 4.6. SEM images of (a,b) CNT, (c,d) PAQ/CNT, (e,f) PPY/CNT.

First, the performance of the individual electrodes was evaluated using cyclic voltammetry (**Figure 4.7a**). As it can be noted by the area of the CV profiles, the capacitance of the PAQ film tested under cathode potentials (56.7 F g^{-1}) is substantially lower than that of PAQ tested under anode potentials (75.7 F g^{-1}). As such, PPY represents a better option as the cathode with a capacitance of 94.2 F g^{-1}. Coin cells were fabricated using a Celgard 2325 (25 μm thick) separator, and their performance was compared to a CT/CT device. **Figure 4.7b** shows the superior capacitance of the polymeric cells with capacitances of 7.2 F g^{-1} and 10.6 F g^{-1} with respect to a carbon-based SC, which correspond to an increase in capacitance of 2 and 3 times that of CT/CT device, respectively. From this it can be noted the importance of a high capacitance cathode. The stability of the devices was evaluated by charge/discharge tests (**Figure 4.7c**) for over 2000 cycles, and CV was recorded for the PAQ/PPY device after 3000 cycles (dotted line from **Figure 4.7b**). It can be seen that the redox peak has disappeared and the capacitance decreased to 6.6 F g^{-1}, which is still twice the capacitance of CT/CT device. While the PAQ/PAQ device showed reduced specific capacitance with respect to the PAQ/PPY device, it showed good stability by retaining 87% of the charge after 2000 cycles, compared to 58% for PAQ/PPY. As expected, the CT/CT device was highly stable and retained 98% of the charge after 2000 cycles. The decrease in stored charge in both polymeric devices can be attributed to polymer backbone degradation as well as the irreversibility associated with the quinone redox groups. Nevertheless, the steady behavior with prolonged cycling corresponds to the stable CNT and the polymer backbone capacitance, and the polymeric devices show an improvement of 1.7 and 2.6

times in specific charge capacity compared to the CT/CT device (**Figure 4.7d**). The PAQ/PPY device also showed a lower charge transfer resistance because of the good conductivity of PPY compared to that of PAQ as cathode material. The PAQ/PPY device showed energy and power densities of 5.9 Wh kg^{-1} and 606 W kg^{-1}, followed by 5.3 and 605 for PAQ/PAQ, and 3.17 and 267 for CT/CT. **Figure 4.7e** shows the charge/discharge profiles for PPY/CT, PAQ/CT single electrodes, and the PAQ/PPY device at a current of 3 mA, and it can be observed that the charge and discharge times of the anode and the cathode are similar, which indicates that the electrodes would make an efficient device. Nonetheless, the device performance is reduced compared to what was expected from the three electrode tests. This may be due to the fact that the CNT mat is still not the optimum substrate material, as the CT/CT device itself presented a reduced performance.

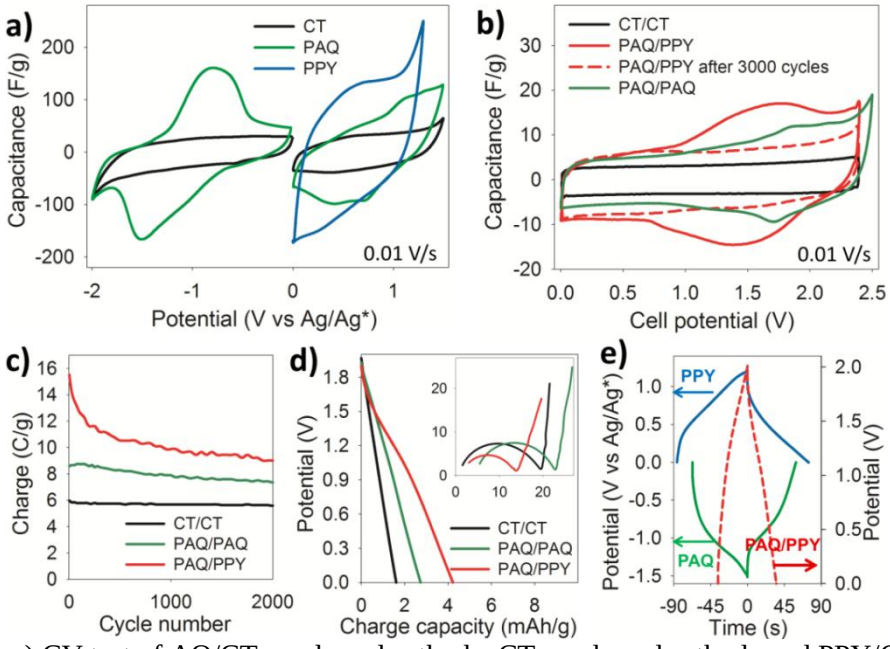

Figure 4.7. a) CV test of AQ/CT anode and cathode, CT anode and cathode and PPY/CT cathode, b) CV of CT/CT, PAQ/PPY and PAQ/PAQ devices, and PAQ/PPY device after 3000 cycles, c) stability of the 3 devices. d) C/D of the 3 devices, inset: EIS, e) C/D profiles for individual electrodes of PAQ/CT (green) and PPY/CT (blue) and the device of PAQ/PPY (red).

4.4 Conclusions

In summary, we have studied the application of poly(1-aminoanthraquinone) for supercapacitor anodes, as this polymer stores charge faradaically in the potential range of 0 to -2 V vs Ag/Ag*. PAQ shows a capacitance of 176 F g^{-1} (at 10 mV s^{-1}) when electrochemically polymerized on stainless steel foil, but poor cycling stability. PAQ was also polymerized on CNT free-standing films, which provided a conductive matrix for the polymer and enhanced the films stability. Single electrode capacitances of up to 81 F g^{-1} (at 10 mV s^{-1}) were obtained for PAQ/CT films in 1 M $LiClO_4$ in acetonitrile. A device made of a PAQ/CT anode and a PPY/CT cathode showed a specific power of 606 W kg^{-1} and a specific energy of 5.9 Wh kg^{-1} compared to 267 W kg^{-1} and 3.17 Wh kg^{-1} for CT/CT devices. The device retained 58% of the charge storage capacity after 3000 cycles.

4.5 References

1. Hou, Y.; Cheng, Y.; Hobson, T.; Liu, J., Design and Synthesis of Hierarchical MnO2 Nanospheres/Carbon Nanotubes/Conducting Polymer Ternary Composite for High Performance Electrochemical Electrodes. *Nano Letters* **2010,** 10, (7), 2727-2733.
2. Frackowiak, E.; Khomenko, V.; Jurewicz, K.; Lota, K.; Béguin, F., Supercapacitors based on conducting polymers/nanotubes composites. *Journal of Power Sources* **2006,** 153, (2), 413-418.
3. Yu, G.; Hu, L.; Liu, N.; Wang, H.; Vosgueritchian, M.; Yang, Y.; Cui, Y.; Bao, Z., Enhancing the Supercapacitor Performance of Graphene/MnO2 Nanostructured Electrodes by Conductive Wrapping. *Nano Letters* **2011,** 11, (10), 4438-4442.
4. Peng, C.; Zhang, S.; Jewell, D.; Chen, G. Z., Carbon nanotube and conducting polymer composites for supercapacitors. *Progress in Natural Science* **2008,** 18, (7), 777-788.
5. Fan, L. Z.; Hu, Y. S.; Maier, J.; Adelhelm, P.; Smarsly, B.; Antonietti, M., High Electroactivity of Polyaniline in Supercapacitors by Using a Hierarchically Porous Carbon Monolith as a Support. *Advanced Functional Materials* **2007,** 17, (16), 3083-3087.
6. Hung, P.-J.; Chang, K.-H.; Lee, Y.-F.; Hu, C.-C.; Lin, K.-M., Ideal asymmetric supercapacitors consisting of polyaniline nanofibers and graphene nanosheets with proper complementary potential windows. *Electrochimica Acta* **2010,** 55, (20), 6015-6021.

7. Qin, C.; Lu, X.; Yin, G.; Jin, Z.; Tan, Q.; Bai, X., Study of activated nitrogen-enriched carbon and nitrogen-enriched carbon/carbon aerogel composite as cathode materials for supercapacitors. *Materials Chemistry and Physics* **2011,** 126, (1–2), 453-458.
8. Xie, L.-J.; Wu, J.-F.; Chen, C.-M.; Zhang, C.-M.; Wan, L.; Wang, J.-L.; Kong, Q.-Q.; Lv, C.-X.; Li, K.-X.; Sun, G.-H., A novel asymmetric supercapacitor with an activated carbon cathode and a reduced graphene oxide–cobalt oxide nanocomposite anode. *Journal of Power Sources* **2013,** 242, 148-156.
9. Luan, F.; Wang, G.; Ling, Y.; Lu, X.; Wang, H.; Tong, Y.; Liu, X.-X.; Li, Y., High energy density asymmetric supercapacitors with a nickel oxide nanoflake cathode and a 3D reduced graphene oxide anode. *Nanoscale* **2013,** 5, (17), 7984-7990.
10. Chen, Z.; Weng, D.; Sohn, H.; Cai, M.; Lu, Y., High-performance aqueous supercapacitors based on hierarchically porous graphitized carbon. *RSC Advances* **2012,** 2, (5), 1755-1758.
11. Liu, C.-L.; Chang, K.-H.; Hu, C.-C.; Wen, W.-C., Microwave-assisted hydrothermal synthesis of Mn3O4/reduced graphene oxide composites for high power supercapacitors. *Journal of Power Sources* **2012,** 217, 184-192.
12. Kang, Y. J.; Chung, H.; Kim, W., 1.8-V flexible supercapacitors with asymmetric configuration based on manganese oxide, carbon nanotubes, and a gel electrolyte. *Synthetic Metals* **2013,** 166, 40-44.
13. Niu, Z.; Zhou, W.; Chen, J.; Feng, G.; Li, H.; Ma, W.; Li, J.; Dong, H.; Ren, Y.; Zhao, D.; Xie, S., Compact-designed supercapacitors using free-standing single-

walled carbon nanotube films. *Energy & Environmental Science* **2011,** 4, (4), 1440-1446.

14. Zhou, Y.; Xu, H.; Lachman, N.; Ghaffari, M.; Wu, S.; Liu, Y.; Ugur, A.; Gleason, K. K.; Wardle, B. L.; Zhang, Q. M., Advanced asymmetric supercapacitor based on conducting polymer and aligned carbon nanotubes with controlled nanomorphology. *Nano Energy* **2014,** 9, 176-185.
15. Peng, Y.-J.; Wu, T.-H.; Hsu, C.-T.; Li, S.-M.; Chen, M.-G.; Hu, C.-C., Electrochemical characteristics of the reduced graphene oxide/carbon nanotube/polypyrrole composites for aqueous asymmetric supercapacitors. *Journal of Power Sources* **2014,** 272, 970-978.
16. Nyholm, L.; Nyström, G.; Mihranyan, A.; Strømme, M., Toward Flexible Polymer and Paper-Based Energy Storage Devices. *Advanced Materials* **2011,** 23, (33), 3751-3769.
17. Snook, G. A.; Kao, P.; Best, A. S., Conducting-polymer-based supercapacitor devices and electrodes. *Journal of Power Sources* **2011,** 196, (1), 1-12.
18. Wang, G.; Zhang, L.; Zhang, J., A review of electrode materials for electrochemical supercapacitors. *Chemical Society Reviews* **2012,** 41, (2), 797-828.
19. Deng, W.; Ji, X.; Chen, Q.; Banks, C. E., Electrochemical capacitors utilising transition metal oxides: an update of recent developments. *RSC Advances* **2011,** 1, (7), 1171-1178.

20. Arcila-Velez, M. R.; Roberts, M. E., Redox Solute Doped Polypyrrole for High-Charge Capacity Polymer Electrodes. *Chemistry of Materials* **2014,** 26, (4), 1601-1607.

21. Leguizamon, S.; Diaz-Orellana, K. P.; Velez, J.; Thies, M. C.; Roberts, M. E., High charge-capacity polymer electrodes comprising alkali lignin from the Kraft process. *Journal of Materials Chemistry A* **2015,** 3, (21), 11330-11339.

22. Milczarek, G.; Inganäs, O., Renewable Cathode Materials from Biopolymer/Conjugated Polymer Interpenetrating Networks. *Science* **2012,** 335, (6075), 1468-1471.

23. Tamaki, T.; Ito, T.; Yamaguchi, T., Immobilization of Hydroquinone through a Spacer to Polymer Grafted on Carbon Black for a High-Surface-Area Biofuel Cell Electrode. *The Journal of Physical Chemistry B* **2007,** 111, (34), 10312-10319.

24. Choi, W.; Harada, D.; Oyaizu, K.; Nishide, H., Aqueous Electrochemistry of Poly(vinylanthraquinone) for Anode-Active Materials in High-Density and Rechargeable Polymer/Air Batteries. *Journal of the American Chemical Society* **2011,** 133, (49), 19839-19843.

25. Huskinson, B.; Marshak, M. P.; Suh, C.; Er, S.; Gerhardt, M. R.; Galvin, C. J.; Chen, X.; Aspuru-Guzik, A.; Gordon, R. G.; Aziz, M. J., A metal-free organic-inorganic aqueous flow battery. *Nature* **2014,** 505, (7482), 195-198.

26. Huang, Y. M.; Zhou, F.-f.; Deng, Y.; Zhai, B.-g., Effects of salt 9,10-anthraquinone-2-sulfonic acid sodium on the conductivity of polypyrrole. *Solid State Ionics* **2008,** 179, (27–32), 1305-1309.

27. Park, S.-G.; Kim, H.-I.; Shin, J.-G.; Kim, H.-J.; Park, J.-E.; Osaka, T., High Performance 1,5-Diaminoanthraquinone/Multi-Wall Carbon Nanotube(DAAQ/MWCNT) Composite Materials by Different Synthesis Methods for Supercapacitor. *ECS Transactions* **2007,** 3, (37), 17-22.
28. Naoi, K.; Suematsu, S.; Manago, A., Electrochemistry of Poly(1,5-diaminoanthraquinone) and Its Application in Electrochemical Capacitor Materials. *Journal of The Electrochemical Society* **2000,** 147, (2), 420-426.
29. Algharaibeh, Z.; Pickup, P. G., Charge trapping in poly(1-amino-anthraquinone) films. *Electrochimica Acta* **2013,** 93, 87-92.
30. Kearns, J. T.; Roberts, M. E., Enhanced performance of triarylamine redox electrodes through directed electrochemical polymerization. *Journal of Materials Chemistry* **2012,** 22, (6), 2392-2394.
31. Kearns, J. T.; Roberts, M. E., Synthesis of high-charge capacity triarylamine-thiophene redox electrodes using electrochemical copolymerization. *Journal of Materials Chemistry* **2012,** 22, (48), 25447-25452.
32. Ryu, K. S.; Kim, K. M.; Park, Y. J.; Park, N.-G.; Kang, M. G.; Chang, S. H., Redox supercapacitor using polyaniline doped with Li salt as electrode. *Solid State Ionics* **2002,** 152–153, 861-866.
33. René, A.; Evans, D. H., Electrochemical Reduction of Some o-Quinone Anion Radicals: Why Is the Current Intensity so Small? *The Journal of Physical Chemistry C* **2012,** 116, (27), 14454-14460.

34. Arcila-Velez, M. R.; Zhu, J.; Childress, A.; Karakaya, M.; Podila, R.; Rao, A. M.; Roberts, M. E., Roll-to-roll synthesis of vertically aligned carbon nanotube electrodes for electrical double layer capacitors. *Nano Energy* **2014,** 8, (0), 9-16.

CHAPTER FIVE

REDOX SOLUTE DOPED POLYPYRROLE FOR HIGH-CHARGE CAPACITY POLYMER

5.1 Introduction

A strong demand exists for high energy/high power storage devices for small and large scale applications such as transportation, load leveling, storage for intermittent energy sources and portable technologies. The performance of current energy storage technologies (batteries and supercapacitors) falls short of requirements for using electrical energy efficiently as energy density requirements cannot be achieved while maintaining high-power density needs.[1, 2] In addition to high-performance materials, low cost, environmentally friendly, and highly abundant materials are necessary for cost-effective stationary energy storage.[3]

Supercapacitors provide a bridge to the gap in performance between high energy density batteries and high power density capacitors using an energy storage mechanism based on charge separation in the double layer that forms at the interface between the solid electrode material surface and an electrolytic solution and within the electrode interface.[4] These devices are classified into electrochemical double-layer capacitors (EDLC) and pseudocapacitors based on whether the charge storage is non-faradaic or faradaic. The main components of commercial EDLCs are carbon materials with extremely high surface areas, that are also fairly low cost and are becoming widely available with well-established fabrication techniques.[5] Since no chemical reactions occur in these systems, charge storage is highly reversible in EDLCs, which gives cycling

stabilities higher than 10^6 cycles.[6] The fact that the storage mechanism of EDLCs is superficial allows very fast energy uptake and delivery but also limits the energy density as only a portion of the active material participates in the charge storage process.[4, 7]

Pseudocapacitors have the ability to store greater amounts of charge than EDLCs due to the inherent properties of the faradaic storage mechanism. In these supercapacitors, the bulk redox material stores energy by a transfer of charge between the electrolyte and the electrode.[8] Typical pseudocapacitive electrode materials include transition metal oxides such as ruthenium oxide (RuO_2), iron oxide (Fe_3O_4) and magnesium oxide (MnO_2) due to their multiple valence states, and electroactive conducting polymers (ECPs) such as polypyrroles, polyanilines and polythiophenes.[4, 9] Metal oxides, notably RuO_2 with the highest reported specific capacitance of ca. 850 F g^{-1},[10] have been studied as a possible electrode material for pseudocapacitors due to their high conductivity and cyclability, although their high cost hinders them to reach major markets[11, 12] and many of them present pseudocapacitive behavior over small ranges of potential.[13] Conversely, ECPs are inexpensive compared to metal oxides and have high charge density, good intrinsic conductivity (ranging from a few S cm^{-1} to 500 S cm^{-1} in the doped state),[8, 14, 15] fast charge–discharge rates, fast doping and de-doping processes, and are easily synthesized by electropolymerization. For many years, many research groups have considered the use ECPs in energy devices, but many challenges still limit commercial adaptation. The overall charge capacity and stability of these materials must be improved such that new energy storage devices can deliver and store more energy with high power requirements.[16]

Conducting polymers are promising for many applications due to their unique electrical, optical, mechanical and membrane properties as well as their stability in the presence of air and water.[12, 17] In addition to their reduced cycling stability due to the constant swelling and contracting caused by the insertion and removal of ions to and from the polymer during the charge-discharge cycles, some of the main drawbacks of these materials are their high self-discharge rates and their low capacities due to the low attainable doping degrees.[18]

Redox reactants accumulated in conducting polymers have been widely studied for sensor applications.[17] Recent papers from Milczarek[19, 20] report the synthesis and characterization of materials based on the combination of polypyrrole and lignin derivatives with quinone redox sites. Thin lignin/polypyrrole electrodes (0.5 μm thick) showed specific capacitances in the range of 430-450 F g^{-1} and charge capacities of 70-75 mA h g^{-1}; however, when the thickness was increased to 1.9 μm, the capacitance decreased to 170 F g^{-1}- 270 F g^{-1} and the charge capacity to 27-43 mA h g^{-1}. In this work, we report the use of a high-charge capacity redox solute, 1,4-benzoquinone, to increase the energy density of polypyrrole electrodes, due to its high theoretical charge capacity of 496 mA h g^{-1} [19] compared to 135 mA h g^{-1} for polypyrrole.[21] When incorporated within the electroactive polymer, we show it is possible to entrap an abundant prototypical organic redox molecule like 1,4-benzoquinone (**Figure 5.1**) and obtain specific capacitances as high as 550 F g^{-1} and charge capacities of 104 mA h g^{-1}. The objective of this work is also to show the effect of deposition conditions on the electrochemical properties of redox molecule doped polymer films. This study will enable the

development of supercapacitor materials that combine the high storage capacity properties of redox molecules with the high conductivity and capacitance of electroactive conducting polymers, such as polypyrrole.

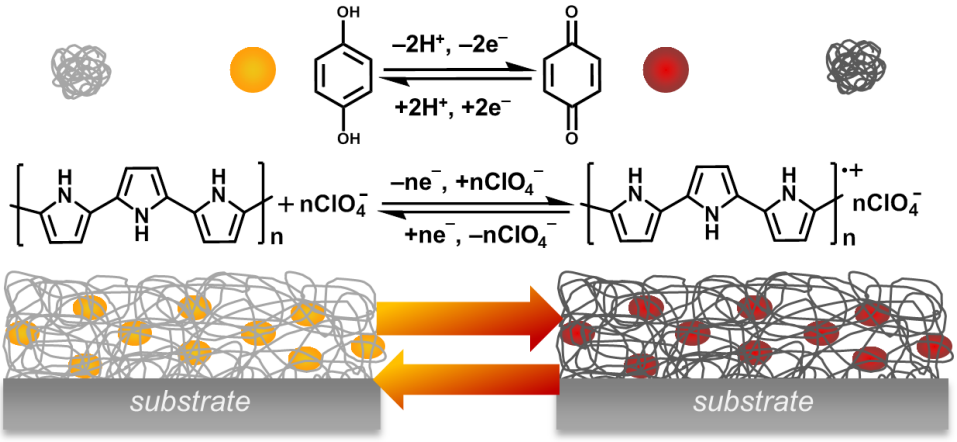

Figure 5.1. Illustrative schematic of the electrochemical processes occurring in a polypyrrole electrode doped with 1,4-benzoquinone.

Conducting polymers have been subject of research due to their interesting electronic, optical, physical and redox properties that make them suitable for applications in electrical energy storage. In these polymers, conductivity is achieved due to the delocalization of π electrons throughout the polymer backbone. In conventional conducting polymers, capacitance is governed by the electrochemical redox reactions of the π-conjugated system, often referred to as doping and de-doping. Polypyrrole can be oxidized with a charge density of one electron per two to three aromatic rings,[22] accompanied by the insertion of a negative ion from the electrolyte for charge compensation, which limits the material to a theoretical specific charge capacity of 135 $mAhg^{-1}$.[21, 23] On the other hand, a well-studied redox molecule like 1,4-benzoquinone has a theoretical specific charge capacity of 496 mA h g^{-1} [19] due to its 2 electron/2 proton

reversible redox process, which may provide a convenient mechanism to increase energy density in supercapacitor electrodes.

Many dopants have been studied extensively in polypyrrole electrodes, such as sulfonates or organosulfonic acids, among which reagents based on aromatic sulfonates are most popular, to achieve high conductivity, desired morphologies and enhance solubility.[24, 25] These dopants, which are used to preserve electrical neutrality, can serve also as surfactants and templates.[26, 27] Some examples are p-toluenesulfonate (PTS),[26, 28-30] dodezylbenzenesulfonate (DBS) and their sulfonic acids,[26, 27] anthraquinone sulfonic acids,[26, 31-34] naphthalene sulfonic acid.[35, 36]

Quinone compounds have been studied for applications in metal-free batteries[37] and supercapacitors [8] but the low cell voltage did not encourage further development and the systems were thought to have no chance for commercial use.[38] Nevertheless, entrapment of quinone-like molecules in polypyrrole has been done in applications for biosensors [39-41] and it has been shown that the polypyrrole acts like a molecular wire between the quinone materials and the base electrode. Polymers functionalized with electroactive moieties[42-46] and the use of quinoid materials as dopants has also been studied[47-50] achieving improved charge storage capacities due to the combined redox processes of polymer and quinoid components.

5.2 Experimental methods

5.2.1 Materials

Pyrrole (99%), 1,4-benzoquinone (98%) and perchloric acid (70%) were purchased from Acros organics, Alfa Aesar and Sigma Aldrich, respectively, and used as received.

5.2.2 Electrode fabrication

Solutions were prepared with 0.092 M 1,4-benzoquinone in aqueous 0.1 M perchloric acid ($HClO_4$), stirred, filtered using a syringe filer (Fisherbrand, Nylon 0.45 μm) and purged with N_2 prior to use. Pyrrole was added with concentrations in the range of 0.075 M to 0.4 M. Quinone-free solutions with similar pyrrole concentrations were prepared for control experiments. Polymer films were grown on 1 cm x 1 cm stainless steel mesh substrates (McMaster-Carr, 200 x 200, specific surface area ~2.65 cm^2) using chronopotentiometry at a current density of 1.9 $mAcm^{-2}$ (referenced to the specific surface area) for 360 sec with a VersaSTAT4 potentiostat/galvanostat and VersaStudio v1.50 Electrochemistry Software (Princeton Applied Research). Prior to film growth, substrates were treated in UV-Ozone (Novascan, PSD-UV8) for 30 minutes in air and at room temperature.

5.2.3 Characterization

Physical properties. Electrode masses were calculated by weighing each substrate on a microbalance (Ohaus, DV215CD, 0.01 mg resolution) before and after film growth. After film growth and characterization, films were allowed to dry overnight in a

vacuum oven (90 ^{o}C, 25 inHg). The surface morphology was observed using scanning electron microscopy (SEM, Hitachi SU-6600) with an accelerating voltage of 20 kV.

Electrochemical properties. Each polymer electrode was characterized in a three-electrode cell containing 0.1 M $HClO_4$ aqueous electrolyte solutions using cyclic voltammetry (CV) (ν = 100, 30, and 10 mVs^{-1}) and galvanostatic charge/discharge cycles (0 – 0.8 V) with current densities in the range of 0.06 $mAcm^{-2}$ to 0.75 $mAcm^{-2}$, which was selected to achieve a total discharge time of ca. 60 sec. The three-electrode cell contained the substrate as the working electrode, an Ag/AgCl reference electrode (ferrocene $E_{1/2}$ = 0.10 V) and a platinum (Pt) mesh counter electrode. QN solutions were tested using a similar three-electrode cell with a Pt disk working electrode (1.6 mm dia.) and a Pt wire counter electrode. To evaluate film stability, CV scans were recorded intermittently while soaking the substrates in fresh electrolyte solution between measurements.

5.3 Results and discussion

The basis of our work is combining two redox materials with very different characteristics to enable electrode materials with new properties conducive for batteries and supercapacitors. In these materials, conductive polymers act as an efficient molecular interface for electron transfer to the redox sites on the quinone, which could not function as a redox electrode alone. To achieve this goal, polypyrrole films were deposited in a saturated 1,4-benzoquinone (0.092 M) solution on stainless steel mesh electrodes. A schematic representation of the resulting composite electrodes, with 1,4-benzoquinone

incorporated in the polymer is shown in **Figure 5.1**, as well as the redox processes occurring within the material during oxidation/reduction. When a positive potential is applied to the polymer electrode, polypyrrole is oxidized (positively charged) and anions from the electrolyte diffuse into the polymeric network to maintain neutrality. It is also likely that positive charges (protons) trapped within the film diffuse out of the electrode during oxidation. At the same time, the reduced form of 1,4-benzoquinone, hydroquinone, oxidizes giving off two protons and two electrons. During dedoping, the polymer accepts electrons from the potentiostat to return to its neutral state, while 1,4-benzoquinone reversibly reduces to hydroquinone. During both of these processes, ions from the electrolyte must travel through the film to maintain charge neutrality.

When electroactive polymers are grown using electrochemical methods, the monomers in solution are irreversibly oxidized at a specific potential, then react with a growing polymer on or near the electrode surface.[51] In the presence of redox solutes, the deposition conditions can vary significantly as the redox solutes will absorb a fraction of the charge. To understand how the presence of 1-4-benzoquinone solutes affects the deposition of the electroactive polymer, the mass of the polypyrrole electrodes was measured using a microbalance for various films prepared with the same applied charge. Electrodes were prepared in the presence and absence of 1,4-benzoquinone with the same current (5 mA) and deposition time (360 s) to maintain a constant deposition charge (Q_{dep} = 1.8 C).

For electrodes prepared using a standard 0.1 M pyrrole in 1,4-benzoquinone solutions (PPy/QN), the mass was significantly reduced (one order of magnitude) relative

to electrodes prepared from reference pyrrole solutions (PPy). As the two redox species compete for the deposition current, we supposed that the film composition and mass could be controlled by varying the pyrrole concentration in the deposition solution while maintaining saturated 1,4-benzoquinone solutions. Reference polypyrrole electrodes were grown with similar pyrrole concentrations for comparison. **Figure 5.2** shows the mass of the grown films with respect to the initial concentration of pyrrole for reference polypyrrole (filled circles) and for PPy/QN electrodes (open circles). The mass of reference polypyrrole electrodes remained fairly constant over the range of deposition conditions and is in accordance with Faraday's law (**Eq 5.1.**)

$$m = \frac{I\,t}{F}\left(\frac{M_m + \gamma M_d}{2+\gamma}\right) \qquad (5.1)$$

where I is the current, t is time, M_m is molar mass of monomer, γ is the doping density (0.33 for polypyrrole),[22] M_d is the molar mass of the dopant and F is Faraday's constant. As expected, we obtained nearly 100% Coulombic efficiency for the polypyrrole growth. However, for the PPy/QN electrodes, the film mass increased linearly with increasing pyrrole concentration. For each PPy/QN film, the film mass was less than reference polypyrrole electrodes, gradually approaching the reference PPy thickness for high monomer concentrations.

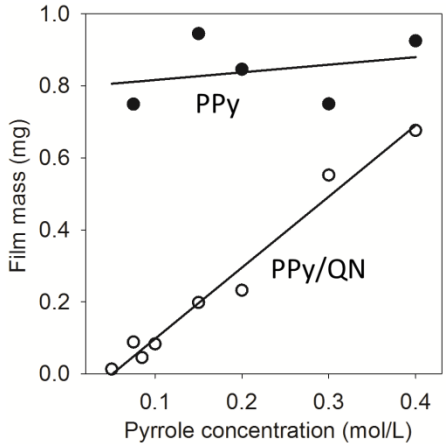

Figure 5.2. Electrode mass vs pyrrole concentration for PPy/QN composite (open circles) and reference PPy (filled circles) films grown with a galvanostatic current density of 1.9 mA cm^{-2} for 360 seconds (total charge of 1.8 C). Amounts weighed in a microbalance (0.01 mg resolution). The quinone concentration is 0.092 M in each film. Linear correlations of the experimental data are displayed as solid lines.

At low pyrrole (Py) monomer concentrations, near that of 1-4-benzoquinone (QN), the amount of mass deposited is small since more QN is available relative to Py at the electrode surface, resulting in a large consumption of current to oxidize the hydroquinone. Conversely, when the concentration of pyrrole is high, these monomers accumulate at the stainless steel electrode surface consuming the majority of current (leaving little to oxidize QN), resulting in higher mass films comparable to reference PPy electrodes. The optimal balance between pyrrole and hydroquinone concentration can be found where the deposition rate and composition of entrapped quinone achieve the highest electrochemical performance.

The effect of 1,4-benzoquinone in the morphology of the films deposited on stainless steel mesh substrates was investigated using scanning electron microscopy (SEM). Reference polypyrrole films show a typically-observed homogeneous granular

texture throughout the stainless steel mesh with a film thickness of 3-4 μm (**Figures 5.3a, 5.3c**), while PPy/QN material (**Figures 5.3b, 5.3d**) showed two different textures, a granular layer coating the substrate and a non-uniform superficial layer of granular clusters and the film thickness is 1.5-2 μm. Compared to reference polypyrrole agglomerate size (~1.5 μm), granular clusters of PPy/QN materials (~0.5 μm) is much smaller and they appeared lighter than the rest of the material. The blurriness in the images of PPy/QN electrodes is due to the lower conductivity of the samples containing QN redox species, which enhances the capacitive, but not to the conductive, properties of the electrodes.

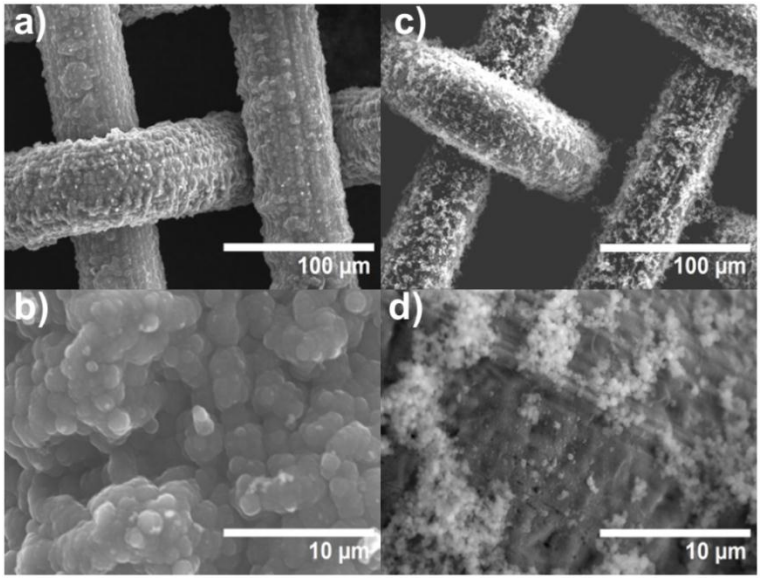

Figure 5.3. Scanning Electron Microscopy (SEM) images showing the morphology of films grown on stainless steel mesh substrates with a pyrrole and quinone concentrations of 0.2 M and 0.092 M, respectively. Reference polypyrrole films are shown for magnification of (a) 500x and (b) 5000x, and PPy/QN films are similarly shown at (c) 500x, (d) 5000x magnification.

The electrochemical properties of the polypyrrole and quinone-doped polypyrrole electrodes were evaluated using cyclic voltammetry and galvanostatic discharge measurements on single electrodes in a three-electrode configuration. As expected, reference polypyrrole electrodes exhibit similar electrochemical properties for all pyrrole concentrations, since the mass of the electrodes remained fairly constant (**Figure 5.4a**). However, when polypyrrole electrodes are doped with hydroquinone, an increase in capacitance is observed as the concentration of pyrrole increases (**Figure 5.4b**). The presence of two redox waves in the CV provides evidences for the integration of the quinone within the electrode during film growth. When comparing PPy/QN to PPy electrodes with greater mass, we observed a higher absolute capacitance of PPy/QN electrodes for those prepared with a concentration greater than 0.3 M, suggesting that the quinone plays a cooperative role with the pyrrole in the electrochemical performance.

To facilitate comparison between materials with different masses, the capacitance of each electrode was normalized by mass. Polypyrrole electrodes displayed similar gravimetric capacitance for all growth concentrations (**Figure 5.4c**); however, the specific capacitance of electrodes grown with hydroquinone (PPy/QN) showed a significant dependence on the monomer concentration during film growth. PPy/ QN films grown with pyrrole concentrations greater than 0.075 M exhibited an increased specific capacitance relative to the reference polypyrrole electrodes (**Figure 5.4d**). Compared to reference PPy electrodes, PPy/QN electrodes displayed two sharp, reversible redox waves, one near 0.2 V and the other around 0.5 V. The redox peak at 0.5 overlaps with the redox characteristics of the redox solute in solution on platinum electrodes, indicating

that the hydroquinone in the film is weakly bound to the polymer matrix. The redox potential at lower potential, however, is broader with a higher peak current. These characteristics are not present in the reference polymer film, and the large shift in performance relative to hydroquinone suggests that the some quinone species are closely bound to the polypyrrole polymer.

The charge capacity of the quinone-doped polypyrrole electrodes was determined using galvanostatic discharge measurements. The discharge profiles of reference PPy electrodes (**Figure 5.4e**) are linear and the capacitances, which were calculated from the inverse of the slopes, ranged from 175 F g^{-1} to 236 F g^{-1} and fall within the expected range.[1, 52-54] From the intersection of the discharge curve with the abscissa, we observe a typical charge capacity of PPy electrode, in the range of 40-50 mA h g^{-1}. On the other hand, the discharge curves for PPy/QN electrodes (**Figure 5.4f**) indicate the presence of the quinone, which leads to higher charge capacities between 65 and 75 mA h g^{-1}.

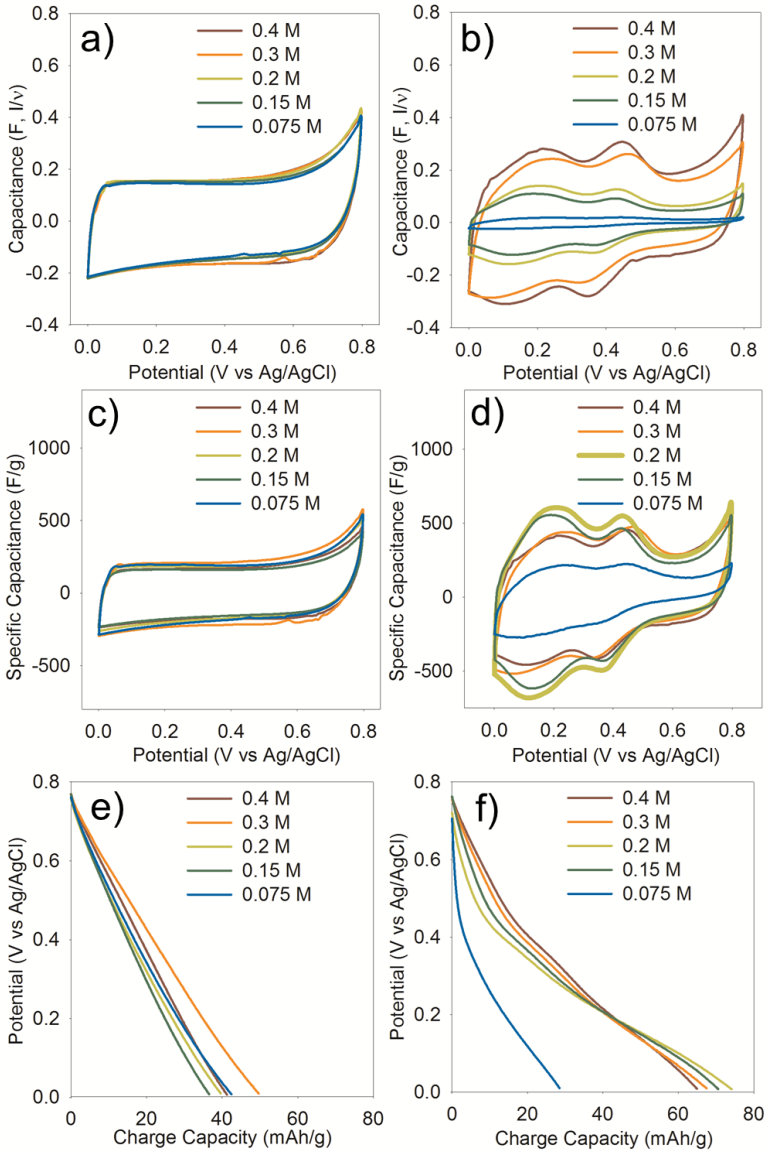

Figure 5.4. Electrochemical properties of reference polypyrrole (left column) and PPy/QN electrodes (right column) grown at different pyrrole concentrations measured in 0.1 M of $HClO_4$. Capacitance (F) vs potential is shown for (a) PPy and (b) PPy/QN, and specific capacitance (F g^{-1}) vs potential is shown for (c) PPy and (d) PPy/QN (0.01 V s^{-1}). Discharge curves, in terms of capacity ($mAhg^{-1}$), are shown for (e) PPy and (f) PPy/QN.

To obtain a clear picture of how the ratio between the Py monomer and the QN affects the electrode properties, PPy/QN electrodes were prepared using pyrrole concentrations ranging between 0.085 M and 0.4 M (**Figure 5.5**). Comparing the

performance of the PPy/QN electrodes with that of the reference pyrrole (**Figure 5.5a**) we found that the highest capacitance corresponded to films with a monomer ratio of pyrrole to quinone of 0.085,with a value of 550 F g^{-1}. The analysis of the discharge curves (**Figure 5.5b**) for the composite films is consistent with previous results.[19] The inverse of the slope of the 0.085 M Py discharge curve that includes the QN redox process equals to 1015 F g^{-1} and with a charge capacity of 104 mA h g^{-1}. Based on these results and knowing that reference pyrrole had a specific capacitance of about 236 F g^{-1}, we can infer a composition of quinone in the electrode of about 40% weight for the highest capacity electrode. To corroborate this estimate, the mass of this film was measured before and after soaking in DI water for nearly 1 month, which resulted in a decrease of 0.032 mg, or about 34% of the films total mass, consistent with our analysis of the discharge curves. The range of quinone composition in PPy/QN films grown with Py concentrations between 0.85 M and 0.4 M was between 40% and 14%, with QN composition decreasing with increasing Py. With an overall charge capacity of the 104 mA h g^{-1}, the estimated contribution of the 1,4-benzoquinone is approximately 200 mA h g^{-1}, which is less than half of its theoretical capacity (496 mA h g^{-1}). This further suggests that some of the hydroxyl groups on the quinone are closely bound to the acidic hydrogens on the polypyrrole and are no longer redox active under the given potential conditions.

When PPy/QN films are grown electrochemically in mixed monomer solutions containing Py and QN, we found that films with the highest charge capacity were obtained for nearly equal concentrations (0.092 M for QN, 0.085 M for Py). At these

conditions, the highest amount of quinone species were reversibly oxidized at the electrode surface and retained within the growing polymer matrix formed by the irreversible oxidization of pyrrole. At lower Py concentrations, redox species that are oxidized at the working electrode surface are able to diffuse away before becoming enveloped by the growing polymer matrix. At higher Py concentrations, the working electrode is saturated with pyrrole thereby limiting the amount of quinone incorporated in the film. The higher pyrrole concentration, however, leads to an increase in the deposition rate of the electrode film (**Figure 5.5c**), albeit with less redox molecules entrapped. **Figure 5.5c** also shows that the highest electrode capacitances are reached at similar concentrations of Py and QN, while the average specific capacitance tends to decrease toward that of reference polypyrrole.

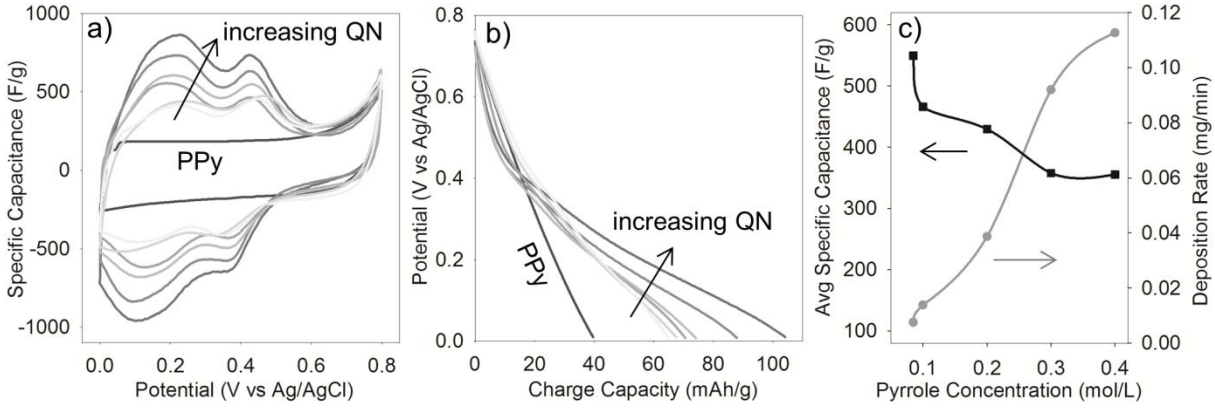

Figure 5.5. a) Specific capacitance vs potential at a scan rate of 0.01 V s^{-1}, b) discharge curves, and c) average specific capacitance/deposition rate vs pyrrole concentration of PPy/QN electrodes deposited with pyrrole concentrations of: 0.085, 0.1, 0.15, 0.2, 0.3 and 0.4 M in the presence of quinone 0.092 M, along with reference polypyrrole control electrode.

As opposed to reference polypyrrole films, PPy/QN films exhibited two sets of reversible redox peaks in their CV profile (**Figure 5.5a**), indicating the presence of quinone in two distinct forms. The nature of the charge transfer reactions in these electrodes was investigated using electrochemical methods in electrolyte solutions with varying pH from 0.46 to 3.2. As a control, 5mM QN solutions were studied in the same electrolytes. Quinone is known to undergo a two electron, two proton charge transfer process in acidic solutions, which is schematically represented above in **Figure 5.1**. As the proton concentration in solution decreases (increasing pH), it is expected that the redox peak(s) associated with this type of process shift by -60 mV/pH.[55] CV profiles for QN solutions (**Figure 5.6a**) display one redox couple with a half-wave potential ($E_{1/2}$) of 0.45 V in the lowest pH solution (pH 0.46). PPy/QN CV profiles, however, display two reversible redox couples, one at $E_{1/2}$ of 0.48 V, which is comparable to QN in solution, and one at $E_{1/2}$ of 0.24 V (**Figure 5.6b**). The insets of **Figures 5.6a and 5.6b** show that the redox behavior of QN species in solution and QN confined within a conducting polymer film exhibit the expected shift in redox potential with pH of 60 mV/pH and 64 mV/pH, respectively. The pH dependent of the redox potential for PPy/QN films is presented in terms of the oxidation peak potential (E_{ox}) rather than $E_{1/2}$ since the cathodic peak was not well-resolved as the pH increased.

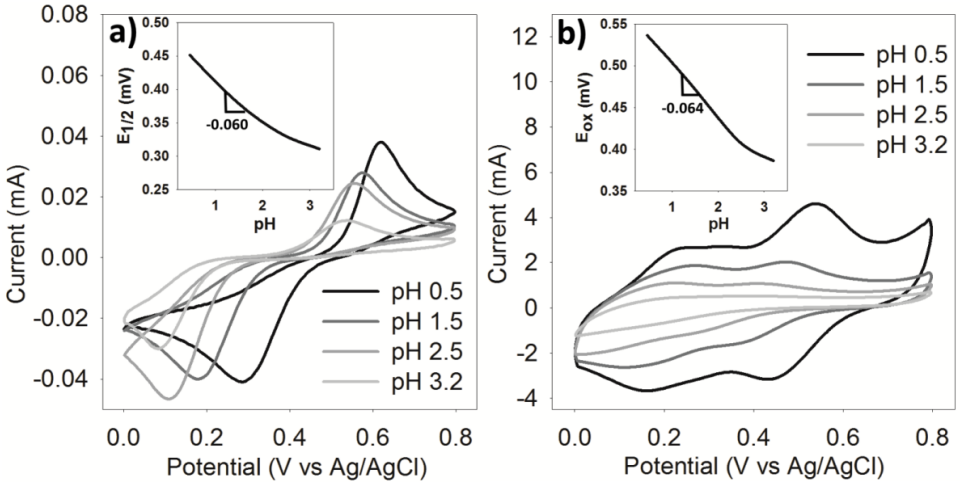

Figure 5.6. Cyclic voltammetry profiles (0.1 V s^{-1}) are shown for a) 5mM QN solutions, and b) PPy/QN films in electrolyte solutions with pH of 0.5, 1.5, 2.5 and 3.2. Figure insets show a) half wave potential ($E_{1/2}$) vs pH and b) oxidation potential (E_{ox}) vs pH.

The stability of the PPy/QN films was evaluated by measuring their electrochemical properties (CV) intermittently while soaking the substrates in electrolyte solution between measurements (**Figure 5.7**). **Figure 5.7b** shows that the performance of reference polypyrrole films remained fairly constant during the testing period, after an initial minor decrease in capacitance. Films containing quinone, however, exhibited a gradual decrease in the capacitance, primarily from the redox couple at 0.48 V (**Figure 5.7c**), which is a consequence of quinone diffusing out from the polymer film while soaking in solution between measurements. The electrochemical behavior of this redox peak is very similar to the redox behavior of the QN measured in solution, as described above. The redox couple at lower potential remains intact, presumably due to a strong interaction between this form of quinone and the acidic protons on polypyrrole. Even though the performance of the composite film decreases, it is predictable that it does not get lower than the reference polypyrrole films.

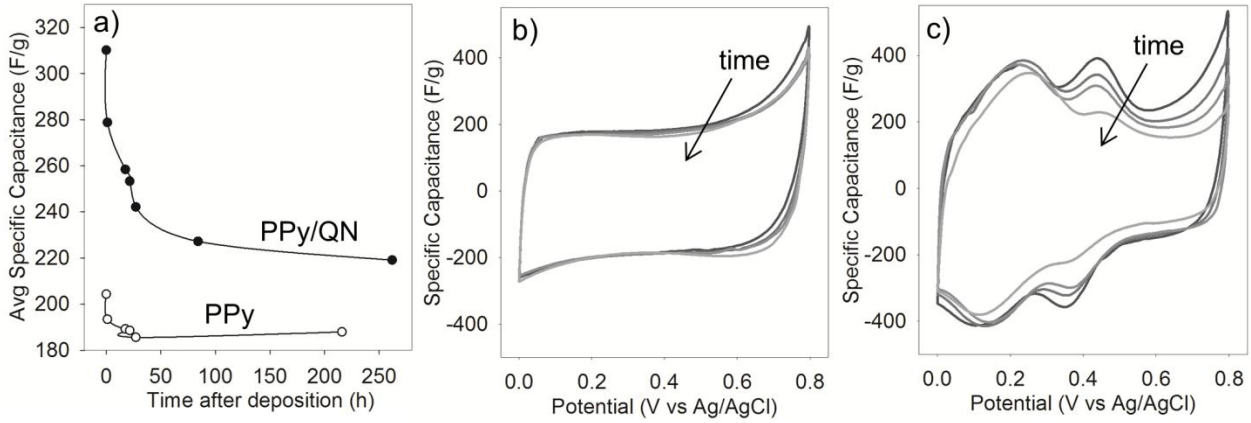

Figure 5.7. Electrode stability of reference polypyrrole and PPy/QN films prepared with 0.4 M pyrrole. a) Average specific capacitance between 0 to 0.8 V vs time in 0.1 M $HClO_4$ aqueous solution. Specific capacitance vs potential is shown for b) Reference polypyrrole and c) PPy/QN electrodes after 1 h, 17.5 h, 21.5 h, 27 h, 84 h, and 262 h. CV profiles are recorded at a scan rate of 0.01 V s^{-1}.

5.4 Conclusions

In order to enhance the charge storage capacity, which ultimately affects the energy density of an electrochemical capacitor, hydroquinone was integrated into a polypyrrole electrode using electrochemical synthesis. The combination of redox events from polypyrrole and hydroquinone result in an electrode with increased charge storage capacity compared to the neat electroactive polymer. In PPy/QN electrodes, the highest average specific capacitance (over the range of 0-0.8V) of 550 F g^{-1} and charge capacity of 104 mA h g^{-1} was achieved when films were grown from solutions with 0.085 M Py and 0.092 M QN, which represents a significant increase over PPy electrodes with typical specific capacitance values of 249 F g^{-1} and 40 mA h g^{-1}. It is important to note that the conditions applied to synthesize the hydroquinone-doped polymer have a significant impact on the resulting electrode performance, and that conditions typically used to

electrochemically synthesize polymer films are not suitable for these materials. Low concentrations of pyrrole, less than 0.075 M, result in insignificant film deposition as the applied current is consumed by the redox process of the quinone. As the concentration is increased, an ideal monomer concentration is observed around 0.085 M, and further increasing the monomer concentrations results in increased deposition rates, but a lower composition of entrapped redox molecules. The consequence of using redox molecule dopants, however, is that some of the quinone diffuses out of the electrode after a few days reducing the charge storage capacity. The redox behavior of the doped electrodes indicates that some of the hydroquinone strongly binds to the polypyrrole background, leading to a sharp redox peak around 0.2V, and the remaining dopants weakly interact with the polymer, yielding a sharp redox peak around 0.5V, similar to its solution redox characteristics. Nonetheless, the results are significant as they demonstrate that materials with diverse redox behaviors and potentials can be combined in an electrochemical system to develop organic electrodes with high specific charge capacities.

5.5 References

1. Burke, A., Ultracapacitors: why, how, and where is the technology. *Journal of Power Sources* **2000,** 91, (1), 37-50.
2. Goodenough, J. B. *Basic Research Needs for Electrical Energy Storage: Report of the Basic Energy Sciences Workshop on Electrical Energy Storage*; Department of Energy: 07/2007, 2007.
3. Winter, M.; Brodd, R. J., What Are Batteries, Fuel Cells, and Supercapacitors? *Chemical Reviews* **2004,** 104, (10), 4245-4270.
4. Simon, P.; Gogotsi, Y., Materials for electrochemical capacitors. *Nature Materials* **2008,** 7, (11), 845-854.
5. Halper, M. S., Ellenbogen, J.C., Supercapacitors: A Brief Overview. In MITRE: http://www.mitre.org/sites/default/files/pdf/06_0667.pdf, 2006; p 41.
6. Pandolfo, A. G.; Hollenkamp, A. F., Carbon properties and their role in supercapacitors. *Journal of Power Sources* **2006,** 157, (1), 11-27.
7. Lota, G.; Fic, K.; Frackowiak, E., Carbon nanotubes and their composites in electrochemical applications. *Energy & Environmental Science* **2011,** 4, (5), 1592-1605.
8. Snook, G. A.; Kao, P.; Best, A. S., Conducting-polymer-based supercapacitor devices and electrodes. *Journal of Power Sources* **2011,** 196, (1), 1-12.
9. Cottineau, T.; Toupin, M.; Delahaye, T.; Brousse, T.; Bélanger, D., Nanostructured transition metal oxides for aqueous hybrid electrochemical supercapacitors. *Applied Physics A* **2006,** 82, (4), 599-606.

10. Dmowski, W.; Egami, T.; Swider-Lyons, K. E.; Love, C. T.; Rolison, D. R., Local Atomic Structure and Conduction Mechanism of Nanocrystalline Hydrous RuO2 from X-ray Scattering. *The Journal of Physical Chemistry B* **2002,** 106, (49), 12677-12683.
11. Deng, W.; Ji, X.; Chen, Q.; Banks, C. E., Electrochemical capacitors utilising transition metal oxides: an update of recent developments. *RSC Advances* **2011,** 1, (7), 1171-1178.
12. Jiang, J.; Li, Y.; Liu, J.; Huang, X.; Yuan, C.; Lou, X. W., Recent Advances in Metal Oxide-based Electrode Architecture Design for Electrochemical Energy Storage. *Advanced Materials* **2012,** 24, (38), 5166-5180.
13. Lu, Q.; Chen, J. G.; Xiao, J. Q., Nanostructured Electrodes for High-Performance Pseudocapacitors. *Angewandte Chemie International Edition* **2013,** 52, (7), 1882-1889.
14. Lota, K.; Khomenko, V.; Frackowiak, E., Capacitance properties of poly(3,4-ethylenedioxythiophene)/carbon nanotubes composites. *Journal of Physics and Chemistry of Solids* **2004,** 65, (2–3), 295-301.
15. Mastragostino, M.; Arbizzani, C.; Soavi, F., Polymer-based supercapacitors. *Journal of Power Sources* **2001,** 97–98, (0), 812-815.
16. Linden, D., Reddy, T.B., *Handbook of Batteries*. 3 ed.; McGraw-Hill: United States, 2001; p 1453.
17. Maksymiuk, K., Chemical Reactivity of Polypyrrole and Its Relevance to Polypyrrole Based Electrochemical Sensors. *Electroanalysis* **2006,** 18, (16), 1537-1551.

18. Nyholm, L.; Nyström, G.; Mihranyan, A.; Strømme, M., Toward Flexible Polymer and Paper-Based Energy Storage Devices. *Advanced Materials* **2011,** 23, (33), 3751-3769.

19. Milczarek, G.; Inganäs, O., Renewable Cathode Materials from Biopolymer/Conjugated Polymer Interpenetrating Networks. *Science* **2012,** 335, (6075), 1468-1471.

20. Nagaraju, D. H.; Rebis, T.; Gabrielsson, R.; Elfwing, A.; Milczarek, G.; Inganäs, O., Charge Storage Capacity of Renewable Biopolymer/Conjugated Polymer Interpenetrating Networks Enhanced by Electroactive Dopants. *Advanced Energy Materials* **2013**, n/a-n/a.

21. Naoi, K., Morita, M., Advanced Polymers as Active Materials and Electrolytes for Electrochemical Capacitors and Hybrid Capacitor Systems. *The Electrochemical Society Interface* **2008,** 17, 44-48.

22. Waltman, R. J.; Bargon, J., Electrically conducting polymers: a review of the electropolymerization reaction, of the effects of chemical structure on polymer film properties, and of applications towards technology. *Canadian Journal of Chemistry* **1986,** 64, (1), 76-95.

23. Novák, P.; Müller, K.; Santhanam, K. S. V.; Haas, O., Electrochemically Active Polymers for Rechargeable Batteries. *Chemical Reviews* **1997,** 97, (1), 207-282.

24. Håkansson, E.; Lin, T.; Wang, H.; Kaynak, A., The effects of dye dopants on the conductivity and optical absorption properties of polypyrrole. *Synthetic Metals* **2006,** 156, (18–20), 1194-1202.

25. Yang, C.; Liu, P., Water-Dispersed Conductive Polypyrroles Doped with Lignosulfonate and the Weak Temperature Dependence of Electrical Conductivity. *Industrial & Engineering Chemistry Research* **2009,** 48, (21), 9498-9503.
26. Ding, C.; Qian, X.; Yu, G.; An, X., Dopant effect and characterization of polypyrrole-cellulose composites prepared by in situ polymerization process. *Cellulose* **2010,** 17, (6), 1067-1077.
27. Wang, J.; Xu, Y.; Yan, F.; Zhu, J.; Wang, J.; Xiao, F., Capacitive characteristics of nanocomposites of conducting polypyrrole and functionalized carbon nanotubes: effects of in situ dopant and film thickness. *Journal of Solid State Electrochemistry* **2010,** 14, (9), 1565-1575.
28. Kaynak, A., Decay of electrical conductivity in p-toluene sulfonate doped polypyrrole films. *Fibers and Polymers* **2009,** 10, (5), 590-593.
29. Little, S.; Ralph, S. F.; Too, C. O.; Wallace, G. G., Solvent dependence of electrochromic behaviour of polypyrrole: Rediscovering the effect of molecular oxygen. *Synthetic Metals* **2009,** 159, (19–20), 1950-1955.
30. Sultana, I.; Rahman, M. M.; Wang, J.; Wang, C.; Wallace, G. G.; Liu, H.-K., All-polymer battery system based on polypyrrole (PPy)/para (toluene sulfonic acid) (pTS) and polypyrrole (PPy)/indigo carmine (IC) free standing films. *Electrochimica Acta* **2012,** 83, (0), 209-215.
31. Huang, Y. M.; Zhou, F.-f.; Deng, Y.; Zhai, B.-g., Effects of salt 9,10-anthraquinone-2-sulfonic acid sodium on the conductivity of polypyrrole. *Solid State Ionics* **2008,** 179, (27–32), 1305-1309.

32. Feng, C.; Ma, L.; Li, F.; Mai, H.; Lang, X.; Fan, S., A polypyrrole/anthraquinone-2,6-disulphonic disodium salt (PPy/AQDS)-modified anode to improve performance of microbial fuel cells. *Biosensors and Bioelectronics* **2010,** 25, (6), 1516-1520.

33. Wang, Y.; Yang, C.; Liu, P., Acid blue AS doped polypyrrole (PPy/AS) nanomaterials with different morphologies as electrode materials for supercapacitors. *Chemical Engineering Journal* **2011,** 172, (2–3), 1137-1144.

34. Wang, Y.; Wang, X.; Yang, C.; Mu, B.; Liu, P., Effect of Acid Blue BRL on morphology and electrochemical properties of polypyrrole nanomaterials. *Powder Technology* **2013,** 235, (0), 901-908.

35. Muthulakshmi, B.; Kalpana, D.; Pitchumani, S.; Renganathan, N. G., Electrochemical deposition of polypyrrole for symmetric supercapacitors. *Journal of Power Sources* **2006,** 158, (2), 1533-1537.

36. Ariyanayagamkumarappa, D. K.; Zhitomirsky, I., Electropolymerization of polypyrrole films on stainless steel substrates for electrodes of electrochemical supercapacitors. *Synthetic Metals* **2012,** 162, (9–10), 868-872.

37. Beck, F., Graphite, Carbonaceous Materials and Organic Solids as Active Electrodes in Metal-Free Batteries. In *Advances in Electrochemical Science and Engineering*, Wiley-VCH Verlag GmbH: 2008; pp 303-411.

38. Beck, F.; Rüetschi, P., Rechargeable batteries with aqueous electrolytes. *Electrochimica Acta* **2000,** 45, (15–16), 2467-2482.

39. Shinohara, H.; Khan, G. F.; Ikariyama, Y.; Aizawa, M., Electrochemical oxidation and reduction of PQQ using a conducting polypyrrole-coated electrode. *Journal of*

Electroanalytical Chemistry and Interfacial Electrochemistry **1991,** 304, (1–2), 75-84.

40. Inoue, T.; Kirchhoff, J. R., Electrochemical Detection of Thiols with a Coenzyme Pyrroloquinoline Quinone Modified Electrode. *Analytical Chemistry* **2000,** 72, (23), 5755-5760.
41. Blitz, J. P., Gun'ko, V., *Surface Chemistry in Biomedical and Environmental Science*. Springer Netherlands: Netherlands, 2006.
42. Naoi, K.; Kawase, K. i.; Mori, M.; Komiyama, M., Electrochemistry of Poly(2,2′-dithiodianiline): A New Class of High Energy Conducting Polymer Interconnected with S–S Bonds. *Journal of The Electrochemical Society* **1997,** 144, (6), L173-L175.
43. Häringer, D.; Novák, P.; Haas, O.; Piro, B.; Pham, M. C., Poly(5-amino-1,4-naphthoquinone), a Novel Lithium-Inserting Electroactive Polymer with High Specific Charge. *Journal of The Electrochemical Society* **1999,** 146, (7), 2393-2396.
44. Yamamoto, T.; Kimura, T.; Shiraishi, K., Preparation of π-Conjugated Polymers Composed of Hydroquinone, p-Benzoquinone, and p-Diacetoxyphenylene Units. Optical and Redox Properties of the Polymers. *Macromolecules* **1999,** 32, (26), 8886-8896.
45. Naoi, K.; Suematsu, S.; Manago, A., Electrochemistry of Poly(1,5-diaminoanthraquinone) and Its Application in Electrochemical Capacitor Materials. *Journal of The Electrochemical Society* **2000,** 147, (2), 420-426.
46. Song, H. K.; Palmore, G. T. R., Redox-Active Polypyrrole: Toward Polymer-Based Batteries. *Advanced Materials* **2006,** 18, (13), 1764-1768.

47. Zinger, B., Electrochemistry of quinoid dopants in conducting polymers. *Synthetic Metals* **1989,** 30, (2), 209-225.

48. Yoneyama, H.; Ii, Y.; Kuwabata, S., Charge-discharge Characteristics of Polypyrrole Films Containing Incorporated Anthraquinone-1-Sulfonate. *Journal of The Electrochemical Society* **1992,** 139, (1), 28-32.

49. Hashmi, S. A.; Suematsu, S.; Naoi, K., All solid-state redox supercapacitors based on supramolecular 1,5-diaminoanthraquinone oligomeric electrode and polymeric electrolytes. *Journal of Power Sources* **2004,** 137, (1), 145-151.

50. Lang, X.; Wan, Q.; Feng, C.; Yue, X.; Xu, W.; Li, J.; Fan, S., The role of anthraquinone sulfonate dopants in promoting performance of polypyrrole composites as pseudo-capacitive electrode materials. *Synthetic Metals* **2010,** 160, (15–16), 1800-1804.

51. Sadki, S.; Schottland, P.; Brodie, N.; Sabouraud, G., The mechanisms of pyrrole electropolymerization. *Chemical Society Reviews* **2000,** 29, (5), 283-293.

52. Wang, J.; Xu, Y.; Chen, X.; Sun, X., Capacitance properties of single wall carbon nanotube/polypyrrole composite films. *Composites Science and Technology* **2007,** 67, (14), 2981-2985.

53. Snook, G. A.; Chen, G. Z., The measurement of specific capacitances of conducting polymers using the quartz crystal microbalance. *Journal of Electroanalytical Chemistry* **2008,** 612, (1), 140-146.

54. Izadi-Najafabadi, A.; Tan, D. T. H.; Madden, J. D., Towards High Power Polypyrrole/Carbon Capacitors. *Synthetic Metals* **2005,** 152, (1–3), 129-132.

55. Senthil Kumar, K.; Natarajan, P., Electrochemical behavior of two and one electron redox systems adsorbed on to micro- and mesoporous silicate materials: Influence of the channels and the cationic environment of the host materials. *Materials Chemistry and Physics* **2009,** 117, (2–3), 365-372.

CHAPTER SIX

CONCLUSIONS AND RECOMMENDATIONS

6.1 Conclusions and recommendations

Throughout this PhD work, carbon materials, conducting polymers, and redox-active polymers and dopants were studied to develop efficient electrodes for supercapacitors. From these materials, carbon nanostructures, an alternative to activated carbon, are the most promising group for the next generation SCs, mainly due to their good stability over multiple thousands of cycles. Faradaic materials do not meet the stability requirements and future research should focus on this issue.

Multiple techniques have been developed to manufacture SC electrodes, in which the active material is directly grown or synthesized on the current collector, or pre-synthesized materials are further processed into pastes, slurries, inks, solution, or suspensions and attached to the current collector (CC) or produced as free-standing electrodes. Direct growth on the CC is advantageous because the active material is strongly attached to the CC, reducing contact resistance and eliminating the need for non-conductive binders. Direct growth also tends to produce homogeneous coatings of active material and synthesis/electrode production occurs in the same step. Pre-synthesis of the active material is attractive because it allows mass production, which is necessary for future commercialization. Some processing techniques of pre-synthesized materials include printing (e.g. ink-jet), spray coating, wet-spinning, which allows the use of well-developed industrial techniques to produce replicable samples and facilitates the possible commercialization. Downsides of these methods include solution processing, which

involves the use of solvents, material waste, and the addition of conductivity enhancers and binders.

6.2 Roll-to-roll synthesis of vertically aligned carbon nanotube electrodes for electrical double layer capacitors

CNTs are attractive due to their remarkable mechanical and electrical properties but the anticipated CNT revolution has not found place yet because the excellent theoretical properties of CNTs apply mainly to SWCNTs, which are difficult to obtain, in the conductive state and purity to fully show their potential. For their outstanding properties, a significant enhancement in electrode performance is foreseen for ordered arrays of single-walled CNTs directly grown on cost-effective CCs. MWCNTs are easier to synthesize, but properties such as conductivity, surface area and capacitance are significantly lower than SWCNTs. Research efforts should be focused on developing processes and tuning conditions that allow for the synthesis of highly conductive and homogeneous SWCNTs with high yield and purity for them to be competitive in the SC field. Nevertheless, the direct growth of MWCNTs on aluminum foil is an important advance towards commercialization, since the synthesis temperature (600 ºC) is low enough to allow the use of this cost-effective substrate, such as aluminum foil. These materials can boost the performance of lithium-ion batteries, as a conductive layer between the active material and the current collector. Additionally, the CC-CNT interfacial resistance is low and no binder is required.

The ordered structure of vertically aligned carbon nanotubes showed advantages, such as increased capacitance due to larger accessible area, important decrease in

resistance due to the shorter path for ion diffusion and close contact of all the tubes with the CC. Randomly oriented CNT electrodes showed larger resistance, as some tubes can be isolated and the electrolyte may not have access to the whole surface.

For deposition times longer than 1 hour, amorphous carbon was observed covering the surface of the VACNTs, which affects the capacitance and power density of the electrodes blocking access of the electrolyte to the pores. To guarantee the best performance of the vertically aligned CNT electrodes, the purity of the material, length of the tubes, and density must be optimized. The longer the deposition times are, the more dense the CNT film and the longer the CNTs, but the larger the content of amorphous carbon. In the future, a conscious selection of the electrolyte salts should be carried out taking in to account the porosity of the materials as the ion size can alter the measured capacitance significantly. According to literature,[1] the highest capacitance of carbon materials is achieved when the size of the ion is about the same size as the pores. Since Brunauer–Emmett–Teller (BET) method to measure the specific surface area of the material overestimates the surface area values,[1] different ion sizes should be tested. Smaller ions (e.g. $LiClO_4$) have given considerably higher capacitance values compared to larger ions (e.g. $TBABF_4$, $TEABF_4$, TBAPF6), but at a concentration of 1M $LiClO_4$ reacts with the aluminum degrading the samples. Acetonitrile should be always considered before propylene carbonate, as its ionic conductivity is substantially higher and larger capacitance values are obtained.

To obtain capacitance values for individual electrodes, they were tested in wide potential ranges from -1 V to +1.2 V (vs Ag/Ag^+), because carbon materials and the

organic electrolyte are stable over a wide range, but when testing conducting polymers only the potential range in which they are active and conductive should be tested. For the SC cell tests, it is recommended to fully charge one electrode and discharge the other one prior to assembling the cell, and the cell should be tested in the range that the materials and electrolyte allows (e.g. 0 V to 2 V).

6.3 A facile and scalable approach to fabricating free-standing polymer-carbon nanotube composite electrodes

The filtration method to fabricate SC electrodes is a simple process that utilizes pre-synthesized CNTs and CPs to yield high capacitance composites. On the downside, the random orientation of the tubes, the tendency to aggregate of both components, and the thickness of the films increased the electrode resistance.

Some difficulties of this method that require attention include the need for better-dispersed materials. Although the separate materials were sonicated prior to filtration, SEM pictures show the presence of large CNT and CP clusters that hinder the electrolyte accessibility to the active material and decreases capacitance due to the unused mass. The CP/CNT ratio needs to be optimized; possibly lower concentrations of well-dispersed CP (< 50 %) in the CNTs can show enhanced mechanical properties and capacitance. Even though water is a preferred solvent for sonication, organic solvents that interact better with the CNTs might be useful, as well as longer sonication times, and a variety of surfactants. The porosity of the filtration membrane used in this project is greater than the dimensions of the CNTs, but the retention of material is efficient because the clusters of

CNTs are larger than the pores. Another recommendation when filtering well-dispersed materials would be to use a low molecular weight cut off ultrafiltration membrane and use a pressurized filtration cell that would speed up the process and increase the retention of CNTs and CP.

The resulting films from the filtration method are resilient, but as the polymer content increases, the film becomes more brittle. The addition of binder would help keep the film structure making it sturdy for easier manipulation. The mechanical and electrochemical properties of films prepared with and without binder should be characterized and compared. Thinner films may also be possible with the use of binder, which is necessary to decrease resistance in the film. When detaching the film from the filter membrane the composite films undergo stress and bending, and a razor blade is also needed, affecting the material consistency. An alternative to peeling off the material from the substrate could be useful, e.g. dissolving the membrane with a method that does not affect the CPs or the CM performance.

An advantage of the absence of a metallic current collector is that any electrolyte can be used in the SC system. Aqueous electrolytes show high capacitance due to their high ionic conductivity, but in the end, the specific energy, which is proportional to the voltage squared, is decisive and (organic) electrolytes with larger potential windows are preferred.

6.4 Pseudo-capacitor anodes comprised of electrochemically synthesized aminoanthraquinone redox polymers

Poly(1-aminoanthraquinone) (PAQ) is a conjugated polymer that shows reversible redox activity in the potential range of 0 to -2 V vs Ag/Ag^{+}, making it an interesting for applications in SC negative electrodes. Its conjugated polyaniline-like backbone allows the polymer to be conductive and p-doped, while the quinone redox sites are electroactive in the negative potentials. Even though quinones possess such high charge capacities and they are one of the most stable redox molecules available, they are less stable than conducting polymers limiting their applications in SCs. PAQ stability was increased by using a free-standing CNT film, where the CNTs served as electron transfer matrix to and from the PAQ redox sites. For future research in polymeric or redox materials for SC anodes, molecules with higher theoretical charge capacity should be studied. The polyaniline back bone is less conductive at negative potentials, affecting the redox activity of the quinone and reducing capacitance due to the unused mass. A material that is conductive and/or active in the negative potentials is needed to provide a conductive support for the redox-active anthraquinone. Since carbon materials work as both anode and cathode, an interesting approach would be to functionalize carbon materials with anthraquinone moieties, to achieve effective charge transport and maximize capacitance.

6.5 Redox solute doped polypyrrole for high-charge capacity polymer electrodes

P-benzoquinone (QN) was integrated into a conducting polymer (polypyrrole) electrode with the purpose of increasing the charge capacity of the electrodes. QN was

entrapped in PPY through electrochemical polymerization and an increase of more than twice the capacitance and charge capacity was achieved, compared to PPY films. The QN/PPY ratio was optimized and the highest capacitance was obtained for a molar ratio of about 1:1. Besides the instability inherent from the redox molecules, part of the QN diffused back in solution after long periods submerged in electrolyte. Since CPs work well as cathodes, composites of redox-active molecules and CPs or carbon materials are promising as positive electrodes for SCs. Stability is also an issue in this case, where the integration with highly conductive carbon materials can enhance performance and stable functionalization or redox molecule-containing polymers would prevent the diffusion of the active molecules back into solution. Our group has also studied entrapping lignin, which is a biopolymer rich in quinone moieties, in polypyrrole, and high capacitances have been achieved.

6.6 References

1. Pandolfo, T., Ruiz, V., Sivakkumar, S., Nerkar, J., *Supercapacitors: Materials, Systems, and Applications*. First ed.; Wiley-VCH Verlag GmbH & Co.: Weinheim, Germany, 2013.